Seasonal Temperature Reconstruction for Northeastern Siberia during the Late Pleistocene from High-Resolution Oxygen Isotope Measurements across Fossil Wood

A Thesis

Presented to the

Graduate Faculty of the

University of Louisiana at Lafayette

In Partial Fulfillment of the

Requirements for the Degree

Master of Science

Collin Moore

Fall 2017

Seasonal Temperature Reconstruction for Northeastern Siberia During the Late Pleistocene from High-Resolution Oxygen Isotope Measurements Across Fossil Wood

Collin Moore

APPROVED:

_____	_____
Brian A. Schubert, Chair Associate Professor of Geology	David M. Borrok Professor and Director of Geology
_____	_____
Brian E. Lock Professor Emeritus of Geology	Mary Farmer-Kaiser Dean of the Graduate School

Moore, Collin. Bachelor of Science Geology Studies, Sam Houston State University, August 2013; Master of Science, University of Louisiana at Lafayette, August 2017
Major: Geology
Title of Thesis: Seasonal Temperature Reconstruction for Northeastern Siberia during the Late Pleistocene from High-Resolution Oxygen Isotope Measurements across Fossil Wood
Thesis Director: Dr. Brian Schubert
Pages in Thesis: 130; Words in Abstract: 247

ABSTRACT

Cellulose is resistant to degradation on geologic timescales and provides a reliable record of the oxygen isotope composition of meteoric water ($\delta^{18}O_{MW}$). A strong empirical relationship between the $\delta^{18}O_{MW}$ value and temperature has been observed in modern settings, allowing researchers to reconstruct mean annual temperature via measurements of the $\delta^{18}O$ value of cellulose ($\delta^{18}O_{cell}$). I present high-resolution intra-annual $\delta^{18}O_{cell}$ measurements across fossil growth rings in mummified wood collected from late Pleistocene sediments (~50,000 to 44,000 ^{14}C BP) within the Yedoma Silt Ice Complex at Duvanny Yar in far northeastern Siberia. These data are used to quantify year-to-year changes in seasonal temperatures at the site, including warm and cold month mean temperatures (T_{max} and T_{min}, respectively). Results suggest T_{max} = 6.4 ± 3.0 °C (average ± 1σ) and T_{min} = -37.7 ± 2.9 °C during the late Pleistocene, which is significantly (T_{max} p = 0.0005, T_{min} p = 0.05) colder than today's values (modern: T_{max} = 13.2 ± 2.1 °C, T_{min} = -34.8 ± 2.6 °C). Assuming a normal distribution for monthly temperatures similar to modern continental climates, I calculate that above-freezing mean monthly temperatures occurred in ~1.6 fewer months during the late Pleistocene than today. These cold conditions allowed for the Arctic to act as a significant carbon sink during the late Pleistocene, despite shorter growing seasons as compared to today. Extrapolation to current Arctic warming suggests that increased temperatures will

allow for longer periods of net carbon release from Arctic soils each summer, despite increased photosynthesis.

ACKNOWLEDGMENTS

I would like to thank my thesis advisor, Dr. Brian Schubert, for giving me the opportunity to work on this important project. Dr. Schubert's knowledge, accessibility, guidance, and generosity in lending laboratory space and materials have provided me with an excellent research environment. His patience and encouragement were appreciated during periods of struggle working through a field of study that was new to me. Visiting and chatting with him during this research has lent me new perspective and a better understanding of our global environment.

I would like to thank my committee members, Dr. David Borrok and Dr. Brian Lock, for taking time to be on my thesis committee and showing interest in my research. Your assistance and advice is greatly appreciated.

I would like to thank Dr. Yingfeng Xu for her time, work, and assistance that were invaluable during the data collection process. I would also like to thank Bill Hagopian, out of the University of Hawaii, for taking time out of his life to travel to the University of Louisiana at Lafayette and spend several long days instructing me on the subsampling and cellulose extraction method. His patience and enthusiasm during my first genuine laboratory experience is truly appreciated. I hope similar projects continue in the Schubert Lab, giving me an opportunity to pay it forward by instructing future graduate students on the cellulose extraction technique for their individual research.

TABLE OF CONTENTS

ABSTRACT iv

ACKNOWLEDGMENTS vi

LIST OF TABLES ix

LIST OF FIGURES x

LIST OF EQUATIONS xii

LIST OF ABBREVIATIONS xiii

1. INTRODUCTION 1

2. MATERIALS AND METHODS 6
- **2.1 Study Site** 6
- **2.2 The Yedoma "Suite" at Duvanny Yar** 8
- **2.3 Sample Age Control** 13
- **2.4 Sample Processing** 16
- **2.5 Oxygen Isotope Analysis** 18

3. RESULTS 20
- **3.1 Resulting Intra-Ring $\delta^{18}O$ Measurements** 20

4. DISCUSSION 24
- **4.1 Quantifying Tmax** 24
  - **4.1.1 Assumption of Cold Month Temperature (T_{min}) for Calculating T_{max}** 26
  - **4.1.2 Assumption of Late Pleistocene Seasonal Precipitation for Calculating T_{max}** 28
- **4.2 Quantifying MAT** 28
- **4.3 Quantifying T_{min} from MAT and T_{max}** 31
- **4.4 Reconstructed Northeastern Siberian Late Pleistocene Seasonal Temperature** 33
- **4.5 Sensitivity Analysis on the Effect Seasonal Precipitation has on Quantifying Seasonal Temperature** 35
- **4.6 Global and Hemispheric Context: Polar Ice Core Records** 39
- **4.7 Regional Context** 41
  - **4.7.1 Regional Context T_{max}** 47
  - **4.7.2 Regional Context T_{min}** 56
  - **4.7.3 Regional Context MART** 58
  - **4.7.4 Regional Context MAT** 58
- **4.8 Modeling Growing Season Length** 59

5. CONCLUSION 73

REFERNCES 76

APPENDIX 101

BIOGRAPHICAL SKETCH 116

LIST OF TABLES

Table 1. Published radiocarbon dates on fossil wood at Duvanny Yar (compiled by Vasil'chuk et al., 2001). Original sources are in Russian. Radiocarbon ages beyond the calibration limit are reported as >54,000 yrs BP 15

Table 2. Preliminary cellulose extraction test results 20

Table 3. Step-by-step summary of equations used to calculate seasonal temperatures from high-resolution oxygen isotope values across consecutive rings 33

Table 4. List of eastern and northern Siberia relevant earlier Kargin interstadial and MIS 3 research, corresponding with Figure 13, including those at Duvanny Yar (Site 1), with their associated paleotemperature reconstructions/interpretations closest to ~45 and >54 ^{14}C kyr BP and their substrate/proxy methods. Dates here reported as infinite in terms of uncalibrated radiocarbon (^{14}C kyr BP) as referenced by the cited authors. Non-radiocarbon derived or calibrated ages referenced by a specific author are presented otherwise here as ka. Note, much of the prior research reported uncalibrated ^{14}C ages in either the kyr BP or ka BP nomenclature, their nomenclature is corrected here as ^{14}C kyr BP * 44

Supplementary Table 1. Tree-ring $\delta^{18}O_{cell}$ values measured from fossil wood samples DY2 and DY4 collected from the study site (68.63 °N, 159.63 °E). $\delta^{18}O_{cell}$ values for sample DY4_R6_6_A was considered an outlier and not included in figure 3 and the paleotemperature reconstructions. Not Detectable (N/D) 101

Supplementary Table 2. Single averaged tree-ring and standard deviation (SD) $\delta^{18}O_{cell}$ values measured from fossil wood samples DY2 and DY4, with $\Delta(\delta^{18}O_{cell})$ calculated from Equation 4 105

Supplementary Table 3. T_{max}, MAT, and T_{min} values calculated from Equations 6-8 and displayed in Figure 8 106

Supplementary Table 4. List of equations from previous literature representing the relationship between $\delta^{18}O_{MW}$ and MAT and T_{month}; $\delta^{18}O_{MW}$ and $\delta^{18}O_{cell}$; and various Richter et al. (2008b) like relationships between $\delta^{18}O_{cell}$ and MAT. Sternberg et al. (2007) equations reported as referenced by Shubert and Jahren (2015). *Regressions manipulated from Richter et al. (2008b) data, *Metasequoia* always excluded following Richter et al. (2008b) 107

Supplementary Table 5. Values calculated for $\delta^{18}O_{MW}$, MAT, and resulting T_{min} using other equations provided in Supplementary Table 4. All T_{min} values calculated using Equation 8 and T_{max} calculated from Equation 6. Average and Standard Deviation (SD) provide for the full eight-year fossil record 108

Supplementary Table 6. Mean monthly temperature values of the single average 33-year modern record from Cherskiy, and modeled mean monthly temperature across each fossil year and the single averaged seven-year fossil record. *Outlier fossil year 112

LIST OF FIGURES

Figure. 1. Location of Duvanny Yar (68.63 °N, 159.15 °E) (pink circle) near Cherskiy, Sakha Republic, Russia (68.74 °N, 161.40 °E) (blue circle) north of the Arctic Circle (66.55 °N) (dashed line) 7

Figure 2. Average monthly temperature across the years (1980-2012) at Cherskiy, Sakha Republic, Russia (National Oceanic and Atmospheric Administration (NOAA), National Climatic Data Center, http://www.ncdc.noaa.gov). The growing season, defined as number of months with T_{month} > 0 °C (dashed line), is only ~4 months long 8

Figure 3. Duvanny Yar field photos taken on 9/10/2014 showing the fossil wood sample collection site (A) with Yedoma silt in place from top to bottom of the exposure, segregated by syngeneic ice wedges along the banks of the Kolyma River (B). (C) Close look showing fossil wood preserved in-situ of lower Yedoma permafrost sediments with fossil wood samples collected lying on top (white box) and viewed in detail in images (D) and (E) 11

Figure 4. Example of non-permineralized fossil wood collected from the lower Yedoma permafrost sediments at Duvanny Yar. (B) Close look at four consecutive fossil tree rings sampled within block (A). Light-colored wood represents earlywood (EW) and darker wood represents latewood (LW). Red arrows indicate the direction of tree ring growth 17

Figure 5. Intra-ring $\delta^{18}O_{cell}$ data for DY2 (A) and DY4 (B) showing a range of values ~15.0 to 19.9‰. Excluding DY2 R1, the range of values is ~16.3 to 19.3‰. Initial value following ring boundaries (vertical axis) denote the first earlywood measurement. Rings numbered in the top left corners. $\Delta(\delta^{18}O_{cell})$ defined as the change between $\delta^{18}O_{cell(max)}$ and $\delta^{18}O_{cell(min)}$ (Eqn. 4) in DY2 and DY4 were on average 2.0 and 1.5‰, respectively 21

Figure 6. Correlation between combined North American and Puerto Rican conifer (red circles) and angiosperm (blue diamonds) δ^{18}Ocell and mean annual temperature including arctic willows (black diamonds). Developed from Richter et al. (2008b), supplementary data found at https://doi.org/10.1016/j.gca.2008.01.030 30

Figure 7. "Correlation between MAT determined by averaging monthly temperature data for all 12 months and MAT calculated as the average temperature determined only using data for the warmest (T_{max}) and coldest (T_{min}) months [Eqn. (8)]. Monthly temperature data used to calculate MAT were from a global dataset determined for all land areas, except Antarctica, at 10' spatial resolution (New et al., 2002)," from Schubert and Jahren (2015) 32

Figure 8. Box and whisker plot showing T_{max} (top row), MAT (middle row), and T_{min} (bottom row) from 1980-2012 at Cherskiy (left column, pink) and for the late Pleistocene (> ~45 to ~50 ^{14}C B.P.) at Duvanny Yar (right column, blue) calculated from Equations 6-8, respectively. DY2 R1 yields an anomalously high range in temperatures (very high T_{max} and very low T_{min}) that is unreasonable compared with the other rings. Modern data

are from the National Oceanic and Atmospheric Administration (NOAA) and National Climatic Data Center, http://www.ncdc.noaa.gov. Each box represents 50% of the temperature values, and line within each box represents the median value. The upper and lower whisker represent the upper and lower quartile of values outside of the box. Lines which cap each whisker represent the highest and least value excluding any outliers, which are shown as points (open circles) 34

Figure 9. Monthly mean precipitation (P, mm) from 1980–2012 in Cherskiy 36

Figure 10. Differences in winter and summer precipitation ($P_{winter} - P_{summer}$) in modern Cherskiy for years 1980 to 2012 37

Figure 11. Sensitivity of calculated late Pleistocene T_{max} (top) with possible seasonal change in precipitation ($P_{winter} - P_{summer}$, mm) in northeastern Siberia and the subsequent effect on T_{min} (bottom). Each box is a range in values of all rings, excluding DY2 R1 outlier 38

Figure 12. The North Greenland Ice Core Project (NGIRP) $\delta^{18}O_{ice}$ record (Site location: 75.10 °N, 42.32 °W) with numbered Dansgaard-Oeschger warming events (1-18) (after Dansgaard et al., 1993; Svensson et al., 2008) and Heinrich cooling periods (H1-H6) (after Hemming, 2004; Kindler et al., 2014; Svensson et al., 2008). Measured $\delta^{18}O_{ice}$ (duplicate) are mean values with a 50 yr resolution. Data from North Greenland Ice Core Project members, 2004 (ftp://ftp.ncdc.noaa.gov/pub/data/paleo/icecore/greenland/summit/ngrip/isotopes/ngrip-d18o-50yr.txt) 40

Figure 13. Map of eastern Siberia showing site locations with relevant Kargin interstadial climate research on northern Yedoma Ice Complex and interior lake permafrost sediments. Numbers correspond to individual sites, including (1) Duvanny Yar, with their associate research and climate reconstruction listed in Table (4). Arctic Circle: dashed line (66.5 °N) 43

Figure 14. Late Pleistocene seasonal temperatures across each year (blue curves) following the normal distribution of the single average of mean monthly change in temperature at modern Cherskiy (bold red line) averaged from each year from 1980-2012 (thin red curves). The bold blue curve represents the late Pleistocene single average of mean monthly change in temperature produced from average T_{max} and T_{min} from all fossil growth rings excluding DY2 R1. The intersection of the red and blue vertical lines with the horizontal dashed line bounds the modern and late Pleistocene growing season ($T \geq 0$ °C), respectively 62

LIST OF EQUATIONS

Equation 1. $\delta_{sample} = (R_{sample} / R_{standard} - 1)1000$ 18

Equation 2. $\Delta(\delta^{18}O_{MW}) = \Delta(\delta^{18}O_{cell}) / 0.66$ 24

Equation 3. $\Delta(\delta^{18}O_{MW}) = \delta^{18}O_{MW(max)} - \delta^{18}O_{MW(min)}$ 24

Equation 4. $\Delta(\delta^{18}O_{cell}) = \delta^{18}O_{cell(max)} - \delta^{18}O_{cell(min)}$ 24

Equation 5. $\Delta(\delta^{18}O_{cell}) = [(17.57T_{max})/(39.89 + 0.44T_{max}) - (17.57T_{min})/(39.89 + 0.44T_{min}) + A(P_{winter} - P_{summer})] * 0.66$ 25

Equation 6. $\Delta(\delta^{18}O_{cell}) = [(17.57T_{max})/(39.89 + 0.44T_{max}) - 0.6109] * 0.66$ 28

Equation 7. $\delta^{18}O_{cell\ (avg)} = -0.00891*MAT^2 + 0.4026*MAT + 26.14$ 30

Equation 8. $MAT = (T_{max} + T_{min}) / 2$ 31

ABBREVIATIONS

^{14}C kyr BP	Radiocarbon Date Thousand Years Before Present
$\delta^{13}C$	Carbon Stable Isotope Composition
$\delta^{18}O_{cell}$	Oxygen Stable Isotope Composition of Tree Ring Cellulose
$\delta^{18}O_{cell(Con\ \&\ Ang)}$	Combined North American and Puerto Rican Conifer and Angiosperm $\delta^{18}O_{cell}$ Values from Richter et al. (2008b)
$\delta^{18}O_{cell(max)}$	Maximum Intra-ring $\delta^{18}O_{cell}$ Value
$\delta^{18}O_{cell(min)}$	Minimum Intra-ring $\delta^{18}O_{cell}$ Value
$\delta^{18}O_{cell(MAT)}$	MAT Reconstructed from Intra-ring $\delta^{18}O_{cell}$ Values
$\delta^{18}O_{cell(Tmax)}$	T_{max} Reconstructed from Intra-ring $\Delta\delta^{18}O_{cell}$ Values
$\delta^{18}O_{cell(Tmin)}$	T_{min} Reconstructed from Intra-ring $\delta^{18}O_{cell}$ Values
$\delta^{18}O_{ice}$	Oxygen Stable Isotope Composition of Ice
$\delta^{18}O_{MW}$	Oxygen Stable Isotope Composition of Meteoric Water
$\delta^{18}O_{PO4(MAT)}$	MAT Reconstructed from Phosphate Oxygen Isotope Values
$\Delta(\delta^{18}O_{cell})$	Intra-annual Change in $\delta^{18}O_{cell}$
$\Delta(\delta^{18}O_{MW})$	Intra-annual Change in $\delta^{18}O_{MW}$
$\Delta(T)$	Mean Change in Temperature
A	Positive Constant = 0.0082‰/mm
ACELL	Alfa Aesar Microcrystalline Cellulose
ARL	Above River Level
CO_{2atm}	Atmospheric CO_2
D	Dansgaard-Oeschger Events
GPP	Gross Primary Production
H	Heinrich Events

JCELL 1	Cellulose Extracted from Eocene Age Fossil Wood Sample Collected from Axel Heiberg Island Fossil Forest: Jahren Lab
JCELL 2	Cellulose Extracted from Eocene Age Fossil Wood Sample Collected from Axel Heiberg Island Fossil Forest: Jahren Lab
IAEA	International Atomic Energy Association
ka	Calibrated Radiocarbon Date (10^3 years)
kyr BP	Thousand Years Before Present
MAT	Mean Annual Temperature
MART	Mean Annual Range in Temperature
MCR	Mutual Climate Range
MIS	Marine Isotope Stage
NPP	Net Primary Production
NGIRP	Northern Greenland Ice Core Project
NOAA	National Oceanic and Atmospheric Administration
R_{eco}	Ecosystem Respiration
SMOW	Standard Mean Ocean Water
T_{max}	Average Warm Month Temperature
T_{min}	Average Cold Month Temperature
T_{month}	Mean Monthly Temperature

1. INTRODUCTION

Historical data suggest that the Arctic is the most sensitive region on the planet to changes in climate (Turner et al., 2007) with mean annual temperature (MAT) rising at two to four times the rate of global temperatures since the beginning of the 20th century (ACIA, 2004; Knutson et al., 2006; Walsh, 2014; Winton, 2006). Since the middle Pliocene, changes in Arctic summer temperature have been 3-4 times larger than those for the rest of the planet (Miller et al., 2010b), and have increased by as much as 8-16 °C across 30 years at some sites (Van Meerbeeck et al., 2011, Lang et al., 1999). The amplified rate of change in Arctic air temperature relative to lower latitudes (Chae et al., 2014; Graversen and Wang, 2009; Overland et al., 2013; Serreze et al., 2009) is largely the result of seasonally related positive feedback mechanisms that exist in Arctic marine and terrestrial ecosystems, and is of significant consequence to global scale climate change (review Miller et al., 2010a; Miller et al., 2010b).

Fossil wood uncovered from permafrost sediments in northeastern Siberia is abundant (Anderson and Lozhkin, 2001; Andreev et al., 2001, 2002a and 2002b; Schirrmeister et al., 2002; Wetterich et al., 2008; Wetterich et al., 2014) and potentially contains valuable information for understanding late Pleistocene climate at annual and seasonal resolution. Such sediments are the regional deposits of silt-dominated permafrost, termed “Yedoma.” The Yedoma is considered a key stratigraphic deposit of the terrestrial Arctic for late Pleistocene environments, and is known to preserve wood fragments and other abundant organic remains of an ancient ecosystem (Kaplina, 1986; Murton et al., 2015; Strauss, 2010; Strauss et al., 2012; Tomirdiaro and Chryornen’kiy, 1987; Wetterich et al., 2011; Vasil’chuk, 1992; Vasil’chuk et al., 2001; Zanina et al., 2011). Located along the banks of the lower

Kolyma River, the Duvanny Yar site is one of the best known and well-studied exposures of Yedoma sediments in northeastern Siberia (Baranova, 1957; Biske, 1957; Guthrie et al., 2006; Hopkins, 1982; Kaplina, 1986; Kaplina et al., 1978; Murton et al., 2015; Sher, 1971, Sher et al., 1979, 1995, 1997; Spencer et al., 2015; Strauss, 2010; Strauss et al., 2012; Tomirdiaro and Chryornen'kiy, 1987; Vasil'chuk, 1992; Vasil'chuk et al., 2001; Vonk et al., 2013; Wetterich et al., 2011; and others within Zanina et al., 2011), and is considered a stratigraphic model for late Quaternary environmental change in northeastern Siberia (Hopkins, 1982; Kaplina et al., 1978; Sher et al., 1975, 1995, and 1997).

Stable isotope data from polar ice cores indicate that the climate was generally colder than today, yet highly unstable in the northern hemisphere, with several abrupt shifts in climate (Dansgaard et al., 1993; NGIRP Project Members, 2004). Previous work suggests that millennial-scale variability in summer temperatures occurred in northeastern Siberia during the Marine Isotope Stage (MIS) 3 and was accompanied by arid conditions (Andreev et al., 2011; Lozhkin and Anderson et al., 2011; Wetterich et al., 2014). Information on seasonality from palaeoecological studies are mixed, however, because pollen data commonly provide only qualitative information (warmer/colder, wetter/drier) in regard to summer climate. Thus, the data are subject to interpretation. However, coupled with stable isotope compositions of ancient ground ice (Meyer, 2001; Strauss, 2010; Streletskaya et al., 2015; Vasil'chuk, 1992), some of the prior literature infers that the climate was more continental than today (i.e. that it featured higher summer temperatures and lower winter temperatures, relative to today) due to an enhanced polar ice sheet with reduced sea levels (Alfimov et al., 2003; Andreev et al., 2001; Andreev et al., 2002a and 2002b; Kienast et al., 2005; Schirrmeister et al., 2002; Sher et al., 2005). Uncertainties regarding the true seasonal climate likely fall within the apparent

temporal and spatial variations characteristic of Siberia during the late Pleistocene (Lozhkin and Anderson et al., 2011), and problems with the qualitative reconstructions have been reviewed by Lozhkin and Anderson (2011), Muller et al., (2010), and Sher et al., (2005). They point out that the presence of certain bioindicators may reflect local environmental controls such as local moisture availability, soil type, and wind conditions, rather than strictly regional temperature (Murton et al., 2015; Sher et al., 2005).

In an effort to quantify past changes in temperature in the critical Arctic region, previous work has measured and analyzed oxygen stable isotope compositions of ancient tree ring cellulose ($\delta^{18}O_{cell}$) (Csank et al., 2013; Jahren and Sternberg et al., 2008; Richter et al., 2008a; Wolf et al., 2012). Multiple empirical studies have shown $\delta^{18}O_{cell}$ principally reflects the $\delta^{18}O$ value of meteoric water ($\delta^{18}O_{MW}$) taken up by plants throughout the growing season (Anderson et al., 2002; Ballantyne et al., 2006; Csank et al., 2013; McCarroll and Loader, 2004; Richter et al., 2008b; Roden et al., 2009; Saurer et al., 1997; Schubert and Jahren, 2015; Sternberg et al., 2007; Waterhouse et al., 2002; McCarroll and Loader, 2004; Saurer et al., 2008; Schubert and Jahren, 2015; Sternberg et al., ., 2007). Cellulose is the wood substrate that contains the most reliable record of $\delta^{18}O_{mw}$ and temperature because it is resistant to degradation and can remain unaltered for millions of years (Hook et al., 2015; Richter et al., 2008a). A strong empirical relationship between the $\delta^{18}O_{MW}$ value and temperature has been observed in modern settings at annual (Dansgaard et al., 1964) and monthly resolution (Bowen, 2008; Schubert and Jahren, 2015), allowing researchers to reconstruct temperature from measurements of $\delta^{18}O_{cell}$. However, the majority of oxygen stable isotope work in modern and ancient polar regions has focused on mean annual climate conditions that fail to capture the seasonal range in temperature, which is often of more

importance to polar ecosystems than MAT. Aside from mutual climate range (MCR) analysis on fossil insects, which happens to show a weaker empirical relationship to winter temperatures (Alfimov et al., 2003; Elias, 1997), previous paleotemperature proxies provide evidence of strictly warm or cold season temperatures alone (Astakhov, 2014; Meyer, 2001; Miller et al., 2010a), thus lacking the ability to provide information on environmental variability at a year-to-year resolution, or the degree of seasonality (e.g., mean annual range in temperature). Though mummified wood preserved in permafrost sediments is abundant, stable isotope research on climate dependent organic substrates is lacking for northeastern Siberia and the late Pleistocene. During this time, the seasonal climate conditions were sufficient for expansion of extensive permafrost and development of a massive carbon stock that remains stored in terrestrial Arctic permafrost today (Strauss et al., 2012 and 2013; Tarnocai et al., 2009; Zimov et al., 2006). The Arctic permafrost, which has acted as a major carbon sink since as early as the Pliocene, is particularly sensitive to changes in seasonal temperatures: modern warming threatens a transition in Artic ecosystem balance from net positive uptake to net positive respiration of carbon (i.e. greenhouse gas sink to source), a decrease in the Arctic terrestrial and marine surface albedo with increased solar heat absorption, and increase in sea levels and disturbance of the ocean thermohaline from increases in river runoff from melted ancient ground ice.

I will provide information on the year-to-year variability and magnitude of seasonal change in temperature within an Arctic environment using high-resolution intra-annual $\delta^{18}O_{cell}$ values measured across consecutive growth rings from two mummified ancient wood samples, collected from the late Pleistocene sediments of the Yedoma Silt Ice Complex at Duvanny Yar. High-resolution stable isotope analyses across annual growth rings have been

used to identify intra-annual (seasonal) patterns in the measured carbon and oxygen isotopic composition of wood tissues (Jahren and Sternberg, 2008). Models have been developed from modern records for relating intra-annual changes in oxygen isotopic composition of modern cellulose to seasonal changes in climate (Schubert and Jahren, 2015). Relative changes in $\delta^{18}O_{cell}$ values across the growing season in the high-resolution $\delta^{18}O_{cell}$ profiles presented in this study allow for absolute late Pleistocene seasonal temperatures to be quantified and modeled across the year. The results provide new information on how the climate has changed in this environment since the late Pleistocene, when global temperature and atmospheric CO_2 (CO_{2atm}) levels were ~200 ppm lower than they are today (Petit et al., 1999).

2. MATERIALS AND METHODS

2.1 Study Site

Fossil wood samples were collected from permafrost sediments of the Yedoma Silt Ice Complex at Duvanny Yar (68.63 °N, 159.15 °E). Duvanny Yar is located ~40 km upstream from the Northeast Science Station in Cherskiy, Sakha Republic, Russia (68.74 °N, 161.40 °E) (Fig. 1) and extends for 10 to 12 km along the right bank of the Kolyma River (facing downstream). Duvanny Yar represents the type-site for the Yedoma silt, a frozen ice-rich silt that spans 2,324,500 km^2 (Grosse et al., 2013) and is exposed within a ~50 m high outcrop at the site (see Section 2.2). The fossil wood samples for this study were collected from the lower 26 m of the section from radiocarbon in the sediment dated to ~42 to 50 ^{14}C BP (Murton et al., 2015), or calibrated ~45 to 54 ka. All radiocarbon ages (^{14}C) here were converted to median calendar ages (ka) using the radiocarbon calibration program CalPal (Danzeglocke et al., 2009). All ^{14}C ages beyond the known calibration limit (50,000 ^{14}C BP or 54,426 ka) are reported here as >54 ka. These ages are consistent with ages of 45.0 ± 3.1 to 48.6 ± 2.9 ka determined for these sediments using optically stimulated luminescence (OSL) (Murton et al., 2015). The upper portion of the section is significantly younger, with radiocarbon ages ranging from ~20 to 34 ka, which are consistent with an OSL date of 21.2 ± 1.0 ka determined for the top of the Pleistocene permafrost (Murton et al., 2015). A more detailed description of the age control can be found in Section 2.3.

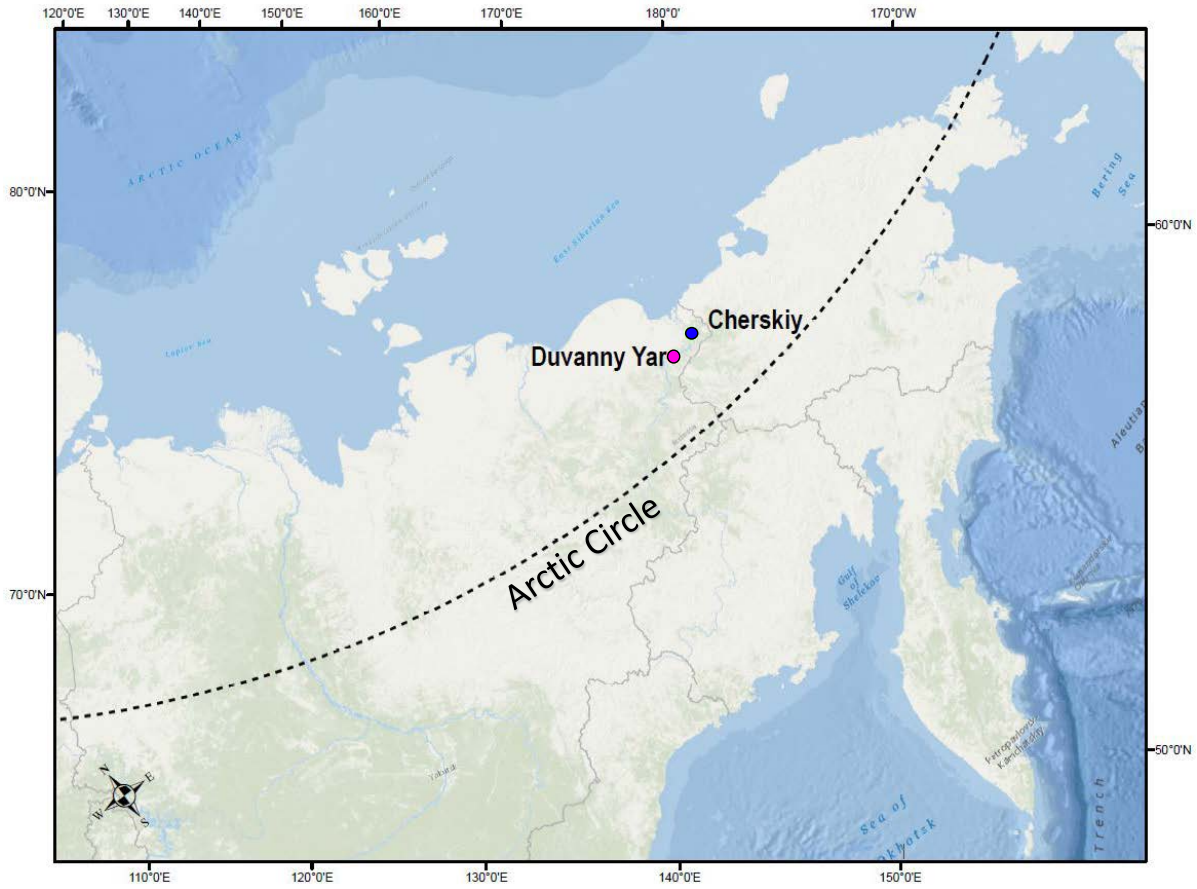

Figure. 1. Location of Duvanny Yar (68.63 °N, 159.15 °E) (pink circle) near Cherskiy, Sakha Republic, Russia (68.74 °N, 161.40 °E) (blue circle) north of the Arctic Circle (66.55 °N) (dashed line).

The present-day Kolyma River valley is a tundra environment with a continental, Arctic climate (Murton et al., 2015). Open *Larix gmelinii* (Dahurian Larch) forest and shrub vegetation cover much of the region (Anderson and Lozhkin, 2001; Zanina et al., 2011). Between 1980 and 2012, the mean annual temperature (MAT) and mean annual precipitation (MAP) at Cherskiy was -10.8 °C and 221.3 mm, respectively (National Oceanic and Atmospheric Administration (NOAA), National Climatic Data Center, http://www.ncdc.noaa.gov). On average, the warmest and coldest months are July and January with average temperatures of 12.9 °C and -32.4 °C, respectively. Mean monthly temperature (T_{month}) at Cherskiy, in general, was normally distributed across each year from

1980-2012 (Fig. 2). The growing season, defined as period with average temperatures > 0 °C, starts in early-mid May and continues until late September. The majority of precipitation falls from June through October. Snowfall begins in late September and reaches its maximum depth in late April (Murton et al., 2015; Strauss, 2010). Strauss (2010) reported similar climate conditions and growing season lengths in the instrumental climate record from nearby Kolymskaya village (68.73 °N, 158.73 °E), located about 20 km northwest of Duvanny Yar.

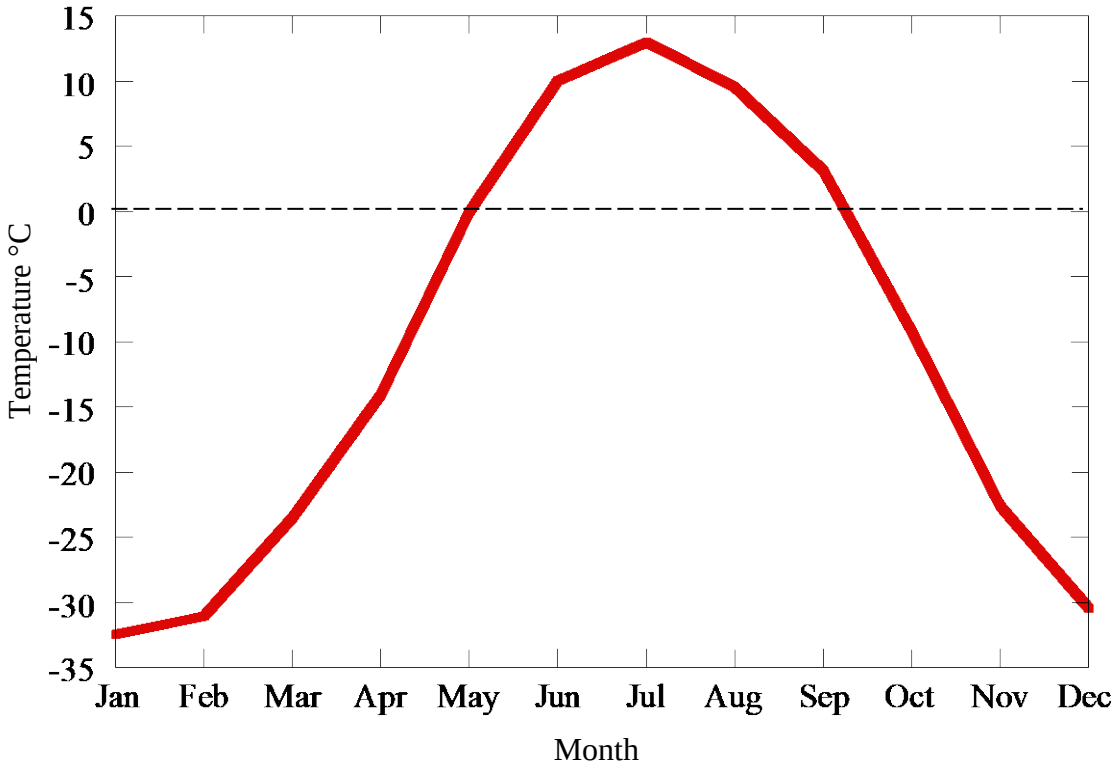

Figure 2. Average monthly temperature across the years (1980-2012) at Cherskiy, Sakha Republic, Russia (National Oceanic and Atmospheric Administration (NOAA), National Climatic Data Center, http://www.ncdc.noaa.gov). The growing season, defined as number of months with T_{month} > 0 °C (dashed line), is only ~4 months long.

2.2 The Yedoma "Suite" at Duvanny Yar

The permafrost underlies 2,324,500 km^2 of lowlands in central and northeastern Siberia (Grosse et al., 2013), and is composed of a distinctive stratigraphic unit of gray-brown silt

and silty sands (Strauss, 2010; Zanina et al., 2011) that was frozen syngenetic with ground ice upon deposition (Grosse et al., 2013; Hopkins et al., 1982, Schirrmeister et al., 2011: Schirrmeister et al., 2013; Vaskovsky, 1963; Zimov et al., 2006). This permafrost unit is termed “Yedoma” or “Yedoma Suite” (Sher, 1997). Stratigraphic interpretations (Kaplina et al., 1978; Sher et al., 1979) and radiocarbon dating (Murton et al., 2015; Strauss, 2010; Vasil’chuk et al., 2001; Zanina et al., 2011) indicate Yedoma formed during the middle to late Weichselian Glaciation (Wisconsinan equivalent) of the Late Pleistocene. At Duvanny Yar, thermokarst mounds, resulting from thaw slumping and significant river erosion (Vasil’chuk et al., 2001) reveal the most complete and thickest Yedoma exposure in northern Siberia (Kaplina et al., 1978), with the exception of the Laptiv Sea region to the west (Sher et al., 2005). Since the 1950s, the exposure has been a well-studied reference site for terrestrial Arctic history during the late Pleistocene (Baranova, 1957; Biske, 1957; Guthrie et al., 2006; Hopkins, 1982; Kaplina, 1986; Kaplina et al., 1978; Murton et al., 2015; Sher, 1971, Sher et al., 1979, 1995, and 1997; Spencer et al., 2015; Strauss, 2010; Strauss et al., 2012; Tomirdiaro and Chyornen’kiy, 1987; Vasil’chuk, 1992; Vasil’chuk et al., 2001; Vonk et al., 2013; Wetterich et al., 2011; and others within Zanina et al., 2011).

Wood fragments were observed in greater abundance in the lower section just above river level (ARL) relative to the upper sections of the exposure, in concordance with recent literature (Fig. 3) (Murton et al., 2015; Strauss, 2010; Strauss et al., 2012; Wetterich et al., 2011a). This study finds the collection point to be most analogous to the “DY-05-B” and possibly the “DY-05-C” section recorded during the joint Russian-German Beringia/Kolyma 2008 expedition reported by Wetterich et al. (2011), Strauss (2010), and Strauss et al. (2012); and the lower sediments of the ~38 m “CY” section recorded in 2009 and reported by Murton

et al (2015). Both sections profile the lower ≤ 7m ARL at the time of study. In agreement with 2014 field observations, both sections were rich in woody roots and wood fragments (**Ø** 2-4 mm, max. 20 mm; Wetterich et al., 2011) in DY-05-B between 2-6 m ARL, and 4 m ARL in CY. The sediments are primarily coarse silt (mean grain size in DY-05-B = 16-32 μm), but range from fine silt to silty sand (Strauss, 2010).

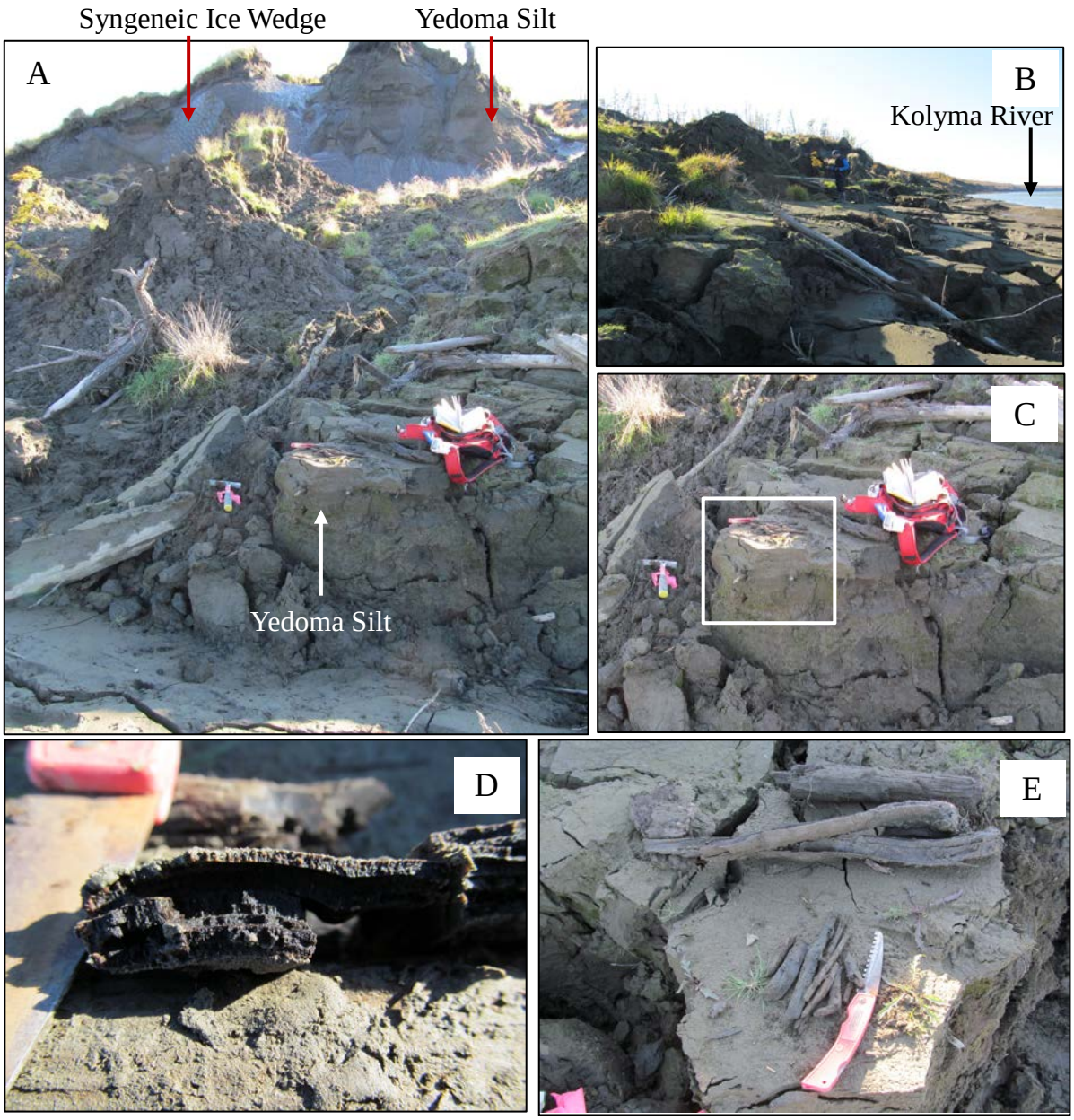

Figure 3. Duvanny Yar field photos taken on 9/10/2014 showing the fossil wood sample collection site (A) with Yedoma silt in place from top to bottom of the exposure, segregated by syngeneic ice wedges along the banks of the Kolyma River (B). (C) Close look showing fossil wood preserved in-situ of lower Yedoma permafrost sediments with fossil wood samples collected lying on top (white box) and viewed in detail in images (D) and (E).

Multiple hypotheses have been proposed for the origin and depositional history of the

Yedoma silt. The most recent paleoenvironment interpretations at Duvanny Yar suggest that

Yedoma is a loess deposit formed primarily from the aeolian (wind-driven) accumulation of

sediments (Murton et al., 2015). Others have favored a polygenetic accumulation with more equal sediment contribution from aeolian, alluvial (water-driven), lacustrine, and in-situ frost weathering process to account for several lacustrine, allochthonous peat layers bounded by Yedoma (Sher, 1997; Strauss, 2010; Zanina et al., 2011). However, scientists are in agreement that deposition occurred in a sub-aerial, non-glaciated steppe-tundra region within a highly continental and harsh permafrost climate characterized as having high summer temperatures and very low winter temperatures when sea levels were much lower than today, as a result of increased polar ice (Schirrmeister et al., 2013; Wetterich et al., 2011).

Yedoma sediments are rich in ground ice with an absolute ice content of 30-40 wt% in the upper ~9-40 m, and ~50-65 wt% in the lower 7 m of the Duvanny Yar sections (Strauss et al., 2012). Large ice wedges penetrate and divide Duvanny Yar and reach up to 6-8 m wide and up to 30-40 km high (Fig. 2) (Sher, 1977; Zanina et al., 2011). The large ice wedges are the most recognizable ice structures of Yedoma deposits and formed syngeneticaly with soil accumulation (Black, 1974; Vasil'chuk, 1992). The presence of such large ice wedges is a direct indication of a prior stable permafrost climate lasting on a multi-millennial scale (Washburn, 1981; Vasil'chuk et al., 2001). Homogenous sediment and grain size distribution through the entire Yedoma section further indicates a continuous and stable depositional environment (Murton et al., 2015; Strauss, 2010; Strauss et al., 2012). The frozen sediments preserve an excellent archive of the terrestrial late-Pleistocene paleoenvironment. Preserved organic remains include rodent burrows and plant, insect, and vertebrate fossils, including mammoth bones (Kaplina et al., 1978; Murton et al., 2015; Sher et al., 1979; Strauss, 2010, Vasil'chuk et al., 2001; Wetterich et al., 20l1a).

2.3 Sample Age Control

Radiocarbon analyses of organic material within the host silt suggest that deposition at Duvanny Yar occurred from ~ >50 to 13-16 ^{14}C BP (Murton et al., 2015; Willerslev et al., 2014; Zanina et al., 2011), and perhaps as recently as 9890 ^{14}C BP (Strauss, 2010). Previous ^{14}C analysis of organic material within the host silt and ice wedges have led to conflicting ages through Yedoma, particularly in the lower ~26 m (Gubin, 1999; Kaplina, 1986; Tomirdiaro and Chryornen'kiy, 1987; Vasil'chuk, 1992; Vasil'chuk et al., 2001; Zanina et al., 2011). Age discrepancies have been attributed to time differences between sampling. Also, a considerable amount of allochthonous material can be admixed in Yedoma from cryoturbation, thawing, and redeposition of organic material (Vasil'chuk et al., 2001; Wetterich et al., 2014), and possible contamination by material that has slumped from higher sections (Murton et al., 2015).

Murton et al. (2015) conducted the most recent and intensive ^{14}C analysis on mostly in-situ roots in the CY section. The section can be subdivided into 4 age ranges starting with the near-surface silt section in the top 1.5 m with modern ages between 830 and 70 ^{14}C BP. Underlying the near-surface silt, 31-37 m ARL dated between ~25,000 and 16,850 ^{14}C BP and 30-26.5 m ARL dated between ~31,700 and 34,100 ^{14}C BP. A long-term Yedoma depositional hiatus followed between ~34,000 and 42,000 ^{14}C BP that is marked by a paleaosol disconformity at ~42,000 ^{14}C BP. The lower < 26.5m ARL dated between ~42,000-44,000 and >48,700 ± 3500 ^{14}C BP.

The analysis revealed stratigraphic order in ^{14}C dates > 10m ARL, with some scatter in the lowest 10m ARL (>49,000 to >45,000 ^{14}C BP, 31,600 ± 500 to 33,500 ± 2000 ^{14}C BP) (Murton et al., 2015). Based on dates from Murton et al. (2015) for the CY section, I attribute

ages younger than 44,000 ^{14}C BP in the lower 10m ARL to reworked material slumped from higher in the outcrop, as ages between ~12 m and ~23 m ARL were consistently between ~44,000 ^{14}C BP and >49,000 ^{14}C BP. The lower 23 m have ages that are close to the maximum for ^{14}C dating, and dating errors are greatest closest to the detection limit. However, OSL dated quartz grains obtained by Murton et al. (2015) of 45.0 ± 3.1 ka at 14.5 m ARL and 48.6 ± 2.9 ka at 3.5 m ARL near the larger wood fragments reported at 4 m ARL helps to confirm the lower section ^{14}C dates. This is consistent with the >46,690 ^{14}C BP date obtained by Strauss (2010) from plant remains in DY-05-B, interpreted to be a paleocyrosol sequence (Strauss, 2010) at 2.7 ARL. A date of ~40,080 ^{14}C at 10 m ARL in DY-05-C (Strauss, 2010), however, is inconstant with the CY section.

The fossil wood collected for this study is interpreted here as being from the early part of the terrestrial Karginsky interstadial (55,000–25,000 cal BP e.g., Murton et al., 2015, Willerslev et al., 2014) or Marine Isotope Stage 3 (MIS 3 60–27 kyr). More specifically, the time frame in which the fossil wood grew is likely between 45,000 and 50,000 ^{14}C BP or ~47 to 54 ka, and certainly not younger than 42,000 ^{14}C BP or ~45 ka (after Danzeglocke et al., 2017). The collected fossil wood falls within the lower 12m of the section, which Murton et al. (2015) assigned calibrated dates of 45,700 up to 50,000 ± 4000 ka BP based upon the author's own age height model. Several relatively older studies obtained radiocarbon dates of >53,370 to 42,600 ± 1200 ^{14}C BP directly from fossil wood at Duvanny Yar between 6-19 m reported above sea level (ASL) (Table 1) (review Vasil'chuk et al., 2001 and Strauss, 2010).

Table 1. Published radiocarbon dates on fossil wood at Duvanny Yar (compiled by Vasil'chuk et al., 2001). Original sources are in Russian. Radiocarbon ages beyond the calibration limit are reported as >54,000 yrs BP.

^{14}C Date (yrs BP)	Calendar Date (yrs BP)	ASL (m)	Source
>53,370	>54,000	8	Kaplina (1986)
>45,000	>48,246	6	
>50,000	>54,000	14	Tomirdiaro and Chyornen'kiy, 1987
>53,370	>54,000	14	
42,600 ± 1200	46,319	19	Vasil'chuk (1992)
45,200 ± 1100	48,566	9	

* After Danzeglocke et al., 2009

The fossil wood samples collected from Duvanny Yar could be in age up to 57 ka based upon the uncertainties in the absolute lowest ARL radiocarbon dates (Murton et al., 2015) and assuming the differences between ^{14}C and corrected (ka) ages are similar beyond the ^{14}C calibration limit at 50,000 ^{14}C BP. The standard deviation of the lowest OSL date 48.6 ± 2.9 ka is evidence to the contrary, however. Dates from OSL are superior to radiocarbon dates in aeolian-dominated environments (Lee et al., 2009), such as those at Duvanny Yar during the late Pleistocene, and their dates more reflect the timing of deposition (Murton et al., 2015). Potential contamination of older carbon can occur in permafrost (Vasil'chuk et al., 2001). Murton et al. (2015) could not rule out the possibility of Yedoma silt being deposited well before 50 ka with a further possibility of modern carbon contamination turning infinite dates into false finite dates. Likewise, I accept the possibility that the fossil wood samples collected at Duvanny Yar could be substantially older than 50 ka and may predate the Yedoma suite. In concordance with prior studies, no underlying disconformable peat and stratified silt layers attributed to the mid-Pleistocene were observed (Giterman et al., 1982; Kaplina; 1978; Sher et al., 1979), but these are exposed upstream from the final Yedoma hill (Giterman et al.,

1982; Kaplina; 1978; Murton et al., 2015; Sher et al., 1979).

2.4 Sample Processing

Two fossil wood samples were selected from those collected at Duvanny Yar for high-resolution oxygen isotope analysis based upon ring width, ring geometry, sample quality, and cellulose yields from preliminary test results. Ring widths (1.1–2.5 mm) were measured with a Fisher Scientific Digital Caliper. Four consecutive rings from each sample representing two sets of four consecutive growth years were subsampled by hand into 8-12 slices (50-400 µm) using a razor blade. Each subsample weighed 1-3 mg (mean = 1.63 mg); preliminary data showed this to be the minimum amount of whole wood needed to obtain sufficient amounts of cellulose for $\delta^{18}O$ analysis.

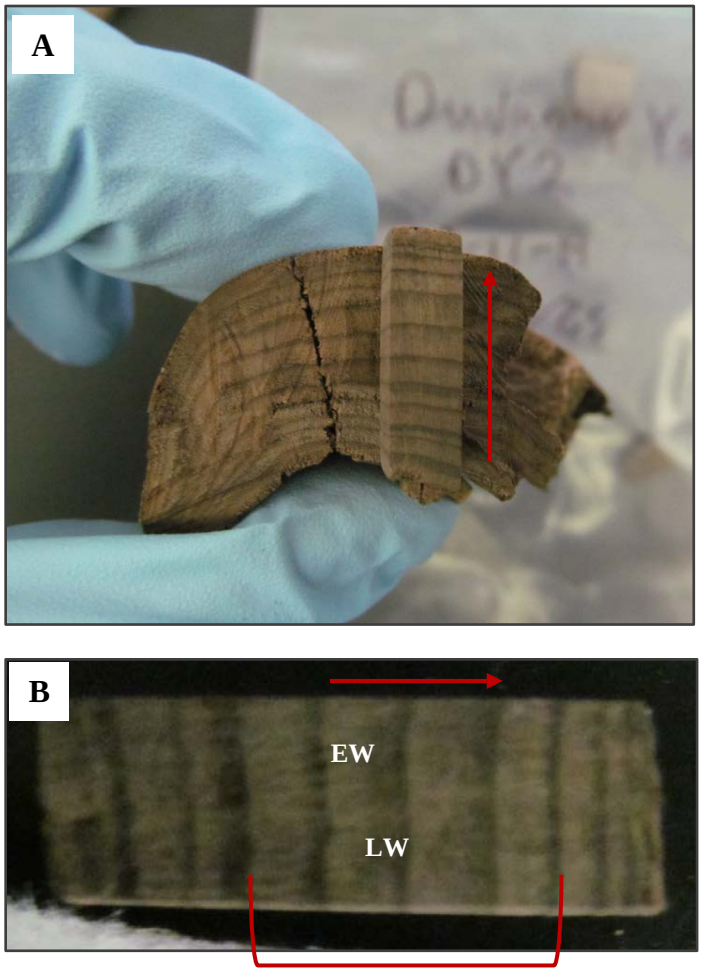

Figure 4. Example of non-permineralized fossil wood collected from the lower Yedoma permafrost sediments at Duvanny Yar. (B) Close look at four consecutive fossil tree rings sampled within block (A). Light-colored wood represents earlywood (EW) and darker wood represents latewood (LW). Red arrows indicate the direction of tree ring growth.

Cellulose was isolated from a total of 81 subsamples of fossil wood using a method modified from Brendel and Stewart (2000). The subsamples were placed into 1500 µl polypropylene micro centrifuge tubes and a 10:1 ratio of 80% acidic acid to 70% nitric acid was added to the samples. The subsamples were then agitated using a standard vortex mixer (Fisher Scientific), centrifuged for a minimum of 5 min at 12,000 rpm, and heated in an aluminum block at 120 °C for 30 min before being allowed to cool to room temperature. The liquid was decanted and the subsamples were rinsed twice with 1000 µl of 99% ethanol and once with

1000 µl of deionized water. Next, 300 µl of a 17% sodium hydroxide (NaOH) solution was added, and after 10 minutes, the subsamples were rinsed with 1000 µl of deionized water. A solution containing 36 µl acidic acid and 260 µl deionized water was then added, followed by a final rinse with 300 µl of 99% ethanol and 300 µl of acetone in successive steps. The subsamples were then dried overnight in a drying oven (Thermo Scientific Precision) set to ~50 °C resulting in 126-438 µm (avg = 275 µm) of pure α-cellulose.

2.5 Oxygen Isotope Analysis

Pure cellulose, weighing ~ 50 to ~100 µg, was weighed (in duplicate) into silver capsules for oxygen isotope analysis. $\delta^{18}O_{cell}$ values were determined using a Delta V Advantage Isotope Ratio Mass Spectrometer (IMRS) joined with a high temperature conversion elemental analyzer (TC/EA) (Thermo Fisher, Bremen, Germany) configured with a zero-blank autosampler (Costech Analytical, Valencia, CA) at the University of Louisiana at Lafayette. The resulting tree-ring cellulose isotope values were expressed in delta notation ($\delta^{18}O_{cell}$) in units per mille (‰) with respected to reference Standard Mean Ocean Water (SMOW) (‰):

$$\delta_{sample} = (R_{sample} / R_{standard} - 1)1000 \qquad \text{Equation 1}$$

where R_{sample} and $R_{standard}$ are the molar ratios of $^{18}O/^{16}O$ in the tree-ring cellulose sample and reference standards, respectively. Two internal laboratory reference materials referenced to SMOW were used (ACELL, cellulose, $\delta^{18}O_{cell} = 32.33 \pm 0.06$ ‰; JCELL 1, cellulose, $\delta^{18}O_{cell} = 17.64 \pm 0.09$ ‰). The standards were characterized by measuring against the following internationally distributed reference materials supplied by the International Atomic Energy Agency (IAEA): IAEA 601 and IAEA 602. One quality control sample (JCELL 2, cellulose, $\delta^{18}O_{cell} = 20.44 \pm 0.1$‰) was analyzed within each batch of extracted pure cellulose. Over the

course of the analysis, the JCELL 2 quality control sample averaged 20.58 ± 0.22‰ (± 2σ) (n=29), which is in agreement with the calibrated reference value.

3. RESULTS

3.1 Resulting Intra-ring $\delta^{18}O$ Measurements

Samples Duvanny Yar 2 (DY2) and Duvanny Yar 4 (DY4) were selected for high-resolution oxygen isotope analysis based upon their greatest cellulose yields in preliminary low-resolution $\delta^{18}O_{cell}$ extractions (Table 2). Figure 5 displays the resulting high-resolution intra-ring profiles of four consecutive growth years from DY2 and DY4.

Table 2. Preliminary cellulose extraction test results.

Sample ID	Average Cellulose Yield (%)	Average $\delta^{18}O_{meas}$ (‰)	n
DY1	9.0	17.91 ± 0.00	2
DY2	19.9	18.15 ± 0.70	3
DY3	12.4	16.92 ± 0.09	3
DY4	16.4	17.8 ± 0.37	3

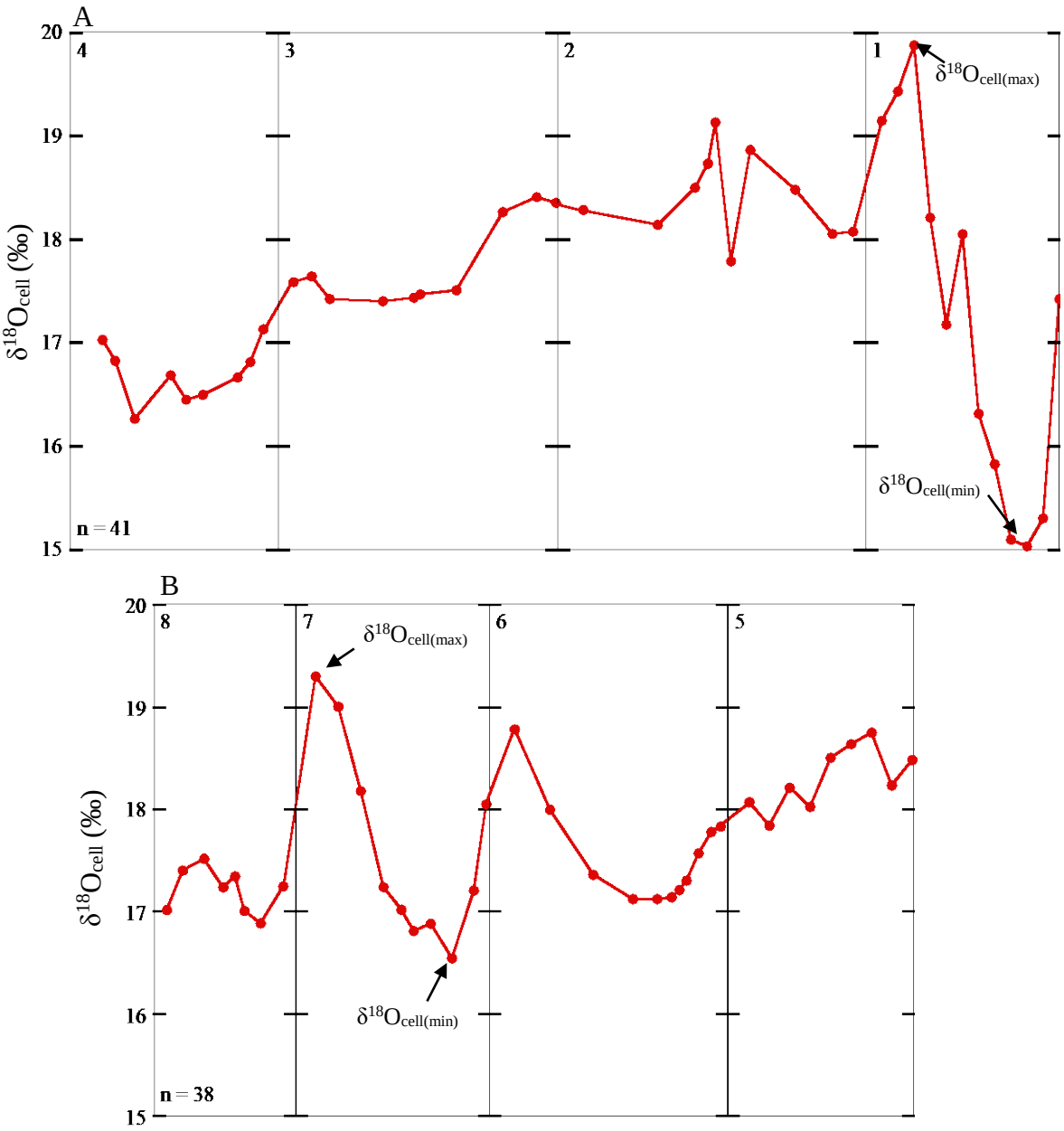

Figure 5. Intra-ring $\delta^{18}O_{cell}$ data for DY2 (A) and DY4 (B) showing a range of values ~15.0 to 19.9‰. Excluding DY2 R1, the range of values is ~16.3 to 19.3‰. Initial value following ring boundaries (vertical axis) denote the first earlywood measurement. Rings numbered in the top left corners. $\Delta(\delta^{18}O_{cell})$ defined as the change between $\delta^{18}O_{cell(max)}$ and $\delta^{18}O_{cell(min)}$ (Eqn. 4) in DY2 and DY4 were on average 2.0 and 1.5‰ respectively. Mean $\delta^{18}O_{cell}$ values did not differ significantly between DY2 and DY4, with mean $\delta^{18}O_{cell}$ being 17.6 ± 0.7‰ and 17.7 ± 0.5‰, respectively (Table S2 in Appendix A).

Similar mean $\delta^{18}O_{cell}$ values suggest similar water sources and mean annual temperature. Using an equation developed by Csank et al. (2013) representing the relationship between $\delta^{18}O_{cell}$ and $\delta^{18}O_{MW}$, single averaged $\delta^{18}O_{cell}$ of all eight fossil rings yields $\delta^{18}O_{MW}$ -25.5 ± 0.9‰ (Table S3 and S4 in Appendix B). Using three equations representing the relationship between $\delta^{18}O_{cell}$ and $\delta^{18}O_{MW}$ from Sternberg et al. (2007) (e.g., Schubert and Jahren, 2015), the singled averaged $\delta^{18}O_{cell}$ of all 8 fossil rings yields $\delta^{18}O_{MW}$ -22.7 ± 2.1‰, or a total range -19.1 to -25.7 ‰, across all three equations (Table S3 and S4 in Appendix B). Average fossil $\delta^{18}O_{MW}$ values calculated using equations from both Csank et al. (2013) and Sternberg et al. (2007) align more with modern $\delta^{18}O_{MW}$ in polar regions than those in non-polar regions (Bowen, 2013; Bowen and Revenaugh, 2003; Bowen and Wilkinson, 2002). Fossil $\delta^{18}O_{MW}$ calculated from Supplementary Equation 6 (Appendix B) fall near the modern $\delta^{18}O_{MW}$ values in the Lower Kolyma region ~ -20.4‰ generated by the Online Isotopes in Precipitation Calculator (OIPC v 2.2) (Bowen, 2013). Average fossil $\delta^{18}O_{MW}$ values calculated using equations from both Csank et al. (2013) and Sternberg et al. (2007) (Supplementary Equation. 3-6 in Appendix B) align more with modern $\delta^{18}O_{MW}$ in polar regions than those in non-polar regions (Bowen, 2013; Bowen and Revenaugh, 2003; Bowen and Wilkinson, 2002). Yet, fossil $\delta^{18}O_{MW}$ is still depleted relative to the modern region, already an indication of a colder climate during the late Pleistocene.

The results displayed in Figure 5 show increases and decreases in $\delta^{18}O_{cell}$ values through each growth year with intra-annual change ($\Delta(\delta^{18}O_{cell})$) (Eqn. 4) from all 8 rings, ranging from 0.63 to 4.8‰ with an average of 1.75‰. The intra-ring profiles show various $\delta^{18}O_{cell}$ patterns, but the minimum $\delta^{18}O_{cell}$ value ($\delta^{18}O_{cell(min)}$) occurred closer to the ring boundary

than the middle of the ring in the majority of the rings sampled. Similar $\delta^{18}O_{cell}$ patterns across consecutive rings have been observed in high-resolution $\delta^{18}O_{cell}$ values in modern conifers from colder climate sites in Alaska and Norway (Dodd et al., 2008; Jahren and Sternberg, 2008; Schubert and Jahren, 2015), and a single analogous site above the Arctic Circle (latitude > 66.5 °N) in Harstad, Norway (Schubert and Jahren, 2015).

4. DISCUSSION

4.1 Quantifying T_{max}

Models have been developed relating the seasonal changes in the stable oxygen isotope composition of modern wood cellulose to seasonal changes in climate. Schubert and Jahren (2015) compiled intra-annual $\delta^{18}O_{cell}$ profiles from modern angiosperm and conifer tree rings (n = 792) at 33 globally distributed sites, and monthly $\delta^{18}O_{MW}$ data at each site provided by the International Atomic Energy Agency (IAEA) Global Network of Isotopes in Precipitation (GNIP) database (IAEA/WMO, 2006), and found a global scale empirical relationship between the intra-annual change (seasonal) in the oxygen isotope composition of cellulose [$\Delta(\delta^{18}O_{cell})$] and intra-annual (seasonal) change in the oxygen isotope composition of meteoric water $\delta^{18}O_{MW}$ [$\Delta(\delta^{18}O_{MW})$]:

$$\Delta(\delta^{18}O_{MW}) = \Delta(\delta^{18}O_{cell}) / 0.66 \qquad R^2 = 0.74 \qquad \text{Equation 2}$$

where $\Delta(\delta^{18}O_{MW})$ was the difference between the maximum ($\delta^{18}O_{MW(max)}$) and minimum ($\delta^{18}O_{MW(min)}$) monthly $\delta^{18}O_{MW}$ values,

$$\Delta(\delta^{18}O_{MW}) = \delta^{18}O_{MW(max)} - \delta^{18}O_{MW(min)} \qquad \text{Equation 3}$$

and where $\Delta(\delta^{18}O_{cell})$ was the difference between the maximum ($\delta^{18}O_{cell(max)}$) and minimum ($\delta^{18}O_{cell(min)}$) intra-ring $\delta^{18}O_{cell}$ values measured within each individual ring (Fig. 4):

$$\Delta(\delta^{18}O_{cell}) = \delta^{18}O_{cell(max)} - \delta^{18}O_{cell(min)} \qquad \text{Equation 4}$$

Multiple empirical relationships have been developed between various environmental parameters (e.g., temperature and precipitation) and the oxygen isotopic composition of meteoric water (Bowen, 2008; Dansgaard, 1964; Fricke and O'Neil, 1999; Rozanski et al.,

1992; Sternberg et al., 2009). Plants use meteoric water taken up through their roots to build plant tissue (i.e. cellulose) during photosynthesis (Keel et al., 2016; McCarroll and Loader, 2004; Roden et al., 2000). The significant relationship between $\delta^{18}O_{MW}$ and temperature (Dansgaard, 1964) and $\delta^{18}O_{MW}$ and precipitation (Schubert and Jahren, 2015) is therefore recorded in tree ring cellulose.

With $\delta^{18}O_{MW}$ and $\delta^{18}O_{cell}$ providing an excellent climate record, Schubert and Jahren (2015) used monthly resolved temperature, precipitation, and $\delta^{18}O_{MW}$ values from global IAEA GNIP sites (n = 365) spanning 158º of latitude, and developed a relationship between $\Delta(\delta^{18}O_{MW})$ and seasonal changes in temperature and precipitation. Combined with the relationship expressed in Equation 3, Schubert and Jahren (2015) produced an empirical global relationship relating $\Delta(\delta^{18}O_{cell})$ to seasonal changes in temperature and precipitation expressed in the following equation:

$$\Delta(\delta^{18}O_{cell}) = [(17.57T_{max})/(39.89 + 0.44T_{max}) - (17.57T_{min})/(39.89 + 0.44T_{min}) + A(P_{winter} - P_{summer})] * 0.66 \quad \text{Equation 5}$$

where T_{max} and T_{min} are the average warm month temperature and the average cold month temperature (°C), respectively, and P_{winter} and P_{summer} are the average 6-month winter (November through April) and summer (May through October) precipitation periods, respectively, as defined by Schubert and Jahren (2015). The term "A" is a positive constant that scales the effect of P_{winter} and P_{summer} on $\Delta(\delta^{18}O_{cell})$ and was determined to be a depletion rate of 0.82‰ per 100 mm change in $P_{winter} - P_{summer}$ (Schubert and Jahren, 2015).

The focus on relative changes in $\delta^{18}O_{cell}$ and temperature values as opposed to absolute values avoids issues of different $\delta^{18}O_{cell}$ values among species growing in similar environments (Schubert and Jahren, 2015) that result from varying amounts of evaporative enrichment in leaves during transpiration and biochemical fractionation during cellulose synthesis (Gessler et al., 2013; McCarroll and Loader, 2004; Roden et al., 2000; Saurer et al, 1997).

4.1.1 Assumption of late Pleistocene seasonal precipitation for calculating T_{max}.

Temperature is the primary control on the oxygen isotopic composition of meteoric water and therefore, cellulose (Csank et al., 2013; Roden et al., 2000). However, intense precipitation during the summer months can cause significant depletion in the heavier ^{18}O isotope relative to the lighter ^{16}O isotope of $\delta^{18}O_{MW}$ and $\delta^{18}O_{cell}$; this process is known as the "amount affect" (Bonel et al., 2000; Bowen, 2008; Dansgaard, 1964, Li et al., 2011; Miller et al., 2006; Poussart et al., 2004; Roden et al., 2009; Xu et al., 2015). The effect of summer rainfall and total precipitation (mm) on $\delta^{18}O_{cell}$ is accounted for by the term P_{winter} - P_{summer} within Equation 5. Schubert and Jahren (2011) developed an equation for quantifying P_{winter}/P_{summer} using intra-annual measurements of the carbon stable isotope composition ($\delta^{13}C$) of evergreen bulk wood tissue. However, the method is not applicable to deciduous wood, for which the intra-annual change in $\delta^{13}C$ value across growth rings reflects a switchover from the use of stored carbon to the use of actively photosynthesized carbon rather than seasonal changes in climate (Helle and Schleser, 2004).

Murton et al. (2015) reports relatively high amounts of evergreen *Pinus* (haploxylon) and deciduous *Betula* spp. (tree-birch) and *Alnus* (alder) pollen in the lower 26 m of Yedoma at Duvanny Yar. Evidence of deciduous *Larix* is not abundant in Yedoma because Larix pollen

is poorly preserved and distributed (Murton et al., 2015; Lozhkin and Anderson, 2011). The possible persistence of *Larix* in the lower Kolyma region during the late Pleistocene is not ruled out as Zanina et al. (2011) reported the presence of *Larix* seed macrofossils within fossil borrows at Duvanny Yar. Plant macrofossils suggest forest-scale populations of *Larix* and *Betula* from 48 to 34 ka BP in the Yana, Indigirka, and Kolyma lowlands (Anderson and Lozhkin, 2001).

Schubert and Jahren (2011) and Schubert et al. (2012) showed that average P_{winter} and P_{summer} could be quantified from evergreen species, if MAP was known. However, a quantitative estimate of MAP for northeastern Siberia during the late Pleistocene is not available. Previous studies suggested general aridity in Siberia with a prevailing consensus that the Siberian late Pleistocene climate was continuously as arid to slightly more arid than present throughout the early- to mid-MIS 3 interstadial (Anderson and Lozhkin, 2001; Astakhov, 2014; Kienast et al., 2005; Lozhkin and Anderson, 2011; Murton et al., 2015; Schirrmeister et al., 2002; Sher et al., 2005; Wetterich et al., 2008; Wetterich et al., 2014). With this, we can calculate T_{max} without the need for prior estimates of MAP and $\Delta(\delta^{13}C)$ measurements by reasonably assuming that seasonal precipitation in the Kolyma River valley has not significantly changed since the late Pleistocene; and the P_{winter} - P_{summer} term in Equation 5 can be set to the average difference between winter and summer precipitation measured at Cherskiy from 1980 to 2012 [Avg (P_{winter} - P_{summer}) = -74.5 mm] (National Oceanic and Atmospheric Administration (NOAA), National Climatic Data Center, http://www.ncdc.noaa.gov). Given that MAP has been suggested to be equal or slightly less than the low levels present today, the effect of P_{winter} - P_{summer} is likely not significant. Sensitivity analysis on the effect of possible differences between winter and summer

precipitation in the Arctic on reconstructed seasonal temperature is presented in section 4.5.

4.1.2 Assumption of Cold Month Temperature (T_{min}) for Calculating T_{max}. Tree ring cellulose does not record the true $\delta^{18}O_{MW(min)}$ as trees do not use significant meteoric water from the soil outside of the growing season. Therefore, measured $\delta^{18}O_{cell(min)}$ reflects the minimum temperature during the growing season rather than the yearly coldest month temperature. The coldest month at Cherskiy is usually January, but it can also occur in December or February (National Oceanic and Atmospheric Administration (NOAA), National Climatic Data Center, http://www.ncdc.noaa.gov). Averaging the coldest month mean temperature from each year between 1980 and 2012 yields an average of modern T_{min} = -34.7 ± 2.7 °C. I define the growing season as months with average temperatures > 0 °C, and set the final unknown term (T_{min}) to equal zero (after Schubert and Jahren, 2015). With the assumptions regarding seasonal precipitation and average temperature of the cold month, the average warm month temperature for northeastern Siberia during the late Pleistocene can be quantified from the intra-annual change in oxygen isotope composition of tree-ring cellulose by modifying Equation 5 to solve for T_{max} using the following equation:

$$\Delta(\delta^{18}O_{cell}) = [\ (17.57T_{max})/(39.89 + 0.44T_{max})\ - 0.6109\ ] * 0.66 \qquad \text{Equation 6}$$

4.2 Quantify Mean Annual Temperature

A strong empirical relationship between $\delta^{18}O_{MW}$ and mean annual temperature has been observed in modern settings (Bowen, 2008; Dansgaard, 1964; Fricke and O'Neil, 1999; Rozanski et al., 1992; Schubert and Jahren, 2015). Studies have also shown that modern $\delta^{18}O_{MW}$ has an empirical relationship with modern $\delta^{18}O_{cell}$ (Anderson et al., 2002; Ballantyne et al., 2006; Csank et al., 2013; Richter et al., 2008b; Saurer et al., 1997; Schubert and

Jahren, 2015; Sternberg et al., 2007; Waterhouse et al., 2002), allowing researchers to reconstruct mean annual temperature from $\delta^{18}O_{MW}$ reconstructions via measurements of $\delta^{18}O_{cell}$ (Ballantyne et al., 2006; Csank et al., 2013). However, in an effort to limit some uncertainty in implementing the relationship between $\delta^{18}O_{cell}$ and $\delta^{18}O_{MW}$ to derive MAT, I selected an approach to calculate MAT directly from $\delta^{18}O_{cell}$ measurements.

Richter et al. (2008b) found that $\delta^{18}O_{cell}$ values extracted from modern tree bulk wood can reflect modern MAT on a continental scale. Richter et al. (2008b) extracted α-cellulose from cut and grounded bulk wood sampled from angiosperm and conifer woody species (Total n=20) collected from 35 North American and Caribbean sites. Monthly temperature recorded by the Meteorological Service of Canada and the National Oceanic and Atmospheric Administration was obtained from weather stations nearest to each site. The authors developed separate continental scale hyperbolic models relating angiosperm $\delta^{18}O_{cell}$ measurements (n = 123) with MAT ($R = 0.91$, $p < 0.001$), and conifer $\delta^{18}O_{cell}$ measurements (n=109) with MAT ($R = 0.95$, $p < 0.001$) for a region that included sites stretching from Puerto Rico to northern Alaska. Conifers species were separated from the angiosperms, as conifers were more often enriched in $\delta^{18}O_{cell}$ relative to angiosperms (Richter et al., 2008b). Each equation can be applied to the appropriate fossil wood species if identified (Richter et al., 2008a). Because the small wood fragments collected from Duvanny Yar were not conducive to identifying the species, I combined both Richter et al. (2008b) conifer and angiosperm models to create a single model relating total conifer and angiosperm $\delta^{18}O_{cell}$ [$\delta^{18}O_{cell\ (Con\ \&\ Ang)}$] with MAT (Fig. 4).

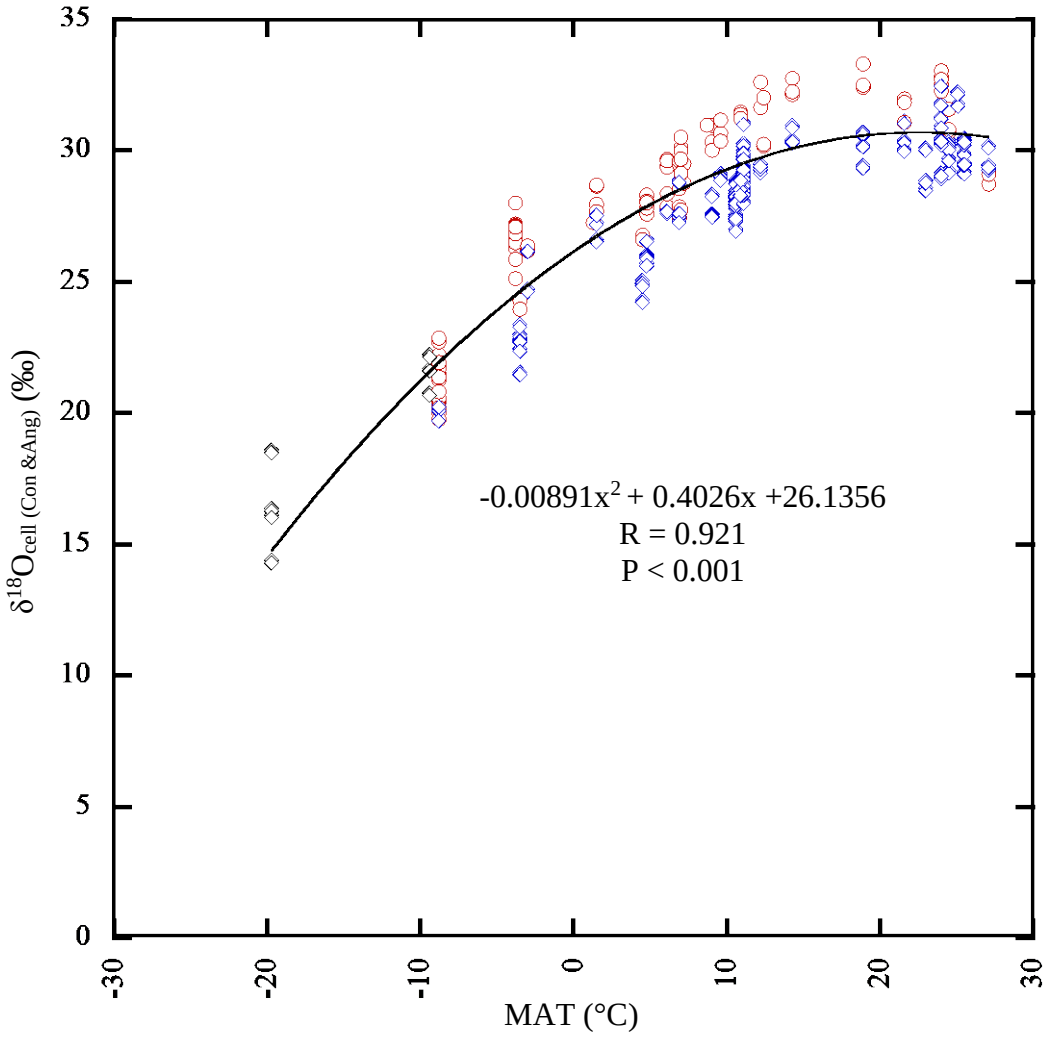

Figure 6. Correlation between combined North American and Puerto Rican conifer (red circles) and angiosperm (blue diamonds) $\delta^{18}O_{cell}$ and mean annual temperature including arctic willows (black diamonds). Developed from Richter et al. (2008b) supplementary data found at https://doi.org/10.1016/j.gca.2008.01.030.

In order to extend the relationship to high-latitude sites, unlike Richter et al. (2008b), I chose to include data on Arctic willows, *Salix arctica* (n = 3) and "another *Salix* species" (n = 3) (Richter et al., 2008b), growing north of the North American tree line at 79.55 ˚N, -89.03 ˚E and 63.05 ˚N, -69.71 ˚E, respectively. The combined hyperbolic model yielded the following equation (R = 0.92) (Fig 4):

$$\delta^{18}O_{cell\ (avg)} = -0.00891*MAT^2 + 0.4026*MAT + 26.14 \qquad \text{Equation 7}$$

where $\delta^{18}O_{cell\ (avg)}$ is the average of $\delta^{18}O_{cell}$ values measured within each individual Duvanny Yar ring. Richter et al. (2008b) elected to not include arctic willows in their quadratic relationships, reasoning that the arctic willows are structurally different than the other samples in the study and were not growing in forested sites. However, Figure 4 shows that the Arctic Willow data fits well with the general quadratic trend represented by the trees growing at relatively warmer sites.

4.3 Quantifying T_{min} from MAT and T_{max}

New et al. (2002) interpolated monthly temperatures from 1961 and 1990 using 12,783 climate stations across the globe, excluding Antarctica. Schubert and Jahren (2015) used this dataset to show that the average of T_{max} and T_{min} given by:

$$MAT = (T_{max} + T_{min}) / 2 \qquad \text{Equation 8}$$

correlates well with MAT calculated as the average of all 12 months of the year ($R^2 = 0.997$).

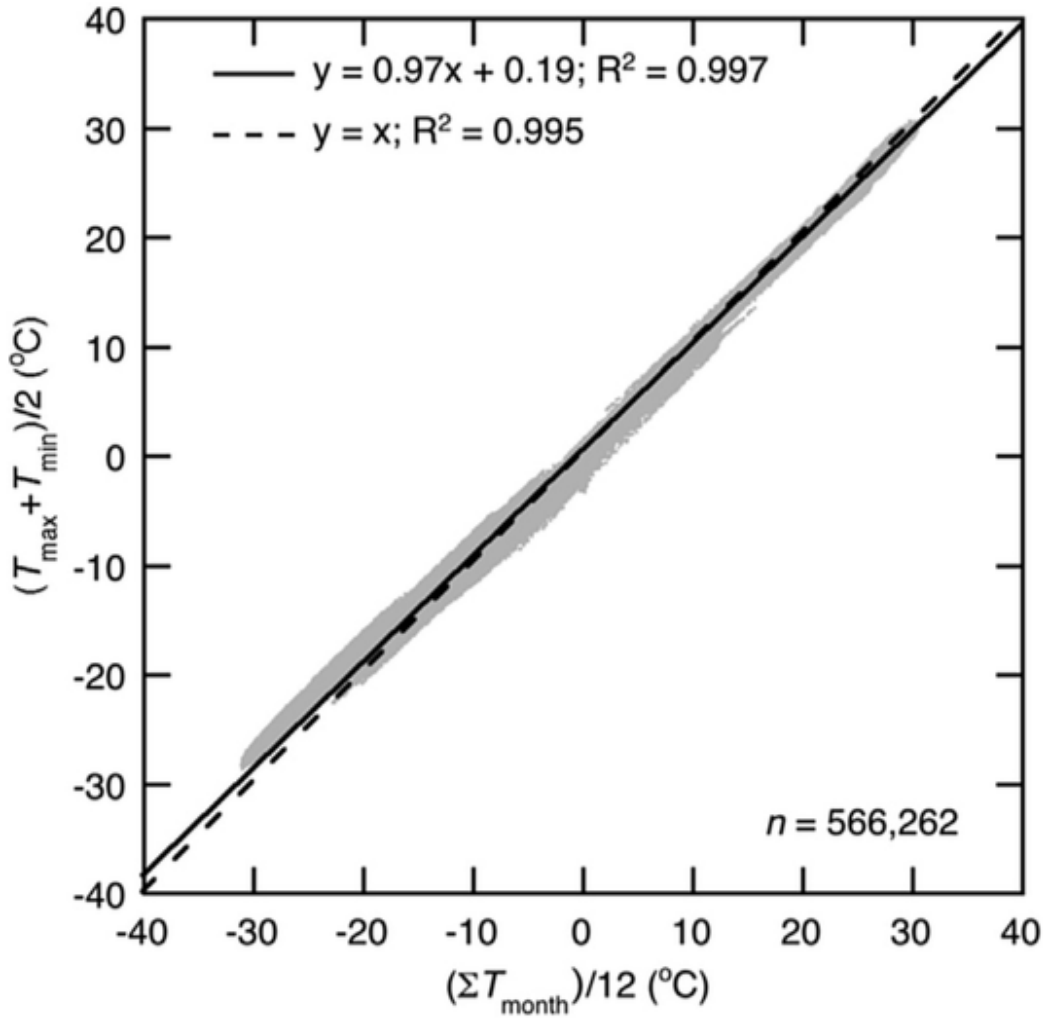

Figure 7. "Correlation between MAT determined by averaging monthly temperature data for all 12 months and MAT calculated as the average temperature determined only using data for the warmest (T_{max}) and coldest (T_{min}) months [Eqn. (8)]. Monthly temperature data used to calculate MAT were from a global dataset determined for all land areas, except Antarctica, at 10' spatial resolution (New et al., 2002)," from Schubert and Jahren (2015).

A simple rearrangement of Equation 7 allows for an approximation of T_{min} from T_{max} and MAT calculated from Equations 6 and 7, respectively. Following the process outlined in Table 3, the high-resolution $\delta^{18}O_{cell}$ data (Fig. 5) allows for the variability and magnitude of seasonal changes in late Pleistocene temperature to be compared with modern climate.

Table 3. Step by step summary of equations used to calculate seasonal temperatures from high-resolution oxygen isotope values across consecutive rings.

No.	Equation	Determine	Reference
4	$\Delta(\delta^{18}O_{cell}) = \delta^{18}O_{cell(max)} - \delta^{18}O_{cell(min)}$	$\Delta(\delta^{18}O_{cell})$	Schubert and Jahren (2015)
6	$\Delta(\delta^{18}O_{cell}) = [\ (17.57T_{max})/(39.89 + 0.44T_{max}) - 0.6109\ ] * 0.66$	T_{max}	Modified Schubert and Jahren (2015)
7	$\delta^{18}O_{cell} = 0.00891*MAT*^{2} + 0.4026*MAT + 26.1356$	MAT	Modified Richter et al., (2008)
8	$MAT = (T_{max} + T_{min}) / 2$	T_{min}	Schubert and Jahren (2015)

4.4 Reconstructed Northeastern Siberian late Pleistocene Seasonal Temperature

High-resolution oxygen isotope values measured from tree-ring cellulose within four consecutive rings in two late Pleistocene fossil wood samples were used to quantify T_{max}, MAT, and T_{min} for each year based on modern relationships (Fig. 8). The following comparison between the late Pleistocene with modern seasonality excludes Ring 1 of DY2, which is shown to be an outlier (open circles) in Figure 8 [T_{max} is 16.1 ± 2.9 °C higher and T_{min} is 17.8 ± 3.2 °C lower relative to the other 7 rings as a result of $\Delta(\delta^{18}O_{cell})$ being 3.5 ± 0.7 °C higher than the other 7 rings (Fig. 5)].

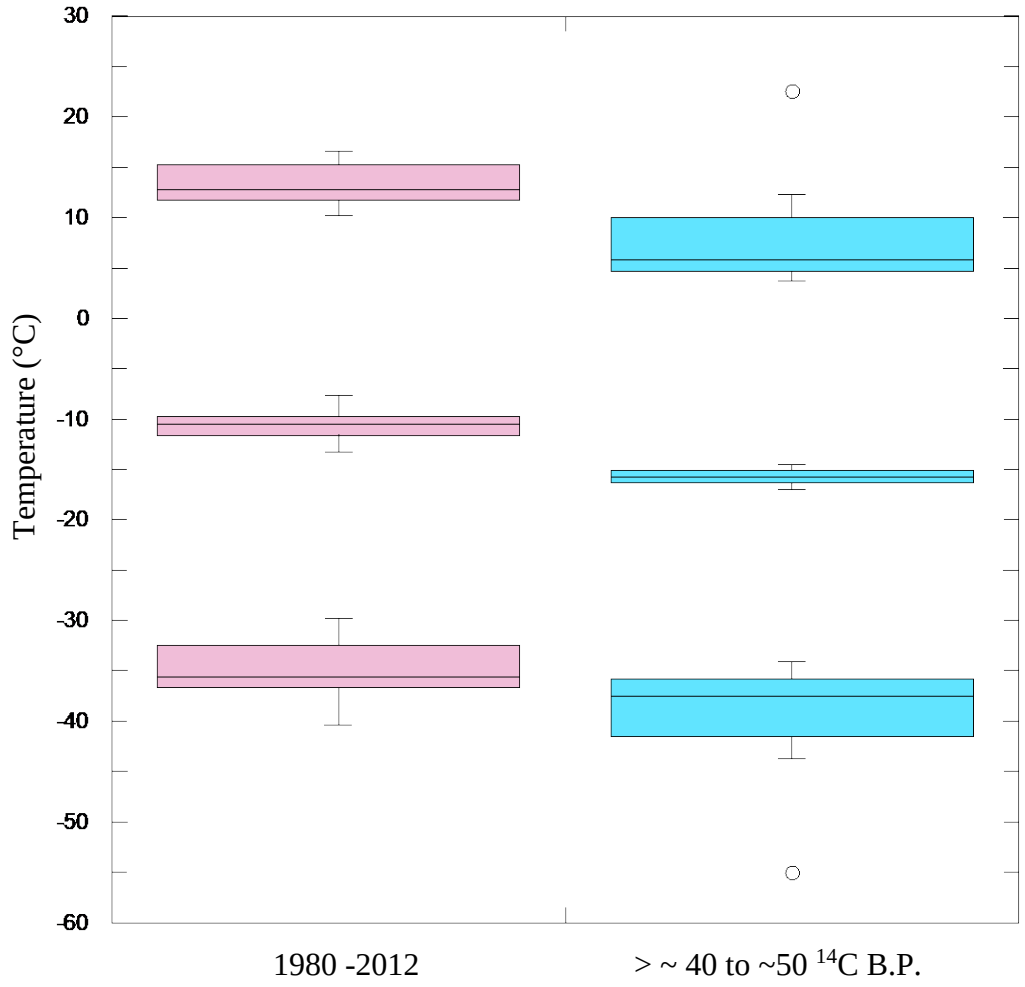

Figure 8. Box and whisker plot showing T_{max} (top row), MAT (middle row), and T_{min} (bottom row) from 1980-2012 at Cherskiy (left column, pink) and for the late Pleistocene (> ~45 to ~50 ^{14}C B.P.) at Duvanny Yar (right column, blue) calculated from Equations 6-8, respectively. DY2 R1 yields an anomalously high range in temperatures (very high T_{max} and very low T_{min}) that is unreasonable compared with the other rings. Modern data are from the National Oceanic and Atmospheric Administration (NOAA), National Climatic Data Center, http://www.ncdc.noaa.gov. Each box represents 50% of the temperature values, and line within each box represents the median value. The upper and lower whisker represent the upper and lower quartile of values outside of the box. Lines which cap each whisker represent the highest and least value excluding any outliers, which are shown as points (open circles).

Modern Cherskiy T_{max} and T_{min} values were selected from the mean monthly temperature of the single coldest and warmest months of each year within the 33-year instrumental record. Throughout much of the late Quaternary literature, coldest and warmest seasonal temperatures derived from various proxies are often referred to as January and July

temperatures (e.g., Alfimov et al., 2003; Csank et al., 2013; Meyer, 2001; Streletskaya et al., 2015; Vasil'chuck,1992). However, implementing modern day Cherskiy actual coldest and warmest month temperatures is better suited when using the Schubert and Jahren (2015) derived $\delta^{18}O_{cell}$ relationships with seasonal climate since the timing of maximum and minimal temperatures during the year in less than apparent in the intra-annual $\delta^{18}O_{cell}$ tree ring profiles of trees growing at high latitude sites (Fig. 5) (Dodd et al., 2008; Jahren and Sternberg, 2008; Schubert and Jahren, 2015). At modern Cherskiy, July and January commonly represented the warmest and coldest months, where the mean July and January temperature represented T_{max} and T_{min} in 25 and 15 of the 33 years on record.

At modern Cherskiy, T_{max}, MAT and T_{min} were on average 13.2 ± 2.1 °C, -10.6 ± 1.3 °C, and -34.7 ± 2.7 °C, respectively (Fig. 8). Implementing Equations 6–8, T_{max}, MAT and T_{min} for MIS 3 at Duvanny Yar averaged 6.4 ± 3 °C, -15.6 ± 0.9 °C and -37.7 ± 2.9 °C, respectively; with T_{max}, MAT, and T_{min} being 6.8 ± 2.1 °C, 5.0 ± 1.3 °C, and 3.0 ± 2.7 °C colder relative to today, respectively (Fig. 8). The difference between late Pleistocene and modern seasonal climate and MAT is significant (T_{max} $p = 0.0005$, T_{min} $p = 0.05$, MAT $p < 0.001$). Mean annual range in temperature (MART), or seasonality, defined as the difference between T_{max} and $T_{min,}$ averaged 47.9 °C today versus 41.9 °C (DY2) and 45.5 °C (DY4). The difference between late Pleistocene and modern MART was less significant ($p = 0.14$).

4.5 Sensitivity Analysis on the Effect Seasonal Precipitation has on Quantifying Seasonal Temperature

As previously discussed in section 4.1.1, the summer precipitation "amount affect" on $\delta^{18}O_{cell}$ is most prominent during the summer rainy season at tropical sites between latitudes 37 ºN and 37 ºS (Brienen et al., 2012; Harada et al., 2014; Schubert and Jahren, 2015;

Sternberg et al., 2007; Verheyden et al., 2004; Xu et al., 2015), but can also be significant at some mid-latitude sites with strong monsoonal climates (Dansgaard, 1964: Johnstone et al., 2013; Li et al., 2011; Nakatsuka et al., 2002). The “amount effect” is minimal in high-latitude arid environments (Dansgaard, 1964; Schubert and Jahren 2015) such as the lower Kolyma River valley, where mean annual precipitation at Cherskiy equaled 221.3 +/- 39.9 mm across 33 years of climate data and the wettest months were June through October (1980-2012) (Fig. 9) (National Oceanic and Atmospheric Administration (NOAA), National Climatic Data Center, http://www.ncdc.noaa.gov). Excluding 1982 as an outlier, when winter precipitation exceeded summer precipitation in a seemingly inverse manor relative to the norm (Fig. 10), average P_{winter} and P_{summer} at Cherskiy was 147.9 mm and 73.4 mm, respectively, and P_{winter} - P_{summer} ranged between -157.9 mm and -14.1 mm.

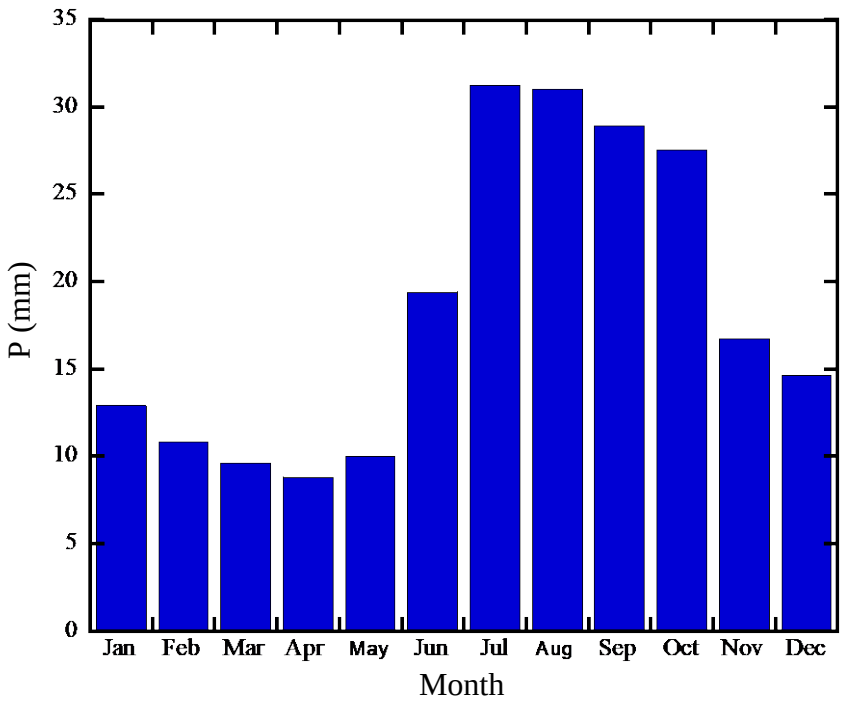

Figure 9. Monthly mean precipitation (P, mm) from 1980–2012 in Cherskiy.

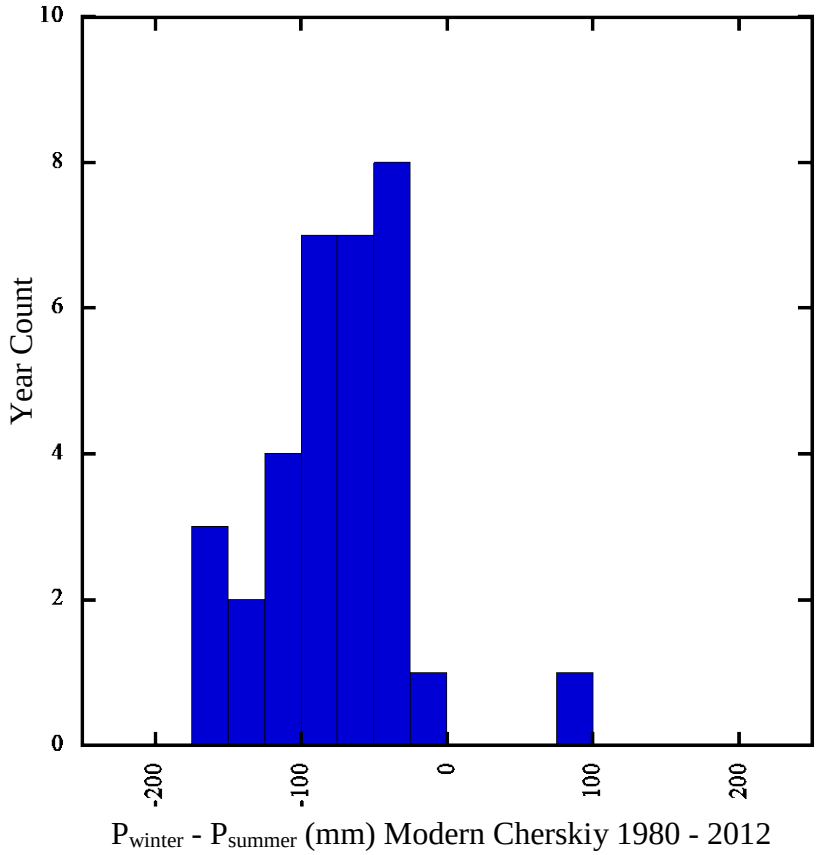

Figure 10. Differences in winter and summer precipitation ($P_{winter} - P_{summer}$) in modern Cherskiy for years 1980 to 2012.

Equation 5 indicates that a 1 mm increase in $P_{winter} - P_{summer}$ would decrease $\Delta(\delta^{18}O_{cell})$ by 0.0082‰ (i.e., A). With $\Delta(\delta^{18}O_{cell})$ known, a sensitivity analysis was performed to determine if changes Siberian Arctic seasonal precipitation significantly affect seasonal temperatures estimated from high-resolution oxygen isotopes measurements from late Pleistocene fossil wood cellulose (Fig. 11).

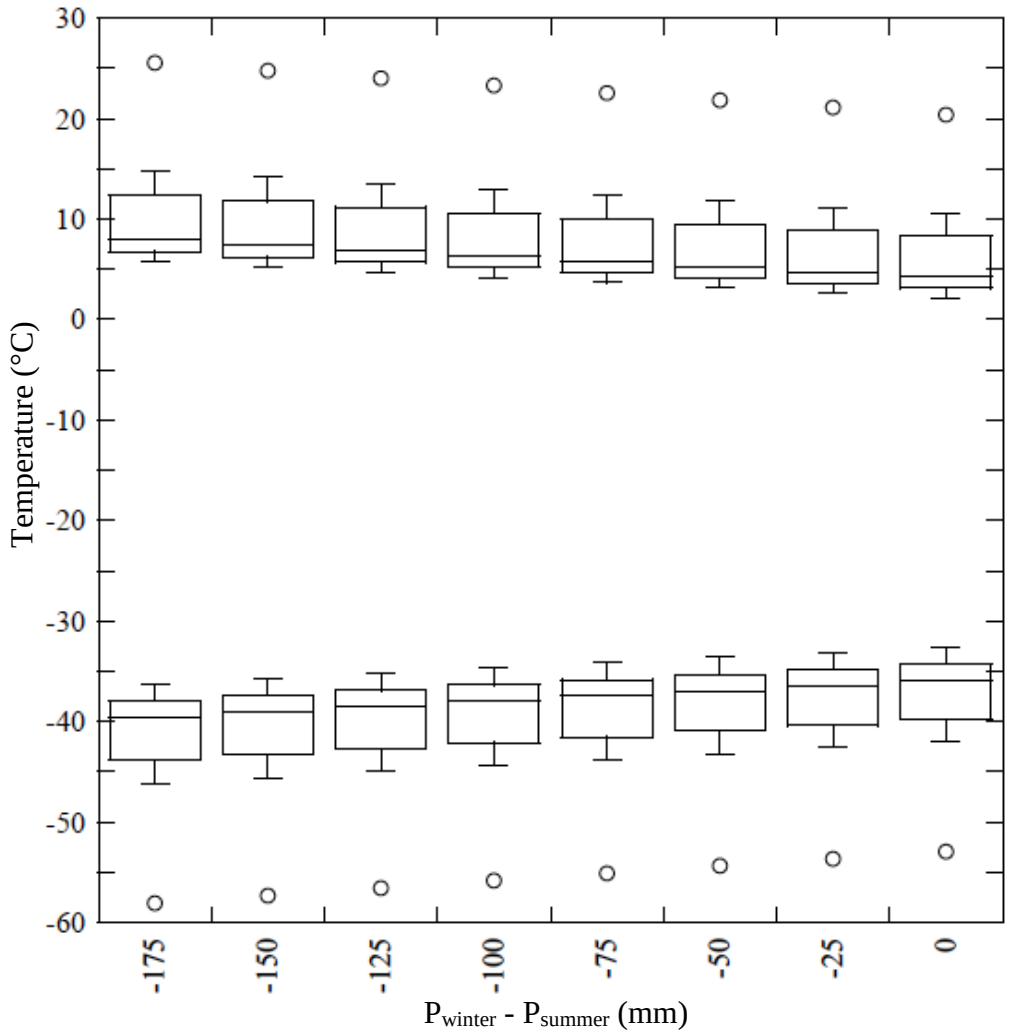

Figure 11. Sensitivity of calculated late Pleistocene T_{max} (top) with possible seasonal change in precipitation ($P_{winter} - P_{summer, mm}$) in northeastern Siberia and the subsequent effect on T_{min} (bottom). Each box is a range in values of all rings excluding DY2 R1 outlier.

Considering the discussion in section 4.1.1, hypothetical values of $P_{winter} - P_{summer}$ (-175 to 0 mm) were selected for Duvanny Yar during the late Pleistocene at 25 mm increments (Fig. 11) based upon modern records at Cherskiy (Fig. 10). Each $P_{winter} - P_{summer}$ value was plugged into Equation 5, deriving modified versions of Equation 6. The resulting analysis revealed a small mean change in temperature [$\Delta(T)$ of 0.54 °C per 25 mm change in $P_{winter} - P_{summer}$ across both samples. The rate of $\Delta(T)$/25 mm varies slightly as $P_{winter} - P_{summer}$ changes, with a mean $\Delta(T)$ = 0.55 °C between $P_{winter} - P_{summer}$ = 175 mm to 0 mm.

Fossil T_{max} ranged from 3.1 to 14.8 °C in Figure 11 when implementing hypothetical values of $P_{winter} - P_{summer}$, compared with the range calculated from Equation 6 of 3.7 to 12.4 °C in Figure 8. Subsequently, fossil T_{min} ranged from -32.6 to -46.2 °C in Figure 11 compared with -35.4 to -43.7 °C in Figure 8. With the modern 33-year range in T_{max} and T_{min} being 16.6 to 10.1 °C and -29.8 to -40.4 °C, respectively (Fig. 8), the general findings in this study are unchanged. The results show that $P_{winter} - P_{summer}$ had a small effect on T_{max}, T_{min}, and seasonality. The northeastern Siberian Arctic was generally colder ~44,000 to 50,000 ^{14}C BP relative to modern day regardless of the $P_{winter} - P_{summer}$ assumed value.

4.6 Global and Hemispheric Context: Polar Ice Core Records

The results of the Duvanny Yar temperatures reconstructed from high-resolution $\delta^{18}O_{cell}$ measurements across fossil tree rings is quantitative evidence of modern terrestrial Artic warming in the Kolyma lowland of ~5 °C across the year relative to the late Pleistocene. The results are in general agreement with the colder environments at the time relative to today as indicated by $\delta^{18}O_{ice}$ (oxygen stable isotope composition of ice) and CO_2 curves from Antarctic ice core record from Vostok (Petit et al., 1999) and Dome C (Luthi et al., 2008), when CO_{2atm} levels and $\delta^{18}O_{ice}$ values were less than today. Changes in Antarctica climate shown in the ice cores were global in scale (Kawamura et al., 2007). The colder Siberian environment in which the fossil wood grew is in further general agreement with the $\delta^{18}O_{ice}$ curves of the European Greenland Ice Core Project (GRIP) (Dansgaard et al., 1993) and the Northern Greenland Ice Core Project (NGIRP) (NGIRP Project Members, 2004) (Fig. 12) records, where $\delta^{18}O_{ice}$ during the late Pleistocene was ~2-7 ‰ less than today, reflecting lower temperatures and lower sea levels during polar ice build.

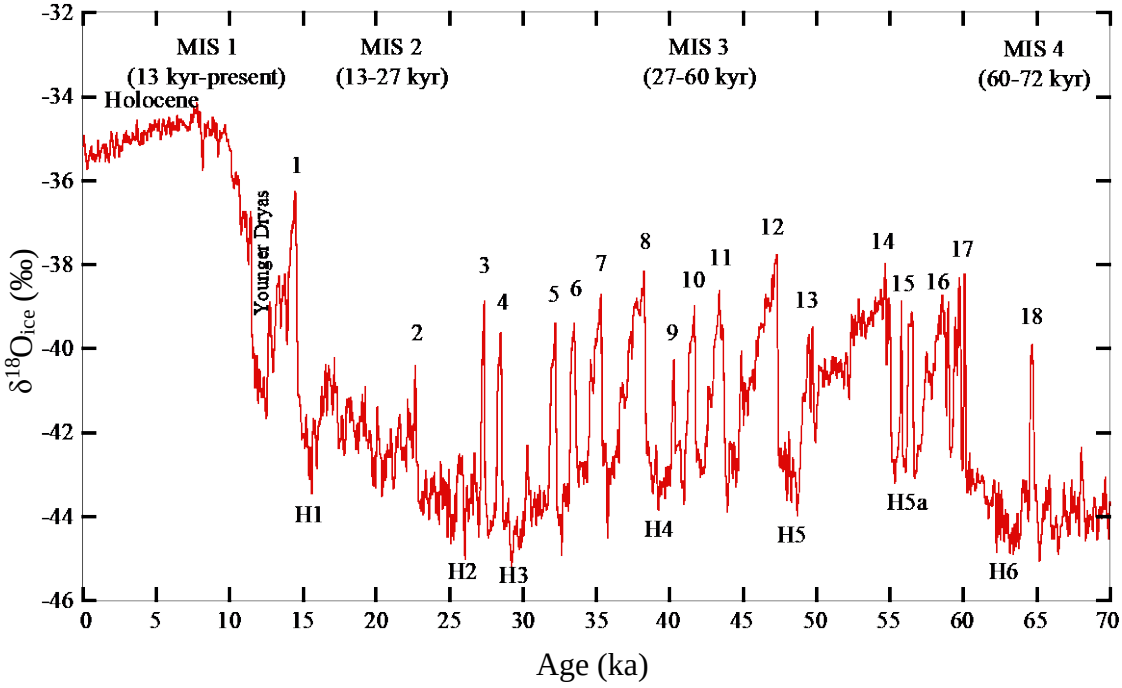

Figure 12. The North Greenland Ice Core Project (NGIRP) $\delta^{18}O_{ice}$ record (Site location: 75.10 °N, 42.32 °W) with numbered Dansgaard-Oeschger warming events (1-18) (after Dansgaard et al., 1993; Svensson et al., 2008) and Heinrich cooling periods (H1-H6) (after Hemming, 2004; Kindler et al., 2014; Svensson et al., 2008). Measured $\delta^{18}O_{ice}$ (duplicate) are mean values with a 50 yr resolution. Data from North Greenland Ice Core Project members, 2004 (ftp://ftp.ncdc.noaa.gov/pub/data/paleo/icecore/greenland/summit/ngrip/isotopes/ngrip-d18o-50yr.txt).

From the polar ice core records, the MIS 3 (Kargin Interstadial) period dates from ~60 to 27 ka (Van Meerbeeck et al., 2011; Svensson et al., 2008), where the $\delta^{18}O_{ice}$ Greenland records show a 33 ka period of high climate variability typical of long term interstadials which define the MIS 3 (Fig. 12) (Capron et al., 2010; Van Meerbeeck et al., 2011; Rasmussen et al., 2014). Climate shifts in the NGRIP record were hemispheric to global in scale (Alley et al., 2007; Rasmussen et al., 2014) and align with the 75 ka $\delta^{18}O_{MW}$ record measured from stalagmites at Hulu Cave (32.5 °N,119.17 °E), ~28 km east of Nanjing, China (Wang et al., 2001). Sudden influxes of massive fresh water supplies into the Atlantic Ocean have been suggested as a triggering mechanism of the MIS 3 unstable climate, with occurrences of

multiple abrupt warmings up to 8-16 °C over a period of a few decades (Huber et al., 2006; Van Meerbeeck et al., 2011) known as Dansgaard-Oeschger events (D) (Fig. 12) (Dansgaard et al., 1993; Melles et al., 2006; Steffensen et al., 2008). Peak temperatures lasted a few centuries and were followed by reorganizations of the north Atlantic thermohaline (Alley et al., 2007; Capron et al., 2010; Dansgaard et al., 1993; Lang et al., 1999; Muller et al., 2010a; Steffensen et al., 2008) accompanied by decadal to millennial scale rapid cooling and polar ice build (Capron et al., 2010; Lowe et al., 2008). Further, several millennial scale periods of enhanced iceberg discharge with minimal hemispheric temperatures occurred known as Heinrich events (H) (Fig. 12) (Heinrich et al., 2008; Van Meerbeeck et al., 2011).

Based upon the hypothetical calibrated ages for DY2 and DY4 (~47 to 54 ka, or up to 57 ka) as discussed in section 2.3, the fossil wood samples likely grew between D (12) and D (15), or before the long-term variable climate between D (3) and D (12) (Fig. 12). The age dating is not sufficiently specific to place these temperature estimates (Fig. 8) within a specific climate event (Figure 12). Though the polar climate was less stable during the MIS 3 than other periods (MIS 1-2, MIS 4), in general, the temperature results determined here fit within the overall MIS 3 climate, when CO_{2atm}, $\delta^{18}O_{ice}$, and sea levels (Lambeck et al., 2002) were never as high as ~10 kyr to present day. To this, the fossil $\delta^{18}O_{cell}$ could have recorded temperatures within northeastern Siberia temperatures during either D (12-15) warm events, H (5-5a) cold periods, or the transitional period between D (14) and H (5).

4.7 Regional Context

Paleoclimate data suggest high summer climate variability during the late Pleistocene, with millennial scale climate patterns resembling the Greenland climate (Andreev et al., 2011; Fig. 8 within Muller et al., 2010) extended to the terrestrial Siberian Arctic during the MIS 3

(Andreev et al., 2002b; Kind et al., 1974; Lozhkin and Anderson, 2011; Muller et al., 2010; Schirrmeister et al., 2002; Tutken et al., 2002 and 2003; Wetterich et al., 2014). There remains disagreement regarding whether the climate was overall warmer, colder, or similar to present day (Table 4) as prior palaeoecological research has uncovered mixed elements of both steppe and Arctic Tundra environments unique to the late Pleistocene northeastern Siberia. Several authors have suggested that lower sea level during the late Pleistocene was the primary environmental factor making the climate of the region more continental than today (Andreev et al., 2002b; Kienast et al., 2005; Schirrmeister et al., 2002; Sher et al., 2005). Increased continentality would suggest lower winter temperatures, but higher summer temperatures and/or longer snow-free periods than today, which contradicts the results in Figure 8. The following subsections within section 4.7 discuss seasonal temperature reconstructions from Figure 8 in relation to prior findings from paleoproxies from a wide range of substrates collected from ancient permafrost sites in eastern and northeastern Siberia (Fig. 13 and Table 4).

Figure 13. Map of eastern Siberia showing site locations with relevant Kargin interstadial climate research on northern Yedoma Ice Complex and interior lake permafrost sediments. Numbers correspond to individual sites, including (1) Duvanny Yar, with their associate research and climate reconstruction listed in Table (4). Arctic Circle: dashed line (66.5 °N).

Table 4. List of eastern and northern Siberia relevant earlier Kargin interstadial and MIS 3 research, corresponding with Figure 13, including those at Duvanny Yar (Site. 1), with their associated paleotemperature reconstructions/interpretations closest to ~45 and >54 ^{14}C kyr BP and their substrate/proxy methods. Dates here reported as infinite in terms of uncalibrated radiocarbon (^{14}C kyr BP) as referenced by the cited authors. Non-radiocarbon derived or calibrated ages referenced by a specific author are presented otherwise here as ka. Note, much of the prior research reported uncalibrated ^{14}C ages in either the kyr BP or ka BP nomenclature, their nomenclature is corrected here as ^{14}C kyr BP *.

Site No.	Site	Region	Location	Substrate/Proxy	Date (^{14}C kyr BP)	Temperature	Source
1	Duvanny Yar	Kolyma Lowland	68.63 °N, 159.15 °E	Wedge Ice Isotopes	Past 40-30 to 13	MWT= -32.5 ºC; Tmin = -47 ºC	Vasil'chuk (1992; In Russian)
				Wedge Ice Isotopes	>46,690 - 16,000	MWT = 4 - 8 ºC colder then today	Strauss (2010)
				Pollen	MIS 3 and MIS 2	No discernible difference	Murton et al., 2015
				Fossil Wood High Res Isotopes	~45 - 50	T_{max}, MAT, T_{min} = 6.4, -15.6, -37.7 ºC	This Study
				Fossil Wood High Res Isotopes	~45 - 50	Tmax, MAT, Tmin was ~6, 5, and 3 ºC lower than today	This Study
2	Molotkovsky Kamen	Kolyma Lowland	68.35 °N, NA	Pollen	*48 - 34	Climate Optimum	e.g., Anderson and Lozhkin, 2001
3	~Molotkovsky Kamen	Kolyma lowland	NA	MCR Insects	*44 - 35	Tmax =12-15.5 ºC	Alfimov et al., 2003 (abstract)
4	El'gygytgyn Lake	Chukotka	67.5 °N, 172.08 °E	Pollen	*46.5 – 25	Cool Summer, nearly glacial	Lozhkin and Anderson, 2011
				Pollen	*54 - 46.5	Transitional	Lozhkin and Anderson, 2011
				Organic Geochem	60-50 ka	Peak MIS 3 warmth	Melles et al., 2007
				Organic Geochem	60-25 ka	Relative warm within past 300ka	Melles et al., 2007
				Diatoms	60-46.4 ka	Relative Warmth	Cherepanova et al., 2007
				Diatoms	60-46.4 ka	Relative Warmth	Cherepanova et al., 2007
				PCR Pollen	MIS 3	Tmax = 2 to 4 ºC, "considerably less than modern"	Lozhkin et al., 2007
5	Bol'shoy Lyakhovsky Island	Laptiv Sea	73.33 °N, 141.5 °E	($\delta^{18}O_{PO4}$) Bones/Tusk	~47.5 – 15 ka	ΔMAT since present = always colder	Tutken et al., 2002, 2003
				Lipids	*~42 - 33	MAT = 4.5 ºC warmer than today	Martens et al., 2016
				Multiple	*>49	Colder relative to present	Wetterich et al., 2014
					*~49 – 48	Early warming	Wetterich et al., 2014

				Multiple	*48 - 38	Summer climate optimum	Wetterich et al., 2014
				Multiple	*50 - 30	Summer = ~8 to 12 similar to today	Andreev et al., 2009
				Mammal Fossil	*44 - 33	Climate Optimization	Andreev et al., 2009
				Wedge Ice Isotopes	*50 - 28.7	Tw, Tmin = 5 – 9 ºC, 11 - 17 ºC < present	Meyer, 2001
				Wedge Ice Isotopes	*60 - 50	Tw, Tmin = 13 ºC, 23 ºC < present	Meyer, 2001
6	Faddeyevskiy Island	Laptiv Seas	75.33 °N, 143.83 °E	Pollen	*43 - 25	At least 4, 2 more than today	Andreev et al., 2001
7	Buor Khaya Peninsula	Laptiv Sea	75.42 °N, 132.08 °E	Lipids	*~49	MAT = 1.6 cooler than today	Martens et al., 2016
8	Bykovsky Peninsula Mamontovy Khayata	Laptiv Sea	71.78 °N, 128.42 °E	Insects	~47-35	Summer warmer or at least not as colder than present	Sher et al., 2005
				Insects	~47-35	Winters much colder than present	Sher et al., 2005
				Pollen/Insects	*48 to 35-33	Slightly warmer summers and colder winters than present	Lozhkin and Anderson, 2011
				Pollen	*48 - 25	Warmer relative to present	Schirrmeister et al., 2002; Andreev et al., 2002b
				Pollen	*48 - 42	slight warming relative to today	Schirrmeister et al., 2002; Andreev et al., 2002b
				Insects/Plant Marco-Fossils	*48- 35	Unstable climate with summers warmer than present	Schirrmeister et al., 2002
				Marco-Fossils	*58 - 53	Very cold	Schirrmeister et al., 2002
				Pollen	*>50	colder summers	Schirrmeister et al., 2002; Andreev et al., 2002b
				Macro-Aquatic Plant Fossils	*~48	(MST) > 12; Tmax > 15	Kienast et al., 2005
				Multiple	*~48 - 35	Applicable to above	Kienast et al., 2005
				Wedge Ice Isotopes	*50 - 28.7	Tw, Tmin = 5 – 9 ºC, 11 - 17 ºC < present	Meyer, 2001
				Wedge Ice Isotopes	*60 - 50	Tw, Tmin = 13 ºC, 23 ºC < present	Meyer, 2001
9	Kurungnakh Island Lena Delta	Laptiv Sea	72.33 °N, 126.3 °E	Pollen & Rhizopod	*~50	Cold Tundra	Schirrmeister et al., 2003
				Pollen & Rhizopod	*~49 - 32	"Relatively" warm summer	Schirrmeister et al., 2003
				Multiple	* >50 to 32	"Relatively" warm summer, but summer colder relative to present	Wetterich et al., 2008

10	Cape Mamontov Klyk, Yedoma, Lower Sand*	Laptiv Sea	73.61 °N, 117.18 °E	Pollen	*45 - 28	Warm Relative to Stadials	Schirrmeister et al., 2008
				Single Celled Organisms	44 - 40	Warm Relative to Stadials	Muller et al., 2009
NA	Regional Summary	Laptiv Sea	NA	Pollen: Climate Simulations	*50 - 30	colder relative to today	Andreev et al., 2011
11	Labaz Lake, Various Sediments and Exposure	Taymyr Lowland	72.00 ° N,99.00 E	Pollen-Based Statistics	>48 to 25	Generally warmer than present	Andreev et al., 2002a
				Pollen-Based Statistics	>48 & ~50-44	Tmax, MAT, Tmin = up to 0.5 & 2.5-3 warmer than present	Andreev et al., 2002a
12	Lake Billyakh, middle Verkhoyansk MT	Lena River Drainage	65.28 °N, 126.78 °E	PCR Pollen	51 - 31 ka	Generally Colder than present, NGIRP climate patterns	Muller et al., 2010
13	Elikchan Lake	Kolyma Upland	60.13 °N, 153.33 °E	Pollen	*45 – 41	Warmer, "not more than present"	Anderson and Lozhkin, 2001
				Pollen	*46.8 - 44.8	Modern	Lozhkin and Anderson, 2011
				Pollen	*48.4 - 46.8	Perhaps colder than present	Lozhkin and Anderson, 2011
				Pollen	*53.4 - 48.4	Perhaps approaching present	Lozhkin and Anderson, 2011
				Pollen	*56.5 - 55.6	Perhaps colder than today	Lozhkin and Anderson, 2011
14	Alut Lake,	Kolyma Upland	60.75 °N, 153.8 °E	Pollen	*45 – 41 ka	"Relatively" Cool	Lozhkin and Anderson, 2011
NA	Multiple	Eastern Siberian Arctic	NA	Wedge Ice Isotopes	MIS 3	Tmin = -38 to -40 MWT = -27 to -29	Streletskaya et al., 2015
NA	Multiple	Yenisei River Drainage (Not Mapped)	Unknown	Likely Palaeoecological	*43 – 33 *45 - 43 *50 - 45	Climate Optimum Cool Warm	Kind et al., 1974 (e.g., Anderson and Lozhkin, 2001)

4.7.1 Regional context: T_{max}. Palaeoecological proxies on persevered organic remains such as vegetation/pollen, insect, plant and mammal macro fossils are common sources of information regarding Arctic Quaternary summer or growing season climates (Miller et al., 2010b). Palaeoecological proxies, such as palynology, commonly provide only qualitative information (warmer/colder, wetter/drier). Such proxies relate the occurrence, frequency, and abundance of indicator species within defined stratigraphic intervals to their modern-day analogs and climate range (Miller et al., 2010b; Sher et al., 2005). Pollen-based approaches lack empirical relationships with modern climate (palynological methods are discussed in detail in Andreev et al. (2011), Miller et al. 2010a, and Muller et al. (2010), and references therein). Various statistical (Andreev et al., 2002a; Andreev et al., 2011; Lozhkin et al., 2007; Muller et al., 2010) and quantitative (Alfimov et al., 2003; Tutken et al., 2002 and 2003) approaches do exist but are largely lacking within Siberia during the MIS 3, focusing more on Eemian and Holocene transitions.

Data on late Pleistocene seasonal climate is limited for the lower regions of the Kolyma River (Anderson and Lozhikin et al., 2001). Outside of the Laptiv Sea region and Duvanny Yar (Fig. 13), only fragmented portions Yedoma permafrost sediments outcrop at locations in the northern lowlands of Siberia, and their radiocarbon ages are suspect (review Anderson and Lozhkin et al., 2001 and Sher et al., 2005). An abundance of *Betula* sect., *Albae*, *Alnaster*, and *Pinus pumila*, and minor *Salix* and *Larix* pollen grains preserved in peat dated to 48-34 ^{14}C kyr BP (Shilo et al., 1987), within the Molotkovsky Kamen section, exposed along the banks of the Malyy Anyuy (Malii Anyuii) River (e.g., Anderson and Lozhkin, 2001 and Sher et al., 2005) (Table 4: Site. 2) inferred summer climate to have been warm as today (Anderson and Lozhkin, 2001). Pollen preserved in the Molotkovsky Kamen section is

evidence for Duvanny Yar reconstructed T_{max} from $\Delta(\delta^{18}O_{cell})$ ($\delta^{18}O_{cell(Tmax)}$) representing climates >48 ^{14}C kyr BP. MCR analysis on fossil insects within the Kolyma River valley (Elias, 1997; Elias, 2000; Elias and Matthews, 2002; Miller et al., 2010a) gives T_{max} values ~12-15 °C, or ~1-4 °C warmer than today during 45,000 – 35,000 ^{14}C BP (Table 4: Site. 3) (Alfimov et al., 2003). The fossil insects were possibly sampled from the same peat within Molotkovsky Kamen. The MCR findings align with fossil insect evidence from the Mamontovy Khayata Ice Complex (Fig. 13 and Table 4: Site. 8) located on the banks of Bykovsky Pennisula, Laptiv Sea (Sher et al., 2005). However, radiocarbon ages for the Molotkovsky Kamen section have been contested (Anderson and Lozhkin et al., 2001; Sher et al., 2005; Zubakov and Borzenkova, 1990). The large age uncertainty may simply indicate optimal summer climates existed in the Kolyma Lowland at least following 45 ^{14}C kyr BP, following cooling as indicated by $\delta^{18}O_{cell(Tmax)}$ (Fig. 8).

Much of the previous palynological research outside of the lower Kolyma River Valley has subdivided the terrestrial Karginsky interstadial and MIS 3 climate into various millennial scale chronologies characterized as relative “warm” and “cold” phases (Anderson and Lozhkin, 2001; Andreev et al., 2002b; Andreev et al., 2011; Kind et al., 1974; Lozhkin and Anderson; 2011; Schirrmeister et al., 2002; Wetterich et al., 2014). However, the timing, magnitude, and variability of climate change is uncertain and difficult to constrain as a result of the wide temporal and spatial scales of the data (Kienast et al., 2005; Lozhkin and Anderson, 2011; Miller et al., 2011a; Murton et al., 2015). Local geography, ecology, and depositional environments can have an important effect on climate reconstructions at any given site (Lozhkin and Anderson, 2011; Murton et al., 2015). Kind (1974) was the first to subdivided the Karginsky interstadial into several radiocarbon chronologies (Table 4)

(Anderson and Lozhkin, 2001; Lozhkin and Anderson, 2011; Miller et al., 2011a; Muller et al., 2010); however, the radiocarbon dates were later found to be too young and were later correlated to the Eemian (~100 ka) (Astakhov, 2014; Sher et a. 1991; Sher et al., 2005).

Pollen records from lacustrine sediments cored within the Kolyma Uplands (Fig. 13: Sites 13 and 14) and multi-proxy records from several Yedoma "Ice Complex" exposures near to or along the Northern Siberian coast (Fig. 13: Sites 5-10), suggest summer climate variability increased towards the Siberian interior with moderate and cool periods at ~53.4-48.4 ^{14}C kyr BP and 48.4-46.8 ^{14}C kyr BP, respectively (Lozhkin and Anderson, 2011) (Table 4: Site. 13). Pollen assemblages from Elikchan Lake and Alut Lake likely integrate across a small geographic region (~10 – 100 km^2) (Lozhkin and Anderson, 2011) and their pollen assemblages may therefore not be indicative of the growing season climate at Duvanny Yar. Several pollen records in the Laptiv Sea region (Fig. 13: Sites 5, 8-10), west of Duvanny Yar, point to three periods of millennial scale changes in climate, but the specific timing appears to be site dependent (Table 4) (Andreev et al., 2001; Andreev et al., 2002b; Andreev et al., 2009; Andreev et al., 2011; Schirrmeister et al., 2002; Schirrmeister et al., 2003; Schirrmeister et al., 2008b; Wetterich et al., 2008; and review Wetterich et al., 2014). Summers were inferred to have been colder than today from ~60 to 50-48 ^{14}C kyr BP, followed by a transitional period of "slight warming" (relative to the prior summer cold stage) from ~50-48 to 40 ^{14}C kyr BP (Schirrmeister et al., 2002) (specific dates are site dependent; e.g., Table 4 and Wetterich et al., 2014). An apparent regional climate optimum, containing the warmest summer climates of MIS 3, started ~44-40 ^{14}C kyr BP and prevailed until ~40-30 ^{14}C kyr BP (review Andreev et al., 2011; Wetterich et al., 2014). Andreev et al., (2011) used multiple stratigraphic sections from around the Laptiv Sea to correlate the

climate chronologies and dated the early warming and climate optimum periods to 50-48 to 40 ^{14}C kyr BP (54.4-51.8 to 43.7 ka) and ~40-32 ^{14}C kyr BP (43.7-36 ka) respectively. Climate trends following 54.4-51.8 to 43.7 ka and 43.7-36 ka agree well with the general $\delta^{18}O_{ice}$ climate trends from events D (14) up to D (11) and D (11) to sharp cooling at 36 ka, respectively (Fig. 12). Interestingly, uncalibrated radiocarbon ages 48-40 ^{14}C kyr BP and 40-32 ^{14}C kyr BP for the early warming and climate optimum periods, respectfully, follows general $\delta^{18}O_{ice}$ climate trends as well. Andreev et al. (2011) concluded the Laptiv Sea regional pollen-based qualitative reconstructions suggested summer temperatures lower than today during ~50-30 ^{14}C kyr BP (review Figure 11 within Andreev et al., 2011).

According to Lozhkin and Anderson (2013) and Wetterich et al. (2014), pollen and other organic matter within a layer of peat described by Zanina et al. (2011) indicates the climate optimum reached the lower Kolyma River valley based upon organic remains in palaeosols dated to ~44,000–42,000 ^{14}C BP with temperatures similar to modern (dates e.g., Zanina et al., 2011). According to Murton et al. (2015; Appendix S5), this layer of peat corresponds with palaeosol 2 located ~11.5 m ARL, and ~7.5 m above the wood fragments in the "CY" section. The ages reported by Zanina et al. (2011) are inconsistent with the Murton et al. (2015) age-height relationship, with ages ~44,000–42,000 ^{14}C BP being much higher up in section "CY." Regardless, based upon the Murton et al. (2015) age model and the DY2 and DY4 sample collection height just above river level, the Laptiv Sea regional pollen-based chronologies and the $\delta^{18}O_{cell(Tmax)}$ results are evidence the fossil wood grew prior to the speculated optimal summer temperatures and during the suggested colder and/or transitional summer environments.

Several pollen studies have assigned the relatively "warm" intervals based upon increased

arboreal pollen occurrence and percentages, suggesting such was reliable evidence of northward advancement of forest line accompanied by relative warmer temperatures (Anderson and Lozhkin, 2001; Andreev et al., 2002b; Kienast et al., 2005; Schirrmeister et al., 2002; Zanina et al., 2011). Other pollen records at Yedoma sites (review Andreev et al., 2011 and Lozhkin and Anderson, 2011), suggested a mostly treeless tundra-steppe vegetation persisted during the MIS 3 as indicated by abundant nonarboreal graminoid herb (Poaceae) with moderate to minimal contribution from arboreal pollen (*Salix, Betula sect*., *Larix, Pinus*, and *Alnus*). According to Murton et al. (2015), the varying amounts of arboreal to nonarboreal pollen at the Duvanny Yar section were likely caused by long distance transport and redeposition by the strong winds responsible for the aeolian depositional environment of the late Pleistocene. Strong southerly winds would have transported pollen from southern upland regions over long distances, and deposited the pollen in the northern lowlands (Andreev et al., 2002b; Astakhov, 2014; Murton et al., 2015). The regional presence of reworked ancient taxa (Pinaceae) suggests that pollen assemblages may be further complicated by redeposition from pre-quaternary deposits into Laptiv Sea Yedoma deposits (~60-45 ^{14}C kyr BP) (Andreev et al., 2011). Therefore, evidence for minor arboreal pollen can be misleading, and their assemblages partially reflect transport in the lower Kolyma River valley and warmer summer climates to the south (Astakhov, 2014; Murton et al., 2015; Sher et al., 2005). Minor increases in small arboreal pollen percentage, even if supported by plant macro-fossil evidence, could more reflect localized hydrological conditions favorable for supporting isolated patches of trees more so than higher summer temperatures accompanied by an advancement in the northern boreal tree line during sea level low stand (Lozhkin and Anderson, 2011; Sher et al., 2005). River valleys, such as the Kolyma, could

have provided adequate moister availability to isolated small groves of Larch or tree birch resulting in sparse tree growth (Muller et al., 2010).

In general, palynology is an indirect proxy and may be less reliable than other palaeoecological and quantitative proxies (Astakhov, 2014). Palynological estimates of vegetation cover and summer temperature are too generalized because the pollen grains were likely transported large distances by wind (Astakhov, 2014). Climate estimates from pollen may therefore reflect environmental controls in addition to growing season temperatures (Astakhov, 2014; Lozhkin and Anderson, 2011; Murton et al., 2015; Sher et al., 2005). Magnitude, duration, and temporal placement of relative "warm" and "cold" intervals are subject to individual interpretation (e.g., Mamontovy Khayata Ice complex exposure, Bykovsky Peninsula; reviewed by Andreev et al., 2002b; Schirrmeister et al., 2002; and Sher et al., 2005, and Lake Billyakh; reviewed by Lozhkin and Anderson, 2011; Muller et al., 2010).

Mammal macro-fossil data indicate climate optimization based upon the steady increase in grazing herd populations (horse and mammoth) from 44-32 ^{14}C kyr BP at Bol'shoy Lyakhovsky Island (Fig. 13: Site. 5) (Andreev et al., 2009) and 44-26 ^{14}C kyr BP at Bykovsky Pennisula (Fig. 13: Site 8) (Figure 11 and 8c within Sher et al., 2005). Well-preserved mammoth carcasses across Siberia indicate absolute warming never reached levels for significant carcass decay during the past 50 ^{14}C kyr BP (Astakhov, 2014). Minimal mammoth populations coupled with a lack of horses at ~44-50 ^{14}C kyr BP (Fig. 8c within Sher et al., 2005) suggests that temperatures were at a minimum during growth of the DY2 and DY4 tree rings. Other bioindicators, such as insect and plant macrofossils, point to colder summer conditions prior to ~53-50 to 48 ^{14}C kyr BP (Kienast et al., 2005; Schirrmeister et

al., 2002; Sher et al., 2005; Wetterich et al., 2008; Wetterich et al., 2014), consistent with the older OSL ages assigned to DY2 and DY4 (~48,000 BP during the H5 cold period) (Fig. 12).

Contrary to the pollen records from the Laptiv Sea region and $\delta^{18}O_{cell(Tmax)}$, pollen records within the Taymyr Lowland (Site. 11) indicate peak warming ~50-44 ^{14}C kyr BP from the presence of open larch forest with shrub birch (Andreev et al., 2002a). Fossil insect assemblages preserved within the Mamontovy Khayata Ice Complex, Bykovsky Peninsula (Site. 8) indicate summer temperatures peaked ~47 ^{14}C kyr BP (Schirrmeister et al., 2002; Sher et al., 2005) and generally decreased steadily until ~24 ^{14}C kyr BP (Astakhov, 2014; Sher et al., 2005). The trend in abundance of "true and southern" xerophile, "northern" tundra xerophile, and Arctic tundra species through the Mamontovy Khayata section, displayed in Sher et al. (2005), aligns well with the Arctic MIS 3 June 60 °N and July 67.5 °N solar insolation trend ~50-25 ka (Berger and Loutre, 1991; Elias and Brigham-Grette, 2013; Melles et al., 2007). However, macrofossil and pollen evidence suggest colder summers occurred ~58-53 ^{14}C kyr BP during peak MIS summer insolation. The persistence of southern steppe insects throughout the Mamontovy Khayata Ice Complex assemblage implied warmer summer temperatures (Schirrmeister et al., 2003; Sher et al., 2005), or at least no colder than today during ~48-36 ^{14}C kyr BP and the Last Glacial Maximum (25-15 kyr BP) (Sher et al., 2005). Several aquatic plant and sub-aerial macrofossils recovered from the Mamontovy Khayata Ice Complex support the timing of peak summer temperatures at 48-43 ^{14}C kyr BP (Schirrmeister et al., 2002) and ~48,000 ^{14}C BP (Kienast et al., 2005), as such species do not exist that far north today. Kienast et al. (2005) suggested the presence of the temperate aquatic plant macrofossil *Callitriche hermaphroditica* at ~48,000 ^{14}C BP and at ~34,000 ^{14}C BP, and a singular steppe fruit of taxon *Thesium* at ~48,000 ^{14}C BP within the

Mamontovy Khayata Ice Complex was evidence of mean summer temperatures > 12 °C and mean July temperatures > 15 °C (i.e., 6 °C higher than those observed today at nearby Tarski, south of Bykovsky Peninsula).

However, according to Lozhkin and Anderson (2010), Bykovsky Peninsula has a low landscape representation and the Mamontovy Khayata records reflects more localized environmental conditions. A single macro-fossil identified by Kienast et al. (2005) may reflect extreme local climate variability rather than regional variability (Andreev et al., 2011). According to Wetterich et al. (2008), the combined Kargin multi-proxy palaeoecological data set on Kurungnakh Island (Fig. 13: Site. 9) in the Lena Delta, Laptev Region, was similar the Kargin data sets from Bykovsky Peninsula. Though the climate was still continental, Wetterich et al. (2008) state that the tundra-steppe site had colder summers >50 to 32 ^{14}C kyr BP relative to today, in contrast to the Bykovsky Peninsula. Wetterich et al. (2008) reasoned Bykovsky Peninsula was biased towards warmer climates due to the vicinity to the Kharaulakh Mountains. Some of the steppe insect species within the relic assemblage exits today within temperatures 12-14 °C, or 5-7 °C warmer than Bykovsky Pennisula today (Sher et al., 2005). However, they exit within isolated areas of the northern lowland and southern upland regions today (Sher et al., 2005; Astakhov et al., 2004), and may not reflect a regional climate. Summer climate simulations (June-August), produced by Andreev et al. (2011) from Laptiv Sea Region pollen data, modeled the difference between modern and Pleistocene temperatures. The Andreev et al. (2011) model aligned well with Pleistocene summer solar insolation patterns. Though not as large of a difference between modern Cherskiy and $\delta^{18}O_{cell(Tmax)}$, the simulation (Figure 11 within Andreev et al., 2011) modeled summer temperatures slightly less than today during ~60-32 ka.

Pollen spectra (Lozhkin and Anderson, 2011 and 2013), organic geochemistry (i.e. TOC) (Melles et al., 2007), and diatom data (Cherepanova et al., 2007) from the El'gygytgyn Lake record, cored in the Chukotka uplands west of Duvanny Yar (Fig. 13: Site. 4), are consistent with the Mamontovy Khayata insect record in regards to climate variability (Lozhkin and Anderson, 2011). Yet, inferred summer temperatures ~60-46 ka, in relation to today, are opposite of those inferred for the Laptiv Sea region. The warmest summer temperatures occurred between ~60-54 ka at El'gygytgyn Lake, followed by "cooling" to ~54-46 ^{14}C kyr BP leading into "colder" summer temperatures ~46-25 ^{14}C kyr BP, as indicted by shrub communities similar to tundra and polar desert communities on present-day Wrangle Island (71.25 °N, 178 °E, ~600 km north of El'gygytgyn Lake and northeast from Duvanny Yar) (Lozhkin et al., 2007; Lozhkin and Anderson, 2011 and 2013). Melles et al. (2007) assigned ~60-25 ka BP as a generally warm period within the past 300 ka BP with summer snow and ice melt, but temperatures may not have been necessarily warmer than today. According to Lozhkin et al. (2007), the palynological data suggest some variability in T_{max} from 2 to 9 °C, but T_{max} mostly ranged from 2.5-4 °C which is ~2-4 °C less than $\delta^{18}O_{cell(Tmax)}$ calculated here for Duvanny Yar. Reconstructed T_{max} was only slightly warmer than the bounding stadial periods (MIS 2 and 4) (Lozhkin et al., 2007), and generally colder than today, which agrees with findings from other statistical and modeling-based approaches (Andreev et al., 2011; Muller et al., 2010). The El'gygytgyn Lake temperature intervals discussed by Melles et al., 2007 and Lozhkin and Anderson (2011) coincide well with both peak July 67.5 °N solar insolation ~50-60 ka BP (e.g., Berger and Loutre, 1991, Melles et al., 2007; Elias and Brigham-Grette, 2013), the $\delta^{18}O_{ice}$ NGRIP record, and in the stacked marine oxygen isotope (MIS) record (Martionson et al., 1987). However, radiocarbon age control is poor within

El'gygytgyn Lake record, and various age corrections and models based on northern hemispheric $\delta^{18}O_{ice}$ (Lozhkin et al., 2007) and paleomagnetism records (Nowaczyk et al., 2007) have been debated (review Lozhkin and Anderson, 2011).

4.7.2 Regional context: T_{min}. Empirical relationships exist between winter temperatures and $\delta^{18}O_{ice}$ stable isotope compositions of modern wedge and ground ice, allowing scientist to reconstruct absolute values for mean winter temperatures (MWT) and T_{min} during the Quaternary form ancient wedge ice (Meyer, 2001; Nikolayev and Mikhalev, 1995; Streletskaya et al., 2016; Vasil'chuk, 1992). Precipitation falls as snow during the cold season, and snowmelt infills frost cracks in the active surface layer from January through mid-May (Meyer, 2002b). Large ice wedges grow syngeneic with permafrost accumulation from the repeated frost cracking and annual infill of snowmelt (Lachenbruch, 1963; Strauss, 2010; Vasil'chuk and Vasil'chuk, 1998), allowing scientist to infer vertical trends in the $\delta^{18}O_{ice}$ values of ancient wedge ice to changes in winter temperature through time (Meyer et al., 2002a and 2002b; Schirrmeister et al., 2002; Wetterich et al., 2014; Opel et al., 2017). Vasil'chuk (1992) was the first to derive quantitative reconstructions of winter temperatures during Yedoma accumulation at Duvanny Yar. According to Appendix S2 from Murton et al. (2015), Vasil'chuk (1992) reconstructed MWT and T_{min} from 13,000 (Vasil'chuk et al., 2001) up to 40,000 – 30,000 ^{14}C yrs BP that were on average -32.5 °C and -47 °C, respectively; with T_{min} being ~12 °C colder relative to modern day Cherskiy. Strauss (2010) measured $\delta^{18}O_{ice}$ beyond 40,000 ^{14}C BP at Duvanny Yar. In the sections dated to >46,690 to 40,880 ± 2100 ^{14}C BP (2.7-10 m ARL, undated < 2.7 m), $\delta^{18}O_{ice}$ values contained the warmest winter signal in the Kargin Interstadial. However, the $\delta^{18}O_{ice}$ values never reached peak Holocene enrichment at Duvanny Yar, and Strauss (2010) concluded that the Yedoma

Ice Complex at Duvanny Yar formed during a stable winter climate characterized as having harsh and cold conditions. Strauss (2010) concluded absolute MWT was ~4-8 °C colder then present during the formation of the Yedoma Ice Complex following the results from Nikolayev and Mikhalev (1995) and Vasil'chuk (1992) derived from developed quantitative methods, supporting the $\delta^{18}O_{cell}$ reconstructed T_{min} ($\delta^{18}O_{cell(Tmin)}$) being 3.0 ± 2.7 °C less than present day.

Vertical trends in the $\delta^{18}O_{ice}$ data of late Pleistocene ice wedges at Bykovsky Peninsula (Meyer et al., 2002a; Schirrmeister et al., 2002) (Fig. 13: Site. 8) and Bol'shoy Lyakhovsky Island (Fig. 13: Site. 5) (Meyer et al., 2002b; Wetterich et al., 2014) Yedoma Ice Complexes provide evidence for late Pleistocene winter conditions signaled at Duvanny Yar were regional across northern Siberia, extending as far west as the Laptiv Sea. In Yedoma sections dated to > 49 ka on Bol'shoy Lyakhovsky Island, $\delta^{18}O_{ice}$ values contained the coldest winter signal in the Kargin Interstadial (Wetterich et al., 2014). A shift to stable $\delta^{18}O_{ice}$ enrichment was observed between ~49 and 48 ^{14}C kyr BP on Bol'shoy Lyakhovsky Island, but was attributed to a change in freezing regime rather than climate (Wetterich et al., 2014). In general, the Laptiv Sea isotope data showed little variation in $\delta^{18}O_{ice}$, indicating winters were continuously colder relative to present (Meyer et al., 2002a; Meyer et al., 2002b; Meyer, 2001; Schirrmeister et al., 2002; Wetterich et al., 2014). Meyer (2001) reconstructed absolute MWT and T_{min} for the entire period of the Yedoma Silt Ice Complex formation (~50 to 28.7 ^{14}C kyr BP) and during ~60-50 ^{14}C kyr BP at Bykovsky Peninsula and Bol'shoy Lyakhovsky Island using novel empirical relationships based on modern wedge ice data. Including both sites, the resulting MWT and T_{min} were 5-9 °C and 11-17 °C, respectively, colder during the entire Yedoma Silt Ice Complex formation relative to present day Bykovsky Peninsula and

Bol'shoy Lyakhovsky Island (modern MWT = ~22 °C, T_{min} = ~31 °C). Again, including both sites, the resulting MWT and T_{min} were 13 °C and 23 °C, respectively, colder during ~60-50 ^{14}C kyr BP formation relative to present day Bykovsky Peninsula and Bol'shoy Lyakhovsky Island. The reconstruction errors were ± 2-3 °C and Meyer (2001) showed a larger change in T_{min} compared to $\delta^{18}O_{cell(Tmin)}$ at Duvanny Yar.

4.7.3 Regional Context: MART. Bioindicators at Mamontovy Khayata coupled with stable isotope data from wedge ice suggest that MART in northeastern Siberia was greater during the late Pleistocene than today (Andreev et al., 2002b; Astakhov, 2014; Kienast et al., 2005; Schirrmeister et al., 2002; Sher et al., 2005), in contrast with the MART results discussed in section 4.4. The authors of the Mamontovy Khayata research speculated higher MART was the result of relatively lower sea levels which lead to a more continental climate in northeastern Siberia during the late Pleistocene. As stated in subsection 4.7.1, the site likely reflected highly localized conditions that climatically favored warmer summers, and subsequently higher MART, than the rest of the Laptiv Sea region.

4.7.4 Regional context: MAT. Change in late Pleistocene MAT relative to present was constrained from lipids preserved at Bol'shoy Lyakhovsky Island and Buor Khaya Peninsula (Fig. 13: Sites 5 and 7). At Bol'shoy Lyakhovsky Island, MAT ~4.5 °C warmer during ~42-33 ^{14}C kyr BP relative to present (Martens et al., 2016) contradicts MAT reconstructed from $\delta^{18}O_{cell}$ ($\delta^{18}O_{cell(MAT)}$) (Fig. 8; $\delta^{18}O_{cell(MAT)}$ ~ -5 °C less). Such large discrepancy and spatial variation in MAT seems unlikely for northeastern Siberia and the Bol'shoy Lyakhovsky Island MAT may reflect the Kargin climate optimum. Lipid constrained MAT at Buor Khaya Peninsula ~1.6 °C less than today at ~49 ^{14}C kyr BP

(Martens et al., 2016) supports the general $\delta^{18}O_{cell(MAT)}$ findings (Fig. 8) for late Pleistocene MAT being lower than present.

A constant colder than present mean annual climate in northeastern Siberia during the MIS 3, up to ~48 ka, is supported by MAT geochemically reconstructed from phosphate oxygen isotope compositions ($\delta^{18}O_{PO4(MAT)}$) of mammal bones/tusks preserved at Bol'shoy Island Lyakhovsky (Table 4) (Tutken et al., 2002 and 2003, e.g., Muller et al., 2010). The $\delta^{18}O_{PO4(MAT)}$ data displayed highly variable but significantly colder mean annual climate relative to today ~48-30 ka, the resembling $\delta^{18}O_{ice}$ curves in Figure 12 (Figure 8 within Muller et al., 2010). The $\delta^{18}O_{PO4(MAT)}$ data did not extend beyond ~48 ka. However, from the excellent alignment between abrupt shifts in $\delta^{18}O_{PO4(MAT)}$ with pollen-sums recorded at Lake Billyakh (Fig. 13: Site 12) (Muller et al., 2010) and $\delta^{18}O_{ice}$ values in the NGIRP record (Fig. 8 within Muller et al., 2010), $\delta^{18}O_{PO4(MAT)}$ could potentially have been ~8 to 12 °C (or perhaps colder) than today when interpolated through H5 (Fig. 12) and up to 51 ka to corresponded with the 48.6 ± 2.9 OSL date provided by Murton et al., (2015) at Duvanny Yar.

4.8 Modeling growing season length

The high rate of atmospheric MAT warming in polar regions, relative to lower latitudes, is the result of marine and terrestrial positive feedback mechanisms that exist in the Arctic (Chae et al., 2014; Gaversen and Wang et al., 2009; Miller et al., 2010a and 2010b; Overland et al., 2013; Serreze et al., 2009; Serreze and Barry; 2011). The magnitude in which positive feedbacks drive Arctic amplification is governed largely by changes in seasonal temperature, primarily during the warm months (mean daily T > 0°C), more so than changes in MAT (ACIA, 2004; Chapin et al., 2000; Walsh, 2014). As discussed in section 4.7, previous

paleoclimate research in northeastern Siberia has lacked uniform understanding of late Pleistocene seasonal climate. Though information regarding winter temperatures is fairly direct, much of the summer climate information is indirect and qualitative. Aside from MCR analysis on fossil insects, though uncertainties quantifying T_{min} exist as mentioned within Alfimov et al. (2003), the entire suite of paleoclimate proxies across the relevant literature was incapable of reasonably estimating both T_{max} and T_{min}, and paleoseasonal temperatures at year-to-year resolution.

However, paleoclimate data (Table 4; Fig. 8) provide sufficient information to suggest northeastern Siberia remained an Arctic-like, arid and cold climate region throughout the past 130 ka (reviewed by Murton et al., 2015). Relative to non-polar regions, ancient Siberia resembled the highly seasonal climate present in the region today (Table 4), having above freezing temperatures during June and July and extreme cold temperatures during November-February of the year. From this, the normal distribution in T_{month} across the year (peak T_{month} in July) (Fig. 2) found across the modern Arctic (ACIA, 2005; Araguas-Araguas et al., 1998; Strauss, 2010; WBG, http://sdwebx.worldbank.org/) is assumed reasonably unchanged since the late Pleistocene. Until now, a single proxy for quantifying ancient seasonal temperatures direct from geochemical analysis on a single organic substrate has been unavailable. To this, following the normal distribution in modern T_{month}, late Pleistocene monthly temperatures can be modeled across the year using T_{max} and T_{min} reconstructed from intra-ring $\delta^{18}O_{cell}$ measurements.

Temperature records at modern Cherskiy show that T_{month} was normally distributed across each year from 1980-2012 (thin red lines in Figure 14) (NOAA, National Climatic Data Center, http://www.ncdc.noaa.gov). Producing a single average of T_{month} for each month

from all 33 years of climate data, expressed by the bold red line (Figs. 2, 14), reveals the single averaged change in T_{month} (T_{min} to T_{max}) was normally distributed as well. Assuming T_{month} during the late Pleistocene at Duvanny Yar followed a normal distribution similar to the single 33-year average at Cherskiy, I used T_{max} and T_{min} calculated from Equations 6 and 8 of each fossil ring to model mean monthly paleotemperature across each year (thin blue lines) during the late Pleistocene (Fig. 14) (Appendix S3).

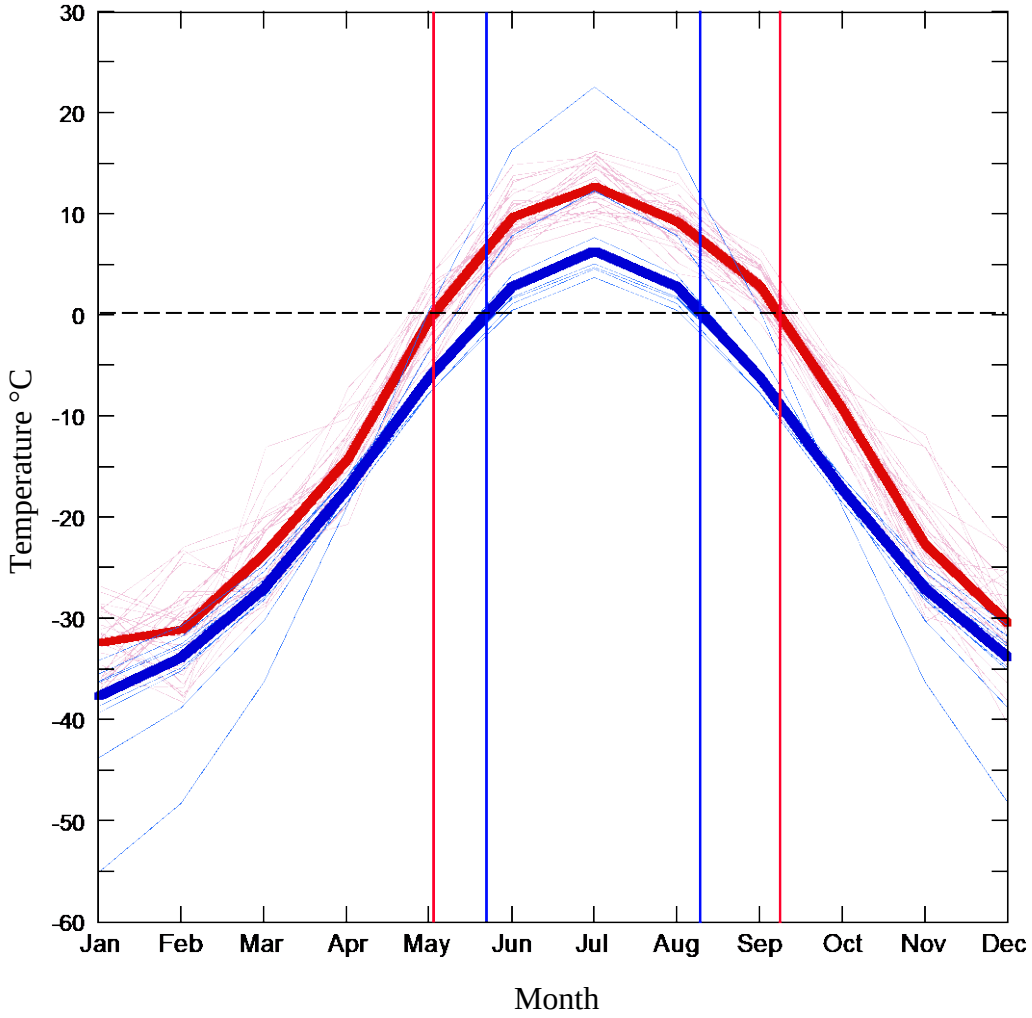

Figure 14. Late Pleistocene seasonal temperatures across each year (blue curves) following the normal distribution of the single average of mean monthly change in temperature at modern Cherskiy (bold red line) averaged from each year from 1980-2012 (thin red curves). The bold blue curve represents the late Pleistocene single average of mean monthly change in temperature produced from average T_{max} and T_{min} from all fossil growth rings excluding DY2 R1. The intersection of the red and blue vertical lines with the horizontal dashed line bounds the modern and late Pleistocene growing season ($T \geq 0$ ^{o}C), respectively.

Average late Pleistocene T_{month}, expressed by the bold blue line (Fig. 14), was produced from single averaged change in T_{month} (T_{max} to T_{min}) from all fossil growth rings in the seven-year record. DY2 R1 was again considered an outlier and excluded from the single averaged fossil T_{month}. The DY2 R1 seasonality seems unlikely given calculated T_{max} and T_{min} fell well outside both modern and fossil MART, and the resulting T_{month} curve has a visually steeper gradient across the year than the other fossil and modern curves. Note, calculated T_{max} for

DY2 R2 and fossil average seven-year record are nearly equal (Appendix S4), and as result, the DY2 R2 T_{month} curve track the single averaged fossil T_{month} curve across the growing season and is not visible within the growing season interval (Fig 14). All fossil calculated $\delta^{18}O_{cell(Tmin)}$, including DY2 R2 calculated T_{min} (-35.6 °C), are visible in Figure 14.

The intersection of the red and blue vertical lines with the horizontal dashed line denotes the modern and late Pleistocene growing season, respectively, I define as the duration with $T \geq 0$ °C in Figure 14. The single average of mean monthly change in temperature produced from all fossil growth rings in the seven-year record shows the late Pleistocene growing season was ~2.6 months in length (late May to early August). Figure 14 shows the modern single averaged growing season is ~4.2 months in length (start of May to mid-September), equating to a 1.6 month increase since the late Pleistocene. Following a general assumption that each month is 30 days in length, Figure 14 reveals growing season duration in northeastern Siberia has increased ~50 days (~76 to ~126) since the late Pleistocene ~45 to 54 ka ago, equating to a 65% increase in duration. The greatest difference between modern T_{month} and late Pleistocene modeled T_{month} occurred during the growing season. Therefore, increased growing season temperatures has been the primary control on enhanced seasonality and growing season extension since the late Pleistocene more so than the increased in cold season temperatures.

Producing a single average of modern T_{month} for each month from all 33 years of climate data results in a lower and higher average for modern T_{max} and T_{min}, respectively, displayed in Figures 2 and 14 compared with those displayed in Figure 8. This is caused by the 33-year average July and January temperatures (July = 12.9 °C, January = -32.4 °C) being lower and higher than the 33-year average of the actual warmest and coldest month, respectively, mean

temperature for each year on record (T_{max} = 13.2 °C, T_{min} = -34.7 °C). As discussed in section 4.4, July and January more often represented T_{max} and T_{min} at modern Cherskiy. For the purposes of modeling late Pleistocene seasonal temperatures across the year following the bold red curve, fossil calculated T_{max} and T_{min} were placed at July and January, respectively, in Figure 14. Thus, the difference between modern and late Pleistocene T_{max}, T_{min}, and MART appears less in Figure 14 than in Figure 8. Findings regarding the absolute change in MAT, T_{max}, T_{min}, and MART since the late Pleistocene should strictly follow the absolute temperature values discussed in section 4.4. Findings regarding changes in modern seasonal temperatures across the year and growing season length since the late Pleistocene should strictly follow the results discussed in this section.

In Figure 14, the prolonged termination of the modern growing season appears to outpace the extension of the start of the modern growing season relative since the late Pleistocene. Such a scenario could have critical implications on future warming as earlier thaw favors an increase in ecosystem carbon uptake, and postponed termination of the growing season favors an increase in ecosystem respiration (R_{eco}) (Van der Molen et al., 2007; Piao et al., 2007). Photosynthesis and carbon uptake is limited by the duration of sunlight at the end of the season, whereas permafrost thaw and carbon respiration is limited by temperatures near to the start of the season and can continue thaw during periods of lower sunlight but with temperatures still above freezing towards the end of the growing season (Van der Molen et al., 2007; Piao et al., 2007). However, the fossil T_{month} record follows a normal distribution modeled from the single averaged 33-year change in T_{month} (T_{max}-T_{min}) rather than the distribution of T_{month} for each month averaged across the 33-year record as displayed by the bold red line (Fig. 14). As such, the blue curves lack the extension of end of the growing

season towards September as seen in the bold red curve. The true shape of late Pleistocene T_{month} curve could have more closely tracked the actual modern T_{month} distribution rather than the modeled, and therefore, the findings from Figure 14 do not provide climate insight regarding the relative timing of the start and end of the late Pleistocene growing season. Regardless of rather the fossil T_{month} followed the modeled or actual modern distribution in T_{month} across the year, the late Pleistocene model (Fig. 14) would still show shorter growing seasons relative to today.

The magnitude and positive change in T_{max} relative to modern contradicts several prior studies in the northeastern Siberia (Table 4). Though the high-resolution $\delta^{18}O_{cell}$ proxy is a more quantitative and direct approach than most previous proxies conducted in the region, yearly snow and permafrost thaw processes may cause intra-annual variability in $\delta^{18}O_{cell}$ values across growth rings (Fig. 5) and $\delta^{18}O_{cell}$ calculated T_{max}. As discussed in subsection 4.7.2, snowmelt infiltrates permafrost cracks and is incorporated into annually thawed soils of the active surface layer during spring and early summer. Plants may uptake depleted $\delta^{18}O_{MW}$ values of winter precipitation and incorporate them into plant tissue during spring growth, depleting early and middle wood $\delta^{18}O_{cell}$ measurements (Roden et al., 2009) as seen in DY2 Rings 2-3, as well as seen through the earlywood and briefly in the middlewood of DY2 R2. Enriched $\delta^{18}O_{cell(max)}$ values nearest to the ring boundary within latewood may reflect enhanced evaporation at the end of the growing season (Roden et al., 2009). Fossil rings with $\delta^{18}O_{cell(max)}$ enrichment nearest to ring boundary within earlywood may indicate plant storage of $\delta^{18}O$ from the prior growing season (Roden et al., 2009) similar to that of $\delta^{13}C$ storage, as seen in Ring 1 of DY2 and Rings 7-8 of DY4. In another possible scenario to explain the occurrence of tree rings with $\delta^{18}O_{cell(max)}$ closest to the ring boundary within

earlier wood, the reactivation of the active surface layer might release enriched evaporate $\delta^{18}O_{MW}$ from the prior end growing season that was frozen following the termination of above freezing temperatures and remained captured in the frozen active surface layer until the following spring thaw.

The method presented in this study for deriving T_{max}, modified from Schubert and Jahren (2015), is not dependent of the timing of $\delta^{18}O_{cell(max)}$ and $\delta^{18}O_{cell(min)}$ within individual growth rings. Yet, possible uptake of snowmelt during the growing season may suppress actual $\delta^{18}O_{cell(max)}$ and subsequently $\Delta(\delta^{18}O_{cell})$ values in some fossil rings, resulting in $\delta^{18}O_{cell}$ calculated T_{max} and T_{min} being lower and higher, respectively, than were actually present during the year. The extent at which snowmelt, seasonal soil thaw, and $\delta^{18}O$ storage interact and effect intra-annual $\delta^{18}O_{cell}$ values of trees growing within Arctic polar sites is not known and requires further study. Though the role permafrost processes had on results from Figures 5, 8, and 14 are unknown, the high-resolution $\delta^{18}O_{cell}$ proxy presented here represents a significant step forward towards uncovering seasonal temperatures and growing season length present in northeastern Siberia during the late Pleistocene.

4.9 Implications

The high-resolution intra-annual $\delta^{18}O_{cell}$ proxy presented in this study is the first of its kind to quantify seasonal and model paleotemperature across the year from a single geochemical proxy applied to a site above the Arctic circle. Findings from this research have critical implications on current and future Arctic and global climates. Data from Jeong et al. (2011) reveal the northern hemisphere (> 30 °N) growing season duration has increased by 9.6 days over years 1982-2008 as a result of significant anthropogenic warming. Findings from Piao et

al. (2007) suggest growing season duration has increased by 0.30 days per year north of 25 °N during the years 1980-2002. Considering that growing season duration likely increases at a higher rate above the Arctic circle more so than lower latitude regions as result of Arctic amplification, findings from Jeong et al. (2011), Piao et al. (2007), and other similar studies regarding modern growing season extension, is evidence to suggest the identified extended and warmed growing season since the late Pleistocene is in large part the result of recent anthropogenic forcing rather than natural planetary or astronomical forcing alone.

The identified shorter growing seasons and colder conditions of the late Pleistocene (Figs. 8 and 14) provided ample conditions for Yedoma permafrost development on a regional scale (Figures 1 within Strauss et al., 2013 and Murton et al., 2015), causing the terrestrial arctic ecosystem to have positive net uptake of carbon and act as a significant global sink of atmospheric and organic carbon at the time (Johnston et al., 2014). Based upon the height ARL in which the fossil wood was sampled from Duvanny Yar, the seasonal temperatures identified from high-resolution $\delta^{18}O_{cell}$ measurements represents the climate in which the sediments of the lowest paleocyrosol sequence ("DY-05-B" ~1-7 m ARL) were deposited. This section contained the highest levels of preserved bulk organic matter within the Yedoma Silt at the Duvanny Yar exposure (Strauss et al., 2012). The late Pleistocene Arctic terrestrial ecosystem had a positive net uptake of carbon due to the trapping of atmospheric carbon sequestered out of the atmosphere during photosynthesis, and organic carbon within frozen and waterlogged soils preventing the microbial degradation of organic matter within the frozen impermeable sediments (Guo et al., 2017; Natali et al., 2014). Organic matter within the active surface layer was incorporated into underlying permafrost from cryoturbation and the vertical rise of the permafrost table though time during continual soil accumulation

(Schuur et al., 2008). This resulted in the sequestering of an ancient carbon stock of critical mass equaling 1672 GT currently present in northern hemisphere sediments (Tarnocai et al., 2009), more than double the current total atmospheric carbon stock (Schuur et al., 2013; Spencer et al., 2015).

Change in Arctic ecosystems which drive Arctic terrestrial climate feedback mechanisms are affected by changes in summer climate more so than winter or mean annual conditions (Astakhov, 2014; Miller et al., 2010a and 2010b; Schuur et al., 2008). Longer growing seasons and amplified summer warming results in and increase in ecosystem carbon uptake due to the increase ecosystem gross primary production (GPP) (defined by Gilabert et al. (2017) from the lengthening of time in which photosynthesis can sequester carbon from the atmosphere during periods of sunlight with mean daily $T > 0$ °C (Churkina et al., 2005; Keenan et al., 2016; Zhang et al., 2014). Enhanced photosynthetic activity, prolonged plant exposure to sunlight with rising summer temperatures, and anthropogenic increase in atmospheric carbon leads to increase in vegetation biomass and changing plant species (Chae et al., 2014; Jeong et al., 2011 and 2012; Piao et al., 2007). Increased vegetation biomass, accompanied by the northward advancement of more productive plant biomes towards northern Siberia, contributes towards a negative (colder) climate feedback (review Anisimov et al., 2007 and Lemke et al., 2007). However, replacing solar reflective barren tundra surfaces with solar insulating dense vegetation during the growing season reduces the Arctic terrestrial surface albedo (i.e., ability to reflect solar radiation and energy), resulting in increased solar energy absorption and warms the arctic terrestrial surface as a positive climate feedback (Chae et al., 2014; Chapin et al., 2005; Jeong et al., 2011; Loranty et al., 2011). Replacement of short growing tundra vegetation, more readily covered by solar

reflective snow during winter, with higher growing shrub vegetation and darker boreal foliage increases solar absorption during both summer and winter season (Chapin et al., 2005; Loranty et al., 2011; Muller et al., 2010a and 2010b; Schuur et al., 2008; Zhao-Ping et al., 2010).

The ability of the Arctic terrestrial surface to reflect solar radiation is critically important during the growing season months when solar radiation is strongest, peaking in June, and solar energy reflection at the surface is at its weakest (Chae et al., 2014; Miller et al., 2011a). Referring to Figure 14, warming has removed 1.6 months of highly reflective snow cover previously present during the late Pleistocene. Approximately 50 days of prior snow cover has been replaced by darker snow free surface, reducing the surface albedo by prolonging the exposer of the snow barren soils and permafrost to solar energy and above freezing temperatures (Serreze and Barry, 2011; Zhang, 2005). To this, the Arctic's terrestrial surface albedo was likely higher during late Pleistocene relative to today, as less solar energy and heat was absorbed and retained by permafrost soils during late Pleistocene relative to today.

While GPP has shown to increase with higher absolute temperatures during the growing season in northeastern Siberia, GPP does not necessarily correlate with longer growing seasons in the terrestrial arctic (Natali et al 2015; Piao et al., 2007; Zhang et al., 2014), particularly in northeastern Siberia (Parmentier et al., 2011b). Longer growing seasons have shown to enhance ecosystem respiration (R_{eco}) by extending the duration in which plants and thawing permafrost respire organic carbon from into the atmosphere (Natali et al., 2015; Parmentier et al., 2011a and 2011b; van der Molen et al., 2007). Prolonged permafrost exposure to increasing growing season temperatures increases permafrost soil temperatures, causing increasing thickness and moister drainage of the active surface layer, erosion such as

thermokarst, and thaw (Anisimov et al., 2007; Natali et al., 2015; Schuur et al., 2008; Schaefer et al., 2014; Vonk et al., 2015; Zhang, 2005; Zhao-ping et al., 2010). Relic permafrost underlying the active surface layer becomes unfrozen and decomposes, making the perennial frozen ancient organic carbon available for dissolution and decay during seasonal thaw (Natali et al., 2015; Schuur et al., 2008 and 2013; Vonk et al., 2015; Zhang, 2005). The dissolved organic matter is converted into CO_2 and methane (CH_4) during microbial degradation and respired into the atmosphere as greenhouse gas during permafrost thaw, erosion, and bacterial respiration once carbon is delivered during fluvial and lacustrine (Lee et al., 2012; Mann et al., 2014; Schuur et al., 2013 and 2015; Spencer et al., 2015; Stubbins et al., 2017; Vonk et al., 2015; Vonk and Gustafsson, 2013; Waldrop et al., 2010; Zimov et al., 2006). Parmentier et al. (2011b) found Arctic terrestrial ecosystems showed a lower net uptake of carbon occurred during years with longer and warmer growing seasons. Increases in Arctic R_{eco} of carbon into the atmosphere have been found to offset most increases in ecosystem carbon uptake (Natali et al., 2014; Schaefer et al., 2014; Parmentier et al., 2011b). Winter R_{eco} has also been shown to further offset any increases in carbon uptake or GPP from as a result of increased growing season length and temperature (Natalie et al., 2014). Increases in carbon uptake with longer growing seasons will be short-term and small at best (Parmentier et al., 2011b; Schaefer et al., 2014).

Arctic river run off sourced from watersheds in the northern lowlands of Siberia, such as Kolyma River valley, is a significant factor controlling the freshwater budget of the Arctic and Atlantic Ocean (Carmack et al., 2016). Continual thaw and melt of frozen ice within Yedoma permafrost results in the subsequent release of ancient freshwater previously frozen alongside ancient organic carbon (Schuur et al., 2008 and 2013; Vonk et al., 2013). The

resulting Yedoma thaw streams are capable of decomposing up to 33% of organic carbon in just 14 days (Vonk et al., 2013). The increased freshwater input into the ecosystem expands the watershed in the Siberian lowlands and increases river erosion, further destabilizing Yedoma permafrost and releasing carbon and freshwater (Schuur et al., 2008). This positive feedback loop is projected to transport high amounts of ancient freshwater and dissolved organic carbon into the Arctic Ocean, potentially disrupting the Atlantic Ocean thermohaline circulation (Carmack et al., 2016; Serreze et al., 2006; Sommerkorn and Hassol, 2009; Spencer et al 2015; Stubbins et al., 2017; Yang et al., 2015).

None of the carbon negative feedback mechanisms will be able to offset carbon release from permafrost thaw and thermokarst development in the long-term future (Schuur et al., 2008; Schaefer et al., 2014; Natalie et al., 2014; Zhao-Ping et al., 2010). Projected Arctic warming is likely to enhance the Arctic carbon sink and carbon uptake (Euskirchen et al., 2006) until the mid 21st century due in part to enhanced net photosynthesis, GPP, and net primary production (NPP) (Xu et al., 2013; Zhang et al., 2014; Zhu et al., 2014), at which point advancing R_{eco} from permafrost thaw and carbon release will outpace NPP (Zhang et al., 2014) causing an Arctic shift from a historical carbon sink to a catastrophic carbon source (Churkina et al., 2005; Grosse et al., 2016; Johnston et al., 2014; Lawrence et al., 2012; McGuire et al., 2009; Schuur et al., 2008 and 2015; Zhu et al., 2014). The abundant ground ice in Yedoma makes the deposits particularly vulnerable to higher growing season temperatures, as significant ice melt leads to permafrost destabilization and collapse (Strauss et al., 2012; Vonk et al., 2013). Of the 211 GT carbon stock present in the Arctic Yedoma region across Siberia and Alaska, equaling about half of the total global planet biomass (350-540 GT), ~83 GT is trapped within the frozen carbon reservoirs of all Yedoma deposits

alone, with the remaining ~128 GT of carbon trapped within refrozen thermokarst deposits of thaw lake basins (Strauss et al., 2013). The release of the massive greenhouse CO_2 and CH_4 pool into the atmosphere during both gradual and abrupt Yedoma thaw, as a result of anthropogenic warming, would be sufficient enough to amplify global warming and accelerate the rate of climate change.

5. CONCLUSION

Cellulose was successfully extracted from mummified ancient growth rings at high-resolution, revealing ancient wood with ample ring geometries and cellulose yields well preserved within late Pleistocene age permafrost soils located in northeastern Siberia. The results from high-resolution $\delta^{18}O_{cell}$ analysis revealed that the ancient cellulose preserved a valuable paleoclimate record at annual and seasonal resolution. The paleoclimate proxy presented here represents a new method for calculating seasonality and modeling monthly temperature across the year from direct geochemical measurements across a single organic substrate. This study is the first of its kind to provide such information regarding a geologic age and Siberian region above the Arctic Circle of critical importance for our future global climate.

Year to year changes in late Pleistocene (~47-54, or perhaps >54 ka) seasonal temperature, characterized as having a lower seasonal range in temperature with shortened growing seasons relative to today, were identified by implementing empirical relationships of seasonal and mean annual changes in modern $\delta^{18}O_{cell}$ and temperature. The results of the reconstructed temperatures for Duvanny Yar provide quantitative evidence of modern terrestrial Artic warming in the Kolyma lowland of ~3-6 °C across the year since the late Pleistocene, adding new information to the Siberian Karginsky interstadial and MIS 3 climate debate. Modern warming was especially pronounced during the warmer months, acting as the primary contributing factor prolonging the critically important growing season.

Colder seasonal temperatures across the year provided ample conditions for Yedoma permafrost development. Despite lower photosynthetic activity and vegetation biomass that accompanies fewer days with T > 0 °, the colder and shorter growing seasons identified for

the late Pleistocene led to ecosystem net uptake of carbon that was likely higher than today due to the entrapment of organic carbon within the frozen sediments, causing the terrestrial Arctic region to behave as a global carbon sink during a time when CO_{2atm} was 200 ppm less than today. Continued increases in T_{max} and T_{min} and growing season length, driven by continual anthropogenic increase in CO_{2atm} levels, threatens a gradual Arctic ecosystem switchover from an ancient carbon sink to a significant modern carbon source. The switchover will be further amplified by terrestrial positive feedback mechanisms, which are largely the result of enhanced growing season length and temperature. Such terrestrial feedbacks include near surface soil and permafrost warming from reduction in Arctic surface albedo, vegetation shifts towards increased solar absorbing biomasses, increased input of fresh melt water into the ocean thermohaline circulation from early snowmelt and permafrost erosion, and continual degradation and thaw of Yedoma and other relic permafrost in the circumpolar region, releasing catastrophic amounts of greenhouse gas into the atmosphere and further compounding greenhouse warming beyond anthropogenic activity alone.

The suggested age of the fossil wood (45 to 50-54 ka) falls near what has previously been debated as either peak MIS 3 warm or cold temperatures. Yet summer and winter temperatures may have continued to decline through the late Pleistocene, leading to even colder permafrost conditions after growth of the Duvanny Yar fossil wood samples based upon the timing of the assumed sample age with historical July 67.5 °C solar insolation levels (Elias and Brigham-Grette, 2013), stacked marine isotope record (Martinson et al., 1987), and the general D12-17 climate in the $\delta^{18}O_{ice}$ NGIRP record (Fig. 12; NGIRP Project Members, 2004). Radiocarbon dating the cellulose samples may help place the $\delta^{18}O_{cell}$ findings in a more constrained context with the highly variable regional and global climate of

the MIS 3. However, chronological complications may yet remain as radiocarbon dating becomes infinite beyond the limit of reliable radiocarbon calibration at ~46.6-50 ka, which has caused more research focused towards younger climate events such as the Pleistocene and Holocene transition. Future work may be required to resolve the temporal and spatial heterogeneity in northeastern Siberia as a means to better understand how an Arctic climate suitable for Yedoma permafrost development has shifted towards a climate where relic permafrost has begun thaw and thermokarst today (Anisimov et al., 2007; Guo et al., 2017; Romanovsky et al., 2007; Zhao-ping et al., 2010). Such work may include but is not limited to: radiocarbon dating cellulose extracted from DY2 and DY4 samples upon further funding, investigating possible environmental impacts on variable intra-ring $\delta^{18}O_{cell}$ profiles within trees growing at permafrost sites, quantifying late Pleistocene northern Siberia MAP, developing Arctic high-latitude specific or Eurasian continental relationships between $\delta^{18}O_{cell}$ and climate, and applying high-resolution $\delta^{18}O_{cell}$ methods similar to those outlined in this study on fossil wood preserved within Yedoma and other permafrost sites across various geological ages of importance to projecting the future climate. Though the effects of snowmelt on the results are uncertain, this proxy represents a positive step forward and a new method towards resolving ancient Arctic seasonal climates from the less quantitative proxies for seasonal temperature and common quantitative proxies of MAT that have dominated the research and understanding of historical late Quaternary Arctic climate.

REFERENCES

ACIA, 2004, Impacts of a Warming Arctic: Arctic Climate Impact Assessment: Cambridge University Press, 144 p.

ACIA, 2005, Arctic Climate Impact Assessment: Cambridge University Press, Ch. 17, pg. 946-988.

Alfimov, A.V., Berman, D. I., and Sher, A.V., 2003, Tundra-steppe insect assemblages and re- constructions of late Pleistocene climate in the lower reaches of the Kolyma River: Zoologicheskiy Zhurnal, v. 82, no. 2 p. 281–300 (in Russian with English Abstract).

Alley, R. B., 2007. Wally was right: predictive ability of the North Atlantic "conveyor belt" hypothesis for abrupt climate change: Annual Review of Earth and Planetary Sciences, v. 35, p. 241-272.

Anderson, P. M., and A. V. Lozhkin, 2001, The Stage 3 interstadial complex (Karginskii/middle Wisconsinan interval) of Beringia: variations in paleoenvironments and implications for paleoclimatic interpretations: Quaternary Science Reviews, v. 20, p. 93-125.

Anderson, W. T., S. M. Bernasconi, J. A. McKenzie, M. Saurer, and F. Schweingruber, 2002, Model evaluation for reconstructing the oxygen isotopic composition in precipitation from tree ring cellulose over the last century: Chemical Geology, v. 182, p. 121–137.

Andreev, A. A., D. M. Peteet, P. E. Tarasov, F. A. Romanenko, L. V. Filimonova, and L. D. Sulerzhitsky, 2001, Late Pleistocene interstadial environment on Faddeyevskiy Island, East-Siberian Sea, Russia: Arctic, Antarctic, and Alpine Research, v. 33, no. 1, p. 28-35.

Andreev, A. A., C. Siegert, V. A. Klimanov, A. Y. Derevyagin, G. N. Shilova, and M. Melles, 2002a, Late Pleistocene and Holocene vegetation and climate on the Taymyr Lowland, northern Siberia: Quaternary Research, v. 57, no. 1, p. 138-150.

Andreev, A. A., L. Schirrmeister, C. Siegert, A. A. Bobrov, D. Demske, M. Seiffert, and H-W. Hubberten, 2002b, Paleoenvironmental changes in northeastern Siberia during the late Quaternary - evidence from pollen records of the Bykovsky Peninsula: Polarforschung, v. 70, p. 13-25.

Andreev, A. A., and 12 additional authors, 2009, Weichselian and Holocene paleoenvironmental history of the Bol'shoy Lyakhovsky Island, new Siberian Archipelago, Arctic Siberia: Boreas, v. 38, p. 72-110.

Andreev, A. A., L. Schirrmeister, P. E. Tarasov, A. Ganopolski, V. Brovkin, C. Siegert, S. Wetterich, and H-W. Hubberten, 2011, Vegetation and climate history in the Laptev Sea region (Arctic Siberia) during late Quaternary inferred from pollen records: Quaternary Science Reviews, v. 30, p. 2182-2199.

Anisimov, O. A., D. G. Vaughan, T. V. Callaghan, C. Furgal, H. Marchant, T. D. Prowse, H. Vilhjamsson, and J. E. Walsh, 2007, Ch. 15 Polar regions (Arctic and Antarctic): Climate Change 2007: Impacts, Adaptation and Vulnerability. Contribution of Working Group II to the Fourth Assessment Report of the Intergovernmental Panel on Climate Change, Cambridge University Press, Cambridge, p. 653-685.

Araguas-Araguas, L., K. Froehlich, and K. Rozanski, 1998, Stable isotope composition of precipitation over southeast Asia: Journal of Geophysical Research, v. 103, no. D22, p. 28,721–28,742.

Astakhov, V., The postglacial Pleistocene of the northern Russian mainland: Quaternary Science Reviews: v. 92, p. 388-408.

Ballantyne, A., N. Rybczynski, P. Baker, C. R. Harington, and D. White, 2006, Pliocene Arctic temperature constraints from the growth rings and isotopic composition of fossil larch: Palaeogeography, Palaeoclimatology, Palaeoecology, v. 242, p. 188-200.

Baranova, Y. P., 1957, Geomorphological sketch of the eastern part of the Kolyma Lowland: Materials on Geology and Minerals of the Northern East USSR, v. 2., p. 208-222 (in Russian).

Berger, A., and M. F. Loutre, 1991, Insolation values for the climate of the last 10 million years: Quaternary Science Reviews, v. 10, p. 297-317.

Black, R. F., 1974, Ice-wedge polygons of northern Alaska: Glacial geomorphology, State University of New York: Binghamton; 247-275.

Biske, S. F., 1957, Quaternary deposits of the Kolyma lowland. In: Materials on Geology and Minerals of the Northern East USSR, v. 2, p. 68-81 (in Russian).

Bonala, D., C. Atgerb, T. S. Barigaha, A. Ferhic, J-M. Guehld, and B. Ferry, 2000, Water acquisition patterns of two wet tropical canopy tree species of French Guiana as inferred from $H_2\ ^{18}O$ extraction profiles: Annals of Forest Science, v. 57, no. 7, p. 717-724.

Bowen, G. J., and B. H. Wilkinson, 2002, Spatial distribution of $\delta^{18}O$ in meteoric precipitation: Geology, v. 30, p. 315-318.

Bowen, G. J., and J. Ravenaugh, 2003, Interpolating the isotopic composition of modern meteoric precipitation: Water Resources Research. doi:10.1029/2003WR002086.

Bowen, G. J., 2008, Spatial analysis of the intra-annual variation of precipitation isotope ratios and its climatological corollaries; Journal of Geophysical Research v. 113, no. D05113, 10 p.

Bowen, G. J., 2013, The Online Isotopes in Precipitation Calculator. http://www.waterisotopes.org, 2.2.

Brendel, I. O., and D. Stewart, 2000, A rapid and simple method to isolate pure alpha-cellulose: Phytochemical Analysis, v. 11, p. 7-10.

Brienen, R. J. W., G. Helle, T. L. Pons, J.-L. Guyot, and M. Gloor, 2012, Oxygen isotopes in tree rings are a good proxy for Amazon precipitation and El Nino-Southern Oscillation variability: Proceedings of the National Academy of Science, v. 109, p. 16957-16962.

Capron, E. and 14 additional authors, 2010, Millennial and sub-millennial scale climatic variations recorded in polar ice cores over the last glacial period: Climate of the Past, v. 6, p. 345-365.

Chae, Y., S. M. Kang, S. J. Jeong, B. Kim, and D. M. W. Frierson, 2015, Arctic greening can cause earlier seasonality of Arctic amplification, Geophysical Research Letters: v. 42, no. 2, p. 536-541.

Chapin III, F. S. and 11 additional authors, 2000, Arctic and boreal ecosystems of western North America as components of the climate system: Global Change Biology, v. 6, p. 211-223.

Carmack, E. C., M. Yamamoto-Kawai, T. W. N. Haine, S. Bacon, B. A. Bluhm, C. Lique, H. Melling, I. V. Polyakov, F. Straneo, M.-L. Timmermans, and W. J. Williams, 2016, Freshwater and its role in the Arctic Marine System: Sources, disposition, storage, export, and physical and biogeochemical consequences in the Arctic and global oceans: Journal of Geophysical Research: Biogeosciences, v. 121, p. 675-717.

Cherepanova, M. V., J. A. Snyder, and J. Brigham-Grette, 2007, Diatom stratigraphy of the last 250 ka at Lake El'gygytgyn, northeast Siberia: Journal of Paleolimnology, v. 37, p. 155-162.

Churkina, G., D. Schimel, B. H. Braswell, and X. Xiao, 2005, Spatial analysis of growing season length control over net ecosystem exchange: Global Change Biology, v.11, p. 1777–1787.

Csank, A, Z., D. Fortier, and S. W. Leavitt, 2013, Annually resolved temperature reconstructions from a late Pliocene–early Pleistocene polar forest on Bylot Island, Canada: Palaeogeography, Palaeoclimatology, Palaeoecology, v. 369, p. 313-322.

Danzeglocke, U., Cologne Radiocarbon Calibration and Paleoclimate Research Package: quickcal2007 ver.1.5, http://www.calpal-online.de, accessed July, 2017.

Dansgaard, W., 1964, Stable isotopes in precipitation: Tellus, v. 16, p. 435-468.

Dansgaard, W., S. J. Johnsen, H. B. Clausen, D. Dahl-Jensen, N. S. Gundestrup, C. U. Hammer, C. S. Hvidberg, J. P. Steffensen, E. Sveinbjornsdottir, J. Jouzel, and G. Bond, 1993, Evidence for general instability of past climate from a 250-kyr ice-core record: Nature, v., 364, p. 218-200. doi:10.1038/364218a0

Dodd, J. P., W. P. Patterson, C. Holmden, and J. M. Brasseur, 2008, Robotic micromilling of tree-rings: a new tool for obtaining subseasonal environmental isotope records: Chemical Geology, v. 252, p. 21-30.

Elias, S. A., 1997, The mutual climatic range method of palaeoclimate reconstruction based on insect fossils: New applications and interhemispheric comparisons: Quaternary Science Reviews, v. 16, no. 10, p. 1217-1225.

Elias, S. A., 2000, Late Pleistocene climates of Beringia, based on analysis of fossil beetles: Quaternary Research, v. 53, p. 229-235.

Elias, S. A., J. V. Matthews Jr., 2002, Arctic North American seasonal temperatures in the Pliocene and early Pleistocene, based on mutual climatic range analysis of fossil beetle assemblages: Canadian Journal of Earth Sciences v. 39, p. 911-920.

Elias, S. A., and J. Brigham-Grette, 2013. Late Pleistocene glacial events in Beringia: Encyclopedia of Quaternary Science, Second Edition, Elsevier, Amsterdam, v. 2, p. 191–201.

Farquhar, G. D., M. H. O'Leary, and J. A. Berry, 1982, On the relationship between carbon isotope discrimination and intercellular carbon dioxide concentration in leaves: Australian Journal of Plant Physiology, v. 9, p. 121-137.

Fricke, H. C., and J. R. O'Neil, 1999, The correlation between 18O=16O ratios of meteoric water and surface temperature: its use in investigating terrestrial climate change over geologic time: Earth and Planetary Science Letters, v. 170, p. 181-196.

Gessler, A., E. Brandes, C. Keitel, S. Boda, Z. E. Kayler, A. Granier, M. Barbour, G. D. Farquhar, and K. Treydte, 2013, The oxygen isotope enrichment of leaf-exported assimilates–does it always reflect lamina leaf water enrichment?: New Phytologist, v. 200, p. 144-157. doi:10.1111/nph.12359

Gilabert, M. A., S. Sanchez-Ruiz, and A. Moreno, 2017, Annual Gross Primary Production from Vegetation Indices: A Theoretically Sound Approach: Remote Sensing, v. 9, no. 3, p. 193-214.

Guo, J., Hu, Y, Xiong, Z., Yan, X., Li, C., and R. Bu, 2017, Variations in growing-season NDVI and its response to permafrost degradation in northeast China: Sustainability, v. 9, no. 4, 551 p.

Graversen, R. G., and M. Wang, 2009, Polar amplification in a coupled climate model with locked albedo: v. 33, no. 5, p. 629-643.

Grosse, G., J. E. Robinson, R. Bryant, M. D. Taylor, W. Harper, A. DeMasi, E. Kyker-Snowman, A., Veremeeva, L. Schirrmeister, and J. Harden, 2013, Distribution of late Pleistocene ice-rich syngenetic permafrost of the Yedoma Suite in east and central Siberia, Russia: U.S. Geological Survey Open File Report 2013-1078, 37p.

Grosse, G., S. Goetz, A. D. McGuire, V. E. Romanovsky, and E. A. G. Schuur, 2016, Changing permafrost in a warming world and feedbacks to the Earth system: Environmental Research Letters, v. 11, no. 4, 10 p.

Gubin, S. V., 1999, Late Pleistocene soil formation in Ice-loess deposits north-east of Eurasia: Doctoral Dissertation in Biological Sciences, Pushchino (in Russian).

Guo, J., Hu, Y., Xiong, Z., Yan, X., Li, C., and R. Bu, 2017, Variations in growing-season NDVI and its response to permafrost degradation in northeast China: Sustainability, v. 9, n0. 4, 15 p.

Guthrie, R. D., 2006, New carbon dates link climatic change with human colonization and Pleistocene extinctions: Nature, v. 441, p. 207-209. DOI:10.1038/nature04604

Harada, M., Y. Watanabe, T. Nakatsuka, S. Tazuru-Mizuno, Y. Horikawa, J. Sugiyama, T. Tsuda, and T. Tagami, 2014, Alpha-cellulose extraction procedure for the tropical tree sungkai (*Peronema canescens* Jack) by using an improved vessel for reliable paleoclimate reconstruction: Geochemical Journal, v. 48, p. 299-307.

Helle, G., and G. H. Schleser, 2004, Beyond CO2-fixation by Rubisco-An interpretation of $^{13}C/^{12}C$ variations in tree rings from novel intra-seasonal studies on broad-leaf trees: Plant, Cell & Environment, v. 27, p. 367-380.

Heinrich, H., 2008, Origin and consequences of cyclic ice rafting in the Northeast Atlantic Ocean during the past 130,000 years: Quaternary Research, v. 29, no. 2, p. 142-152.

Hook, B. A., J. Halfar, J. Bollmann, Z. Gedalof, M. A. Rahman, J. Reyes, and D. J. Schulze, 2015, Extraction of α-cellulose from mummified wood for stable isotopic analysis: Chemical Geology, v. 405, p. 19-27.

Hopkins D. M., J. V. Matthews, C. E. Schweger, S. B. Young, and V. Stanley, 1982, Aspects of the paleogeography of Beringia during the late Pleistocene: Paleoecology of Beringia, New York: Academic Press; p. 3-28.

Huber, C., M. Leuenberger, R. Spahni, J. Flückiger, J. Schwander, T. F. Stocker, S. J. Johnsen, A. Landais, and J. Jouzel, 2006, Isotope calibrated Greenland temperature record over Marine Isotope Stage 3 and its relation to CH4: Earth and Planetary Science Letters, v. 243, p. 504-519.

IAEA/WMO, 2006. Global Network of Isotopes in Precipitation. The GNIP Database Accessible at: http://www.iaea.org/water.

Jahren A. H., and L. S. L. Sternberg, 2008, Annual patterns within tree rings of the Arctic middle Eocene (c. 45 Ma): Isotope signatures of precipitation, relative humidity, and deciduousness: Geology, v. 36, p. 99-102.

Jeong S. J., Ho C. H., Gim, H. J., and M. E. Brown, 2011, Phenology shifts at start vs. end of growing season in temperate vegetation over the northern Hemisphere for the period 1982–2008: v. 17, no. 7, p. 2385-2399.

Jeong, J. H., Kug, J. S., Kim, B. M., Min, S. K., Linderholm, H. W., Chang-Hoi Ho, C. H., Rayner, D., Chen, D., and S. Y. June, 2012, Greening in the circumpolar high-latitude may amplify warming in the growing season: Climate Dynamics, v. 38, no. 7-8, p. 1421-1431.

Johnston, C. E., S. A. Ewing, J. W. Harden, R. K. Varner, K. P. Wickland, J. C. Koch, C. C. Fuller, K. Manies, and M. T. Jorgenson, 2014, Effect of permafrost thaw on CO2 and CH4 exchange in a western Alaska peatland chronosequence: Environmental Research Letters, v. 9, no. 8, 12 p.

Kaplina T. N., 1986, Regularities of development of cryolithogenesis in late Cenozoic in accumulation flood plain of northeastern Asia: Dissertation in Geology and Mineralogy, Permafrost Institute of the Siberian Branch, USSR Academy of Science, Moscow, P. 48 (in Russian).

Kaplina, T. N., R. E. Giterman, O. V., Lakhtina, B. A. Abrashov, S. V. Kiselyov, and A. V. Sher, 1978, Duvanny Yar, a key section of upper Pleistocene sediments of the Kolyma lowland.: Bulletin of Quaternary Commission, v. 48, p. 49-65 (in Russian).

Kawamura. K, and 17 additional authors, 2007, Northern Hemisphere forcing of climatic cycles in Antarctica over the past 360,000 years: Nature, v. 488, p. 912-917.

Keel, S. G., F. Joos, R. Spahni, M. Saurer, R. B. Weigt, and S. Klesse, 2016, Simulating oxygen isotope ratios in tree ring cellulose using a dynamic global vegetation model: Biogeosciences, v. 13, p. 3869-3886.

Keenan, T. F., I. C. Prentice, J. G. Canadell, C. A. Williams, H. Wang, M. Raupach, and G. J. Collatz, 2016, Recent pause in the growth rate of atmospheric CO_2 due to enhanced terrestrial carbon uptake: Nature Communications, v. 7, no. 13428, 7 p.

Kienast, F., T. Lutz, L. Schirrmeister, C. Siegert, and P. Tarasov, 2005, Palaeobotanical evidence for warm summers in the East Siberian Arctic during the last cold stage: Quaternary Research, v. 63, p. 283-300.

Kind, N. V., 1974, Late Quaternary geochronology According to Isotopic Data: Nauka, Moscow, 255 p (in Russian with English abstract).

Knutson, T. R., T. L. Delworth, K. W. Dixon, I. M. Held, J. Lu, V. Ramaswamy, and M. D. Schwarzkopf, 2006, Assessment of twentieth-century regional surface temperature trends using the GFDL CM2 coupled models: Journal OF Climate, v. 19, p. 1624-1651.

Lachenbruch, A. H., 1963, Contraction theory of ice-wedge polygons: A qualitative discussion: Permafrost International Conference, Lafayette, National Academy of Sciences-National Research Council.

Lambeck, K., T. M. Esat, and E. K. Potter, 2002, Links between climate and sea levels for the past three million years: Nature, v. 419, p. 199-206.

Lang, C., M. Leuenberger, J. Schwander, and S. Johnsen, 1999, 16 °C Rapid Temperature Variation in Central Greenland 70,000 Years Ago: v. 286, no. 5441, p. 934-937.

Lemke, P., J. Ren, R. B. Alley, I. Allison, J. Carrasco, G. Flato, Y. Fujii, G. Kaser, P. Mote, R. H. Thomas, and T. Zhang, 2007, Ch. 4 Observations: Changes in Snow, Ice and Frozen Ground. In: Climate Change 2007: The Physical Science Basis. Contribution of Working Group I to the Fourth Assessment Report of the Intergovernmental Panel on Climate Change, Cambridge University Press, Cambridge, United Kingdom and New York, NY, USA, p. 339-383.

Li, Z H., N. Labbee, S. G. Driese, and H. D. Grissino-Mayer, 2011, Micro-scale analysis of tree-ring $\delta^{18}O$ and $\delta^{13}C$ on α-cellulose spline reveals high-resolution intra-annual climate variability and tropical cyclone activity: Chemical Geology, v. 284, p. 138-147.

Loranty, M. M., S. J. Goetz, and P. S. A. Beck, 2011, Tundra vegetation effects on pan-Arctic albedo: Environmental Research Letters, v. 6, no. 024014, 7 p.

Lozhkin, A. V., P. M. Anderson, T. V. Matrosova, and P. S. Minyuk, 2007, The pollen record from El'gygytgyn Lake: implications for vegetation and climate histories of northern Chukotka since the late middle Pleistocene: Journal of Paleolimnology, v. 37, p. 135-153.

Lozhkin, A. V., and P. M. Anderson 2011, Forest or no forest: implications of the vegetation record for climatic stability in Western Beringia during Oxygen Isotope Stage 3: Quaternary Science Reviews, v. 30, p. 2160-2181.

Lozhkin, A. V., and P. M. Anderson 2013, Northern Asia: Encyclopedia of Quaternary Science, 2nd Edition, Elsevier, Amsterdam, v. 4, p. 27-38.

Luthi, D. and 10 additional authors, 2008, High-resolution carbon dioxide concentration record 650,000-800,000 years before present: Nature, v. 453, p. 379-382.

Mann, P. J., and 10 additional authors, Evidence for key enzymatic controls on metabolism of Arctic river organic matter: Global Change Biology, v. 20, no. 4, p. 1089-1100.

Martens, J., S. Kusch, M. Winterfeld, G. Mollenhauer, G. Schwamborn, L. Schirrmeister, S. Wetterich, P., Overduin, and J. Rethemeyer, 2016, A biomarker-based paleoclimatic reconstruction of MIS1, MIS3 and MIS5e based on permafrost deposits from NE Siberia: Presentation at the 11th International Conference on Permafrost, Potsdam, 20 June 2016 - 24 June 2016. doi: 10.2312/GFZ.LIS.2016.001

Martinson, D. G., N. G. Pisias, J. D. Hays, J. Imbrie, T. C. Moore Jr, and N. J. Shackleton, 1987, Age dating of the orbital theory of the Ice Ages: development of a high-resolution 0 to 300,000-year chronostratigraphy. Quaternary Research, v. 27, p. 1-29.

McCarroll, D., and N. J. Loader, 2004, Stable isotopes in tree rings: Quaternary Science Reviews, v. 23, p. 771-801.

Melles, M., J. Brigham-Grette, O. Y. Glushkova, P. S. Minyuk, N. R. Nowaczyk, and H. W. Hubberten, 2007, Sedimentary geochemistry of core PG1351 from Lake El'gygytgyn-a sensitive record of climate variability in the East Siberian Arctic during the past three glacial-interglacial cycles: Journal of Paleolimnology, v. 37, p. 89-104.

Meyer, H., 2001, Late Quaternary climate history of Northern Siberia - evidence from ground ice: PhD Thesis, University of Potsdam, Germany.

Meyer, H., A. Y. Derevyagin, C. Siegelt, and H-W. Hubberten, 2002a, Paleoclimate studies on Bykovsky Peninsula, north Siberia hydrogen and oxygen isotopes in ground ice: Polarforschung, v. 70, p. 37-51.

Meyer, H., A. Y. Derevyagin, C. Siegelt, Lutz Schirrmeister., and Hans-W. Hubberten, 2002b, Palaeoclimate Reconstruction on Big Lyakhovsky Island, North Siberia—Hydrogen and Oxygen Isotopes in Ice Wedges: Permafrost and Periglacial Processes, v. 13, p. 91-105.

Miller, D. L., C. I. Mora, H. D. Grissino-Mayer, C. J. Mock, M. E. Uhle, and Z. Sharp, 2006, Tree-ring isotope records of tropical cyclone activity: Proceedings of the National Academy of Science, v. 103, no. 39, p. 14294-14297.

Miller, G. H., R. B. Alley, J. Brigham-Grette, J. J. Fitzpatrick, L. Polyak, M. C. Serreze, and J. W. C. White, 2010a, Arctic amplification: can the past constrain the future?: Quaternary Science Reviews, v. 29, p. 1779-1790.

Miller, G. H. and 21 additional authors, 2010b, Temperature and precipitation history of the Arctic: Quaternary Science Reviews, v. 29, p. 1679-1715.

Muller, S., A. A. Bobrov, L. Schirrmeister, A. A. Andreev, and P. E. Tarasov, 2009, Testate amoebae record from the Laptev Sea coast and its implication for the reconstruction of Late Pleistocene and Holocene environments in the Arctic Siberia, Palaeogeography, Palaeoclimatology, Palaeoecology, v. 271. p. 301–315.

Muller, S., P. E. Tarasov, A. A. Andreev, T. Tutken, S. Gartz, and B. Diekmann, 2010, Late Quaternary vegetation and environments in the Verkhoyansk Mountains region (NE Asia) reconstructed from a 50-kyr fossil pollen record from Lake Billyakh: Quaternary Science Reviews, v. 29, p. 2071-2086.

Murton, J. B. and 17 additional authors, 2015, Paleoenvironmental interpretation of Yedoma Silt (ice complex) deposition as cold-climate loess, Duvanny Yar, northeast Siberia: Permafrost and Periglacial Process, v. 26, p.208-288.

Natali, S. M., E. A. G. Schuur, E. E. Webb, C. E. H. Pries, and K. G. Crumme, 2014, Permafrost degradation stimulates carbon loss from experimentally warmed tundra: Ecology, v. 95, no. 3, p. 602-608.

New, M., D. Lister, M. Hulme, and I. Makin, 2002, A high-resolution data set of surface climate over global land areas: Climate Research, v. 21, p. 1-25.

Nikolayev, V., and D. V. Mikhalev, 1995, An Oxygen-Isotope paleothermometer from ice in Siberian permafrost: Quaternary Research, v. 43, p. 14-21.

NOAA, National Climatic Data Center, http://www.ncdc.noaa.gov

North Greenland Ice Core Project members, 2004, High-resolution record of Northern Hemisphere climate extending into the last interglacial period: Nature, v. 431, No. 7005, p. 147-151. doi:10.1038/nature02805

Opel, T., S. Wetterich, H. Meyer, A. Y. Dereviagin, M. C. Fuchs, and L. Schirrmeister, 2017, Ground-ice stable isotopes and cryostratigraphy reflect late Quaternary palaeoclimate in the Northeast Siberian Arctic (Oyogos Yar coast, Dmitry Laptev Strait): Climate of the Past, v. 13, p. 587-611.

Overland, J. E., M. Wang, J. E. Walsh, and J. C. Stroeve, 2013, Future Arctic climate changes: Adaptation and mitigation time scales: Earth's Future, v. 2, p. 68-74.

Parmentier, F. J. W., J. van Huissteden, M. K. van der Molen, G. Schaepman-Strub, S. A. Karsanaev, T. C. Maximov, and A. J. Dolman, 2011a, Spatial and temporal dynamics in eddy covariance observations of methane fluxes at a tundra site in northeastern Siberia: Journal of Geophysical Research, v. 116, no. G03016, 14 p.

Parmentier, F. J. W., M. K. van der Molen, J. van Huissteden, S. A. Karsanaev, A. V. Kononov, D. A. Suzdalov, T. C. Maximov, and A. J. Dolman, 2011b, Longer growing seasons do not increase net carbon uptake in the northeastern Siberian tundra: Journal of Geophysical Research, v. 116, no. G04013, 11 p.

Petit, J. R. and 18 additional authors, 1999, Climate and atmospheric history of the past 420,000 years from the Vostok ice core, Antarctica: Nature, v. 339, p. 429-436.

Piao, S., P. Friedlingstein, P. Ciais, N. Viovy, and J. Demarty, 2007, Growing season extension and its impact on terrestrial carbon cycle in the northern Hemisphere over the past 2 decades, Global Biogeochemical Sciences, v. 21, no. GB3018, p. 1-11.

Poussart, P. F., M. N. Evans, and D. P. Schrag, 2004, Resolving seasonality in tropical trees: multi-decade, high-resolution oxygen and carbon isotope records from Indonesia and Thailand: Earth and Planetary Science Letters, v. 218, p. 301-316.

Rasmussen, S. O. and 23 additional authors, 2014, A stratigraphic framework for abrupt climatic changes during the Last Glacial period based on three synchronized Greenland ice-core records: refining and extending the INTIMATE event stratigraphy: Quaternary Science Reviews, v. 106, p. 14-28.

Richter, S. L., A. H. Johnson, M. M. Dranoff, B. A. LePage, and C. J. Williams, 2008a, Oxygen isotope ratio in fossil wood cellulose: Isotope composition of Eocene to Holocene-aged cellulose: Geochimica et Cosmochimica Acta, v. 72, p. 2744-2753.

Richter, S. L., A. H. Johnson, M. M. Dranoff, and K. D. Taylor, 2008b, Continental-scale patterns in modern wood cellulose $\delta^{18}O$: Implications for interpreting paleo-wood cellulose $\delta^{18}O$: Geochimica et Cosmochimica Acta, v. 72, p. 2735-2743.

Roden, J. S., G. Lin, and J. R. Ehleringer, 2000, A mechanistic model for interpretation of hydrogen and oxygen isotope ratios in tree-ring cellulose: Geochimica et Cosmochimica Acta, v. 64, p. 21-35.

Roden, J. S., J. A. Johnstone, and T. E. Dawson, 2009, Intra-annual variation in the stable oxygen and carbon isotope ratios of cellulose in tree rings of coast redwood (*Sequoia sempervirens*): Holocene, v. 19, p. 189-197.

Romanovskya, V. E., T. S. Sazonovaa, V. T. Balobaevb, N. I. Shender, and D. O. Sergueev, 2007, Past and recent changes in air and permafrost temperatures in eastern Siberia: Global and Planetary Change 56 (2007) 399–413

Rozanski, K., L. Araguas-Araguas, and R. Gonfiantini, 1992, Relation between long-term trends of oxygen-18 isotope composition of precipitation and climate: Science, v. 258, p. 981-985.

Saurer, M., S. Borella, and M. Leuenberger, 1997, $\delta^{18}O$ of tree rings of beech (*Fagus silvatica*) as a record of $\delta^{18}O$ of the growing season precipitation. Tellus B, v. 49, p. 80-92.

Saurer, M., P. Cherubini, C. E. Reynolds-Henne, K. S. Treydte, W. T. Anderson, and R. T. W. Siegwolf, 2008, An investigation of the common signal in tree ring stable isotope chronologies at temperate sites: Journal of Geophysical Research. v. 113, G04035.

Schaefer, K., H. Lantuit, V. E. Romanovsky, E. A. G. Schuur, and R. Witt, 2014, The impact of the permafrost carbon feedback on global climate: Environmental Research Letters, v. 9, no. 085003, 9 p.

Schirrmeister, L., C. Siegert, T. Kuznetsova, S. Kuzmina, A. Andreev, F. Kienast, H. Meyer, and A. Bobrov, 2002, Paleoenvironmental and paleoclimatic records from permafrost deposits in the Arctic region of northern Siberia: Quaternary International v. 89, no. 1, p. 97-118.

Schirrmeister, L., and 12 additional authors, 2008, Periglacial landscape evolution and environmental changes of Arctic lowland areas for the last 60,000 years (western Laptev Sea coast, Cape Mamontov Klyk): Polar Research, v. 27, no. 2, p. 249-272.

Schirrmeister L., D. Froese, V. Tumskoy, G. Grosse, and S. Wetterich, 2013, Yedoma: Late Pleistocene Ice-Rich Syngenetic Permafrost of Beringia. The Encyclopedia of Quaternary Science, vol. 3, p. 542-552.

Schubert, B. A., and A. H. Jahren, 2011, Quantifying seasonal precipitation using high-resolution carbon isotope analyses in evergreen wood: Geochimica et Cosmochimica Acta, v. 75, p. 7291-7303.

Schubert, B. A., A. H. Jahren, J. J. Eberle, L. S. L. Sternberg, and D. A. Eberth, 2012, A summertime rainy season in the Arctic forests of the Eocene: Geology, v. 40, no. 6, p. 523-526.

Schubert, B. A., and A. H. Jahren, 2015, Seasonal temperature and precipitation recorded in the intra-annual oxygen isotope pattern of meteoric water and tree-ring cellulose: Quaternary Science Reviews, v. 125, p. 1-14.

Schubert, B. A., and A. Timmermann, 2015, Reconstruction of seasonal precipitation in Hawaii using high-resolution carbon isotope measurements across tree rings: Chemical Geology, v. 417, p. 273-278.

Schuur, E. A. G. and 18 additional authors, 2008, Vulnerability of permafrost carbon to climate change: Implications for the global carbon cycle: Bioscience, v. 58. no. 8, p. 701–714.

Schuur, E. A. G. and 41 additional authors, 2013, Expert assessment of vulnerability of permafrost carbon to climate change: Climatic Change, v. 119, p. 359-374.

Schuur, E. A. G. and 16 additional authors, 2015, Climate change and the permafrost carbon feedback: Nature, v. 520, p. 171-179.

Serreze, M. C., A. P. Barrett, J. C. Stroeve, D. N. Kindig, and M. M. Holland, 2009, The emergence of surface-based Arctic amplification: The Cryosphere, v. 3, p. 11-19.

Serreze, M. C., and R. G. Barry, 2011, Processes and impacts of Arctic amplification: A research synthesis: Global and Planetary Change, v. 77, p. 85-96.

Sher, A.V., 1971, Mammals and stratigraphy of the Pleistocene of the extreme Northeast of the USSR and North America. Nauka, Moscow (in Russian). In English: Pleistocene mammals and stratigraphy of the Far Northeast USSR and North America; Intern. Geology Review, v. 16, no. 7-10, p. 1-284.

Sher, A.V., T. N. Kaplina, R. E. Giterman, A. V. Lozhkin, A. A. Arkhangelov, S.V. Kiselyov Y. V. Kouznetsov, E. I. Virina, and V. S. Zazhigin, 1979, Late Cenozoic of the Kolyma Lowland: XIV Pacific Science Congress, Khabarovsk August 1979, Tour Guide XI. USSR Academy of Sciences: Moscow.

Sher, A. V., 1991, Problems of the last interglacial in Arctic Siberia: Quaternary International, v. 10–12, p. 215-222.

Sher, A., 1995, Is there any real evidence for a huge shelf ice sheet in East Siberia?: Quaternary International, v. 28, p. 39-40.

Sher, A. V., S. Elias, and J. Brigham-Grette, 1997, Yedoma as a store of paleoenvironmental records in Beringia: Beringia Paleoenvironmental Workshop September 1997, Ohana Productions: Nepean, ON, Canada; p. 92-94.

Sher, A. V., S. A. Kuzmina, T. V. Kuznetsova, and L. D. Sulerzhitsky, 2005, New insights into the Weichselian environment and climate of the east Siberian Arctic, derived from fossil insects, plants, and mammals: Quaternary Science Reviews, v. 24, p. 533-569. doi:10.1016/j.quascirev.2004.09.007

Shilo, N. A., A. A. Siderov, Yu. P. Baranova, and A. V. Lozhkin, 1987, Resolutions of Interdisciplinary Stratigraphic Congress for Quaternary Systems of Eastern USSR: Russian Ministry of Geology, USSR Academy of Science, Far East Branch, Magadan, p. 29-69 (in Russian).

Spencer, R. G. M., P. J. Mann, T. Dittmar, T. I. Eglinton, C. McIntyre, R. M. Holmes, N. Zimov, and A. Stubbins, 2015, Detecting the signature of permafrost thaw in Arctic rivers: Geophysical Research Letters, v. 42, p. 2830-2835. doi:10.1002/2015GL063498

Steffensen, J. P. and 19 additional authors, 2008, High resolution Greenland ice core data show abrupt climate change happens in few years: Science, v. 321, p. 680-684.

Sternberg, L. D. L., M. C. Pinzon, P. F. Vendramini, W. T. Anderson, A. H. Jahren, and K. Beuning, 2007, Oxygen isotope ratios of cellulose-derived phenylglucosazone: an improved paleoclimate indicator of environmental water and relative humidity. Geochim Cosmochim Acta v. 71, p. 2463-2473.

Stubbins, A., P. J. Mann, L. Powers, T. B. Bittar, T. Dittmar, C. P. McIntyre, T. I. Eglinton, Zimov, N., and R. G. M. Spencer, 2017, Low photolability of yedoma permafrost dissolved organic carbon: Journal of Geophysical Research Biogeosciences, v. 122, no. 1, p. 200-211.

Strauss, J., 2010, Late Quaternary environmental dynamics at the Duvanny Yar key section, Lower Kolyma, East Siberia: Diploma Thesis, University of Potsdam, Alfred Wegener Institute for Polar and Marine Research, 108 p. DOI: 10013/epic.37551

Strauss, J., L. Schirrmeister, S. Wetterich, A. Borchers, and S. P. Davydov, 2012, Grain-size properties and organic-carbon stock of Yedoma Ice Complex permafrost from the Kolyma lowland, northeastern Siberia: Global Biogeochemical Cycles, v. 26, no. 3, p. 1-12.

Strauss, J., L. Schirrmeister, G. Grosse, S. Wetterich, M. Ulrich, U. Herzschuh, and H. W. Hubberten, 2013, The deep permafrost carbon pool of the Yedoma region in Siberia and Alaska: Geophysical Research Letters, v. 40, p. 6165-6170.

Streletskaya, I. D., A. A. Vasiliev, G. E. Oblogov, and I. V. Tokarev, 2015, Reconstruction of paleoclimate of Russian Arctic in the late Pleistocene-Holocene on the basis of ice wedges: Kriosfera Zemli, 2015, v. 19, no. 2, p. 86-94.

Svensson, A. and 13 authors, A 60,000 year Greenland stratigraphic ice core chronology: Climate of the Past, v. 4, p. 47-57.

Tarnocai, C., J. G. Canadell, E. A. G. Schuur, P. Kuhry, G. Mazhitova, and S. Zimov, 2009, Soil organic carbon pools in the northern circumpolar permafrost region: Global Biogeochemical Cycles, v. 29, GB2023.

Tomirdiaro, S. V., and B. I. Chyornen'kiy, 1987, Cryogenic eolian deposits of eastern Arctic and subarctic, Nauka, 197 p. (in Russian).

Turner, J., J. E. Overland, and J. E. Walsh, 2007, An Arctic and Antarctic perspective on recent climate change: International Journal of Climatology, v. 17, p. 277-293.

Tutken, T., T. V. Kuznetsova, T. W. Vennemann, and H. U. Pfretzschner, 2002. Late Pleistocene-Holocene climate of Siberia deduced from oxygen isotope compositions of mammoth and horse bone phosphate: Geochimica et Cosmochimica Acta, v. 66, A885.

Tutken, T., 2003, The implications of early diagenesis to the preservation of in vivo elemental and isotopic compositions in fossil bones: Ph.D. thesis, Eber-hard-Karls Universitat Tubingen (in German), 343 p.

Van Meerbeeck, C. J., H. Renseen, D. M. Roche, B. Wohlfarth, S. J. P. Bohncke, J. A. A. Bos, S. Engels, K. F. Helmens, M. F. Sanchez-Goni, A. Svensson, and J. Vandenberghe, 2011, The nature of MIS 3 stadial-interstadial transitions in Europe: New insights from model-data comparisons: Quaternary Science Reviews, v. 30, p. 3618-3637.

Van der Molen, M. K., J. Van Huissteden, F. J. W. Parmentier, A. M. R. Petrescu, A. J. Dolman, T. C. Maximov, A. V. Kononov, S. V. Karsanaev, and D. A. Suzdalov, 2007, The growing season greenhouse gas balance of a continental tundra site in the Indigirka lowlands, NE Siberia: Biogeosciences, v. 4, p. 985-1003.

Vasil'chuk, Y, K., 1992. Oxygen isotope composition of ground ice application to paleogeocryological reconstructions: Moscow: Russian Academy of Sciences and Moscow University, v. 2, 264 p. (In Russian with English contents section).

Vasil'chuk, Y. K., and A. C. Vasil'chuk, 1998, ^{14}C and ^{18}O in Siberian syngenetic ice-wedge complexes: Radiocarbon, v. 40, no. 2, p. 883-893.

Vasil'chuk, Y. K., A. C. Vasil'chuk, D. Rank, W. Kutschera, and J. Kim, 2001, Radiocarbon dating of $\delta^{18}O$-δD plots in Late Pleistocene ice-wedges of Duvanny Yar (Lower Kolyma River, northern Yakutia): Radiocarbon, v. 43, no. 2B, p. 503-515.

Vaskovsky, A.P., 1963, Essay of stratigraphy of the Anthropogene (Quaternary) deposits in the Extreme North-east of Asia: Geology of Karyak Highland. Government Scientific-Technical Publisher on Mining, Moscow, p. 143-168.

Verheyden, A., G. Helle, G. H. Schleser, F. Dehairs, H. Beeckman, and N. Koedam, 2004, Annual cyclicity in high-resolution stable carbon and oxygen isotope ratios in the wood of the mangrove tree *Rhizophora mucronata*: Plant Cell and Environment. v. 27, p. 1525-1536.

Vonk, J. E., P. J. Mann, K. L. Dowdy, A. Davydova, S. P. Davydov, N. Zimov, R. G. M. Spencer, E. B. Bulygina, T. I. Eglinton, and R. M. Holmes, 2013, Dissolved organic carbon loss from Yedoma permafrost amplified by ice wedge thaw: Environmental Research Letters, v. 8, no. 3, p. 1-9.

Xu, L. and 20 other authors, 2013, Temperature and vegetation seasonality diminishment over northern lands: Nature Climate Change, v. 3, no. 3, p. 581-586.

Waldrop M. P., K. P. Wickland, R. White III, A. A. Berhe, J. W. Harden, and V. E. Romanovsky, 2010, Molecular investigations into a globally important carbon pool: permafrost-protected carbon in Alaskan soils: Global Change Biology, v. 16, p. 2543-2554.

Walsh, J. E., 2014, Intensified warming of the Arctic: Causes and impacts on middle latitudes: v. 117, p. 52-63.

Wang, Y. J., H. Cheng, R. L. Edwards, Z. S. An, J. Y. Wu, C. C. Shen, and J. A. Dorale, 2001, A high-resolution absolute-dated late Pleistocene Monsoon Record from Hulu Cave, China: Science, v. 294, p. 2345-2348.

Waterhouse, J. S., V. R. Switsur, A. C. Barker, A. H. C. Carter, and O. Robertson, 2002, Oxygen and hydrogen isotope ratios in tree rings: how well do models predict observed values?: Earth and Planetary Science Letters, v. 201, p. 421-430.

Winton, M., 2006, Amplified Arctic climate change: What does surface albedo feedback have to do with it?: Geophysical Research Letters, v. 33, p. 1-4.

Wetterich, S., S. Kuzmina, A. A. Andreev, F. Kienast, H. Meyer, L. Schirrmeister, T. Kuznetsova, and M. Sierralta, 2008, Palaeoenvironmental dynamics inferred from late Quaternary permafrost deposits on Kurungnakh Island, Lena Delta, Northeast Siberia, Russia: Quaternary Science Reviews, v. 27, p. 1523-1540.

Wetterich, S., L. Schirrmeister, and A. L. Kholodov, 2011, The joint Russian-German expedition BERINGIA/KOLYMA 2008 during the international polar year (IPY) 2007/2008: Berichte zur Polar-und Meeresforschung, Reports on Polar and Marine Research, Bremerhaven, Alfred Wegener Institute for Polar and Marine Research, v. 636, 48 p.

Wetterich, S., V. Tumskoy, N. Rudaya, A. A. Andreev, T. Opel, H. Meyer, L. Schirrmeister, and M. Huls, 2014, Ice Complex formation in arctic East Siberia during the MIS3 Interstadial: Quaternary Science Reviews, v. 84, p. 39-50.

Willerslev, E. and 49 additional authors, 2014, Fifty thousand years of Arctic vegetation and megafaunal diet: Nature, v. 506, no. 7486, p. 47-51.

Wolfe, A. P., A. Z. Csank, A. V. Reyes, A. V. McKellar, R. Tappert, and K. Muehlenbachs, 2012 Pristine Early Eocene Wood Buried Deeply in Kimberlite from Northern Canada. PLoS ONE v. 7, no. 9: e45537. doi: 10.1371/journal.pone.0045537

WBG, World Bank Group, The Climate Knowledge Portal, 2015, <http://sdwebx.worldbank.org/climateportal/index.cfm?page=downscaled_data_download&menu=historical> Accessed June, 20, 2017

Zanina, O. G., S. V. Gubin, S. A. Kuzmina, S. V. Maximovich, and D. A. Lopatina, 2011, Late-Pleistocene (MIS 3-2) palaeoenvironments as recorded by sediments, palaeosols, and ground-squirrel nests at Duvanny Yar, Kolyma lowland, northeast Siberia: Quaternary Science Reviews, no. 17-18, v. 30, p. 2107-2123. doi:10.1016/j.quascirev.2011.01.021

Zhang, T., 2005, Influence of the seasonal snow cover on the ground thermal regime: An overview: Reviews of Geophysics, v. 43, no. 4, 23 p.

Zhang, W., C. Jansson, P. A. Miller, B. Smith, and P. Samuelsson, 2014, Biogeophysical feedbacks enhance the Arctic terrestrial carbon sink in regional Earth system dynamics: Biogeosciences, v. 11, p. 5503-5519.

Zhao-ping, Y., Hua, Ou. T., Xing-liang, Xu., Lin, Z., Ming-hua, S., and Z. Cai-ping, 2010, Effects of permafrost degradation on ecosystems: Acta Ecologica Sinica, v. 30, no. 1, p. 33-39.

Zimov, S. A., E. A. G. Schuur, and F. S. Chapin, 2006, Permafrost and the global carbon budget: Science, v. 312, no. 5780, p. 1612–1613. doi: 10.1126/science.1128908

Zubakov, V. A., and I. I. Borzenkova, 1990, Global palaeoclimate of the late Cenozoic: State Hydrological Institute, Leningrad, USSR, Elsevier Science, v. 12, 453 p.

APPENDIX A

High-resolution intra-annual $\delta^{18}O_{cell}$ values measured from the Northeastern Siberian Arctic late Pleistocene fossil wood, north of the Arctic Circle (66.5 °N)

Supplementary Table 1. Tree-ring $\delta^{18}O_{cell}$ values measured from fossil wood samples DY2 and DY4 collected from the study site (68.63 °N, 159.63 °E). $\delta^{18}O_{cell}$ values for sample DY4_R6_6_A was considered an outlier and not included in figure 3 and the paleotemperature reconstructions. $\delta^{18}O_{cell}$ measurements that were not detectable (N/D).

Sample ID	Ring Position (mm)	$\delta^{18}O_{cell}$ (‰) (SMOW)	$\delta^{18}O_{cell}$ (‰) (SMOW) Average	1SD
DY2 R1 = 1.50 mm				
DY2_R1_1_A	1.5	17.58	17.43	0.21
DY2_R1_1_B		17.27		
DY2_R1_2_A	1.38	15.28	15.31	0.04
DY2_R1_2_B		15.33		
DY2_R1_3_A	1.25	15.08	15.03	0.06
DY2_R1_3_B		14.99		
DY2_R1_4_A	1.13	15.06	15.10	0.06
DY2_R1_4_B		15.14		
DY2_R1_5_A	1	15.70	15.83	0.18
DY2_R1_5_B		15.95		
DY2_R1_6_A	0.88	15.91	16.32	0.57
DY2_R1_6_B		16.72		
DY2_R1_7_A	0.75	18.59	18.05	0.76
DY2_R1_7_B		17.52		
DY2_R1_8_A	0.63	17.08	17.18	0.13
DY2_R1_8_B		17.27		
DY2_R1_9_A	0.5	18.47	18.21	0.37
DY2_R1_9_B		17.95		
DY2_R1_10_A	0.38	19.93	19.88	0.07
DY2_R1_10_B		19.83		
DY2_R1_11_A	0.25	19.63	19.44	0.27
DY2_R1_11_B		19.24		
DY2_R1_12_A	0.13	19.05	19.15	0.13
DY2_R1_12_B		19.25		
DY2 R2 = 2.40 mm				
DY2_R2_1_A	2.3	17.93	18.08	0.21
DY2_R2_1_B		18.23		
DY2_R2_2_A	2.14	18.02	18.06	0.06
DY2_R2_2_B		18.10		
DY2_R2_3_A	1.85	18.23	18.48	0.36
DY2_R2_3_B		18.74		
DY2_R2_4_A	1.5	19.00	18.86	0.19

DY2_R2_4_B		18.73		
DY2_R2_5_A	1.35	17.66	17.79	0.18
DY2_R2_5_B		17.92		
DY2_R2_6_A	1.23	19.03	19.13	0.15
DY2_R2_6_B		19.24		
DY2_R2_7_A	1.17	N/D	18.74	N/A
DY2_R2_7_B		18.74		
DY2_R2_8_A	1.07	N/D	18.50	N/A
DY2_R2_8_B		18.50		
DY2_R2_9_A	0.78	18.24	18.14	0.13
DY2_R2_9_B		18.05		
DY2_R2_10_A	0.51	N/D		
DY2_R2_11_A	0.2	18.33	18.29	0.06
DY2_R2_11_B		18.24		
DY2 R3 = 2.15 mm				
DY2_R3_1_A	2.15	18.37	18.36	0.02
DY2_R3_1_B		18.34		
DY2_R3_2_A	2.1	18.49	18.41	0.12
DY2_R3_2_B		18.33		
DY2_R3_3_A	1.74	18.24	18.27	0.04
DY2_R3_3_B		18.30		
DY2_R3_4_A	1.38	17.67	17.51	0.23
DY2_R3_4_B		17.35		
DY2_R3_5_A	1.1	17.41	17.47	0.08
DY2_R3_5_B		17.53		
DY2_R3_6_A	1.05	17.40	17.44	0.05
DY2_R3_6_B		17.47		
DY2_R3_7_A	0.81	17.51	17.41	0.14
DY2_R3_7_B		17.31		
DY2_R3_8_A	0.4	17.22	17.43	0.29
DY2_R3_8_B		17.63		
DY2_R3_9_A	0.26	17.28	17.64	0.52
DY2_R3_9_B		18.01		
DY2_R3_10_A	0.12	17.62	17.59	0.04
DY2_R3_10_B		17.56		
DY2 R4 = 1.60 mm				
DY2_R4_1_A	1.5	17.12	17.13	0.02
DY2_R4_1_B		17.15		
DY2_R4_2_A	1.4	16.80	16.82	0.02
DY2_R4_2_B		16.83		
DY2_R4_3_A	1.3	16.65	16.67	0.03
DY2_R4_3_B		16.69		
DY2_R4_4_A	1.03	16.50	16.50	N/A
DY2_R4_5_A	0.9	16.40	16.45	0.07

DY2_R4_5_B		16.50		
DY2_R4_6_A	0.78	16.69	16.69	0.00
DY2_R4_6_B		16.69		
DY2_R4_7_A	0.5	15.93	16.27	0.47
DY2_R4_7_B		16.60		
DY2_R4_8_A	0.35	16.83	16.83	0.00
DY2_R4_8_B		16.83		
DY2_R4_9_A	0.25	17.05	17.03	0.03
DY2_R4_9_B		17.01		
DY 4 R5 = 1.45 mm				
DY4_R5_1_A	1.45	18.39	18.48	0.13
DY4_R5_1_B		18.57		
DY4_R5_2_A	1.29	18.11	18.23	0.17
DY4_R5_2_B		18.35		
DY4_R5_3_A	1.13	18.75	18.75	N/A
DY4_R5_3_B		N/D		
DY4_R5_4_A	0.97	18.67	18.64	0.04
DY4_R5_4_B		18.60		
DY4_R5_5_A	0.81	18.40	18.50	0.14
DY4_R5_5_B		18.60		
DY4_R5_6_A	0.65	18.33	18.02	0.44
DY4_R5_6_B		17.71		
DY4_R5_7_A	0.49	17.93	18.21	0.40
DY4_R5_7_B		18.49		
DY4_R5_8_A	0.33	17.78	17.84	0.09
DY4_R5_8_B		17.91		
DY4_R5_9_A	0.17	18.45	18.07	0.54
DY4_R5_9_B		17.69		
DY4 R6 = 1.85 mm				
DY4_R6_1_A	1.78	17.87	17.83	0.06
DY4_R6_1_B		17.79		
DY4_R6_2_A	1.72	17.72	17.78	0.08
DY4_R6_2_B		17.83		
DY4_R6_3_A	1.6	17.65	17.57	0.12
DY4_R6_3_B		17.48		
DY4_R6_4_A	1.55	N/D	17.30	N/A
DY4_R6_4_B		17.30		
DY4_R6_5_A	1.5	17.21	17.21	N/A
DY4_R6_5_B		N/D		
DY4_R6_6_A	1.44	18.62	17.14	N/A
DY4_R6_6_B		17.14		
DY4_R6_7_A	1.3	17.04	17.12	0.11
DY4_R6_7_B		17.20		
DY4_R6_8_A	1.1	17.06	17.12	0.10

DY4_R6_8_B		17.19		
DY4_R6_9_A	0.75	17.30	17.36	0.09
DY4_R6_9_B		17.42		
DY4_R6_10_A	0.5	18.23	17.99	0.34
DY4_R6_10_B		17.75		
DY4_R6_11_A	0.25	18.68	18.78	0.14
DY4_R6_11_B		18.88		
DY4 R7 = 1.55 mm				
DY4_R7_1_A	1.54	17.72	18.05	0.46
DY4_R7_1_B		18.37		
DY4_R7_2_A	1.44	17.44	17.21	0.33
DY4_R7_2_B		16.97		
DY4_R7_3_A	1.26	16.60	16.54	0.08
DY4_R7_3_B		16.49		
DY4_R7_4_A	1.09	16.88	16.88	N/A
DY4_R7_4_B		N/D		
DY4_R7_5_A	0.95	N/D	16.81	N/A
DY4_R7_5_B		16.81		
DY4_R7_6_A	0.85	16.80	17.02	0.30
DY4_R7_6_B		17.23		
DY4_R7_7_A	0.71	17.28	17.24	0.06
DY4_R7_7_B		17.20		
DY4_R7_8_A	0.53	18.30	18.18	0.17
DY4_R7_8_B		18.06		
DY4_R7_9_A	0.34	18.87	19.00	0.18
DY4_R7_9_B		19.13		
DY4_R7_10_A	0.16	19.22	19.30	0.11
DY4_R7_10_B		19.37		
DY R8 = 1.10 mm				
DY4_R8_1_A	1.01	17.25	17.25	N/A
DY4_R8_1_B		N/D		
DY4_R8_2_A	0.84	16.90	16.88	0.02
DY4_R8_2_B		16.87		
DY4_R8_3_A	0.71	N/D	17.01	N/A
DY4_R8_3_B		17.01		
DY4_R8_4_A	0.66	17.39	17.35	0.06
DY4_R8_4_B		17.31		
DY4_R8_5_A	0.54	17.32	17.23	0.13
DY4_R8_5_B		17.14		
DY4_R8_6_A	0.39	17.55	17.51	0.05
DY4_R8_6_B		17.48		
DY4_R8_7_A	0.23	N/D	17.40	N/A
DY4_R8_7_B		17.40		
DY4_R8_8_A	0.1	17.10	17.01	0.12

DY4_R8_8_B	16.93

Supplementary Table 2. Single averaged tree-ring and standard deviation (SD) $\delta^{18}O_{cell}$ values measured from fossil wood samples DY2 and DY4, with $\Delta(\delta^{18}O_{cell})$ calculated from Equation 4.

Ring	Averaged $\delta^{18}O_{cell}$ (‰) (SMOW)	SD $\delta^{18}O_{cell}$ (‰) (SMOW)	$\Delta(\delta^{18}O_{cell})$ (‰)
DY2 R1	17.24	1.74	4.85
DY2 R2	18.41	0.42	1.34
DY2 R3	17.75	0.42	1.01
DY2 R4	16.71	0.28	0.87
DY4 R5	18.30	0.30	0.91
DY4 R6	17.56	0.51	1.66
DY4 R7	17.62	0.96	2.75
DY4 R8	17.21	0.22	0.63
Average	17.60		1.75
SD	0.57		1.42

APPENDIX B

Supplementary Table 3. T_{max}, MAT, and T_{min} values calculated from Equations 6-8 and displayed in Figure 8.

Ring	T_{max} (Eqn. 6)
DY2 R1	22.55
DY2 R2	6.42
DY2 R3	5.13
DY2 R4	4.59
DY4 R5	4.74
DY4 R6	7.7
DY4 R7	12.34
DY4 R8	3.7
Average	8.4
Standard Deviation	6.33
Ring	MAT (Eqn. 7)
DY2 R1	-16.25
DY2 R2	-14.53
DY2 R3	-15.5
DY2 R4	-17.01
DY4 R5	-14.68
DY4 R6	-15.78
DY4 R7	-15.69
DY4 R8	-16.3
Average	-15.72
Standard Deviation	0.83
Ring	T_{min} (Eqn. 8)
DY2 R1	-55.04
DY2 R2	-35.48
DY2 R3	-36.13
DY2 R4	-38.61
DY4 R5	-34.11
DY4 R6	-39.25
DY4 R7	-43.72
DY4 R8	-36.3
Average	-39.83
Standard Deviation	6.39

Supplementary Table 4. List of equations from previous literature representing the relationship between $\delta^{18}O_{MW}$ and MAT and T_{month}; $\delta^{18}O_{MW}$ and $\delta^{18}O_{cell}$; and various Richter

et al. (2008b) like relationships between $\delta^{18}O_{cell}$ and MAT. Sternberg et al. (2007) equations reported as referenced by Shubert and Jahren (2015). *Regressions manipulated from Richter et al. (2008b) data, *Metasequoia* always excluded following Richter et al. (2008b).

Eqn No	Supplementary Equation	R^2	Reference
S1	$\delta^{18}O_{MW} = 0.695(MAT) - 13.6$	N/A	Dansgaard, 1964
S2	$\delta^{18}O_{cell} = \{[(17.57)(T_{month})] / [39.89 + (0.44)(T_{month})]\} - 12.33$	0.64	Schubert and Jahren, 2015
S3	$\delta^{18}O_{cell} = 0.61(\delta^{18}O_{MW}) + 33.21$	0.70	Csank et al., 2013
S4	$\delta^{18}O_{cell} = 0.61(\delta^{18}O_{MW}) + 32.4$	0.54	Sternberg et al., 2007 (All Data)
S5	$\delta^{18}O_{cell} = 0.60(\delta^{18}O_{MW}) + 31.9$	0.58	Sternberg et al., 2007 (Excludes Tucson, AZ)
S6	$\delta^{18}O_{cell} = 0.89(\delta^{18}O_{MW}) + 35.9$	0.78	Sternberg et al., 2007 (Excludes Sugarloaf Key, FL)
S7	$\delta^{18}O_{cell} = 0.59(\delta^{18}O_{MW}) + 35.11$	0.90	$\delta^{18}O_{MW}$ Richter et al., 2008b (Conifers)
S8	$\delta^{18}O_{cell} = 0.54(\delta^{18}O_{MW}) + 33.10$	0.75	$\delta^{18}O_{MW}$ Richter et al., 2008b (Angiosperm)
S9	$\delta^{18}O_{cell} = -0.01(MAT)^2 + 0.49(MAT) + 26.84$	0.95	MAT Richter et al., 2008b (Conifers)
S10	$\delta^{18}O_{cell} = -0.01(MAT)^2 + 0.48(MAT) + 24.99$	0.91	MAT Richter et al., 2008b (Angiosperm, Excludes Willow)
S12*	$\delta^{18}O_{cell} = -0.01(MAT)^2 + 0.43(MAT) + 26.09$	0.83	MAT Richter et al., 2008b (Eqn. S9 and S10 Combined Data)
S12*	$\delta^{18}O_{cell} = -0.01(MAT)^2 + 0.37(MAT) + 25.4$	0.91	MAT Richter et al., 2008b (Angiosperm, Includes Willow)

Supplementary Table 5. Values calculated for $\delta^{18}O_{MW}$, MAT, and resulting T_{min} using other equations provided in Supplementary Table 4. All T_{min} values calculated using Equation 8

and T_{max} values calculated from Equation 6. Average and Standard Deviation (SD) provided for the full eight-year fossil record.

Ring	$\delta^{18}O_{MW}$ (Eqn. S3)
DY2 R1	-26.13
DY2 R2	-24.22
DY2 R3	-25.3
DY2 R4	-27
DY4 R5	-24.39
DY4 R6	-25.6
DY4 R7	-25.51
DY4 R8	-26.19
Average	-25.54
SD	0.93
Ring	MAT (Eqn. S1) ($\delta^{18}O_{MW}$ Eqn. S3)
DY2 R1	-18.02
DY2 R2	-15.28
DY2 R3	-16.82
DY2 R4	-19.28
DY4 R5	-15.52
DY4 R6	-17.27
DY4 R7	-17.13
DY4 R8	-18.11
Average	-17.18
SD	1.33
Ring	T_{min} (MAT Eqn. S1) ($\delta^{18}O_{MW}$ Eqn. S3)
DY2 R1	-58.6
DY2 R2	-36.99
DY2 R3	-38.77
DY2 R4	-43.15
DY4 R5	-35.79
DY4 R6	-42.23
DY4 R7	-46.6
DY4 R8	-39.92
Average	-42.76
SD	7.29
Ring	MAT (Eqn. S2) ($\delta^{18}O_{MW}$ Eqn. S3)

DY2 R1		-23.28	
DY2 R2		-20.8	
DY2 R3		-22.22	
DY2 R4		-24.36	
DY4 R5		-21.03	
DY4 R6		-22.61	
DY4 R7		-22.49	
DY4 R8		-23.36	
Average		-22.52	
SD		1.19	
Ring		T_{min} (MAT Eqn. S1) ($\delta^{18}O_{MW}$ Eqn. S3)	
DY2 R1		-69.11	
DY2 R2		-48.03	
DY2 R3		-49.56	
DY2 R4		-53.31	
DY4 R5		-46.8	
DY4 R6		-52.92	
DY4 R7		-57.32	
DY4 R8		-50.41	
Average		-53.43	
SD		7.16	
Ring	$\delta^{18}O_{MW}$ (Eqn. S4)	$\delta^{18}O_{MW}$ (Eqn. S5)	$\delta^{18}O_{MW}$ (Eqn. S6)
DY2 R1	-24.85	-24.43	-20.4
DY2 R2	-22.94	-22.49	-19.09
DY2 R3	-24.01	-23.58	-19.83
DY2 R4	-25.72	-25.32	-21
DY4 R5	-23.11	-22.66	-19.21
DY4 R6	-24.32	-23.89	-20.04
DY4 R7	-24.22	-23.8	-19.97
DY4 R8	-24.91	-24.49	-20.44
Average	-24.26	-23.83	-20
SD	0.93	0.94	0.64
Ring	MAT (Eqn. S1) ($\delta^{18}O_{MW}$ Eqn. S4)	MAT (Eqn. S1) ($\delta^{18}O_{MW}$ Eqn. S5)	MAT (Eqn. S1) ($\delta^{18}O_{MW}$ Eqn. S6)
DY2 R1	-16.18	-15.58	-9.79
DY2 R2	-13.44	-12.79	-7.9
DY2 R3	-14.98	-14.36	-8.96

DY2 R4	-17.44	-16.86	-10.65
DY4 R5	-13.68	-13.04	-8.07
DY4 R6	-15.42	-14.81	-9.27
DY4 R7	-15.29	-14.67	-9.17
DY4 R8	-16.27	-15.67	-9.84
Average	-15.34	-14.72	-9.21
SD	1.34	1.36	0.92
Ring	T_{min} (MAT Eqn. S1) ($\delta^{18}O_{MW}$ Eqn. S4)	T_{min} (MAT Eqn. S1) ($\delta^{18}O_{MW}$ Eqn. S5)	T_{min} (MAT Eqn. S1) ($\delta^{18}O_{MW}$ Eqn. S6)
DY2 R1	-54.92	-53.71	-42.12
DY2 R2	-33.3	-32	-22.23
DY2 R3	-35.09	-33.84	-23.05
DY2 R4	-39.47	-38.31	-25.89
DY4 R5	-32.1	-30.81	-20.88
DY4 R6	-38.55	-37.31	-26.23
DY4 R7	-42.91	-41.67	-30.68
DY4 R8	-36.24	-35.04	-23.39
Average	-39.07	-37.84	-26.81
SD	7.29	7.31	6.89
Ring	MAT (Eqn. S9)	MAT (Eqn. S10)	MAT (Eqn. S12)
DY2 R1	-15	-12.75	-16.63
DY2 R2	-13.49	-11.13	-14.66
DY2 R3	-14.35	-12.05	-15.78
DY2 R4	-15.67	-13.47	-17.5
DY4 R5	-13.63	-11.28	-14.84
DY4 R6	-14.59	-12.31	-16.09
DY4 R7	-14.51	-12.23	-16
DY4 R8	-15.04	-12.8	-16.69
Average	-14.53	-12.25	-16.02
SD	0.73	0.78	0.95
Ring	T_{min} (MAT Eqn. S9)	T_{min} (MAT Eqn. S10)	T_{min} (MAT Eqn. S12)
DY2 R1	-52.54	-48.05	-55.8
DY2 R2	-33.41	-28.69	-35.75
DY2 R3	-33.82	-29.23	-36.68
DY2 R4	-35.92	-31.53	-39.58
DY4 R5	-32	-27.3	-34.43
DY4 R6	-36.87	-32.32	-39.88

DY4 R7	-41.36	-36.8	-44.33
DY4 R8	-33.79	-29.3	-37.07
Average	-37.46	-32.9	-40.44
SD	6.74	6.79	6.48

Ring	MAT (Eqn. S11)	T_{min} (MAT Eqn. S11)
DY2 R1	-15.08	-52.72
DY2 R2	-13.48	-33.38
DY2 R3	-14.39	-33.91
DY2 R4	-15.8	-36.19
DY4 R5	-13.62	-31.99
DY4 R6	-14.65	-36.99
DY4 R7	-14.57	-41.47
DY4 R8	-15.13	-33.97
Average	-14.59	-37.58
SD	0.78	6.78

Ring	$\delta^{18}O_{MW}$ (Eqn. S7)	$\delta^{18}O_{MW}$ (Eqn. S8)
DY2 R1	-30.28	-29.36
DY2 R2	-28.31	-27.21
DY2 R3	-29.42	-28.42
DY2 R4	-31.19	-30.35
DY4 R5	-28.48	-27.4
DY4 R6	-29.74	-28.77
DY4 R7	-29.64	-28.66
DY4 R8	-30.35	-29.43
Average	-29.68	-28.7
SD	0.96	1.05

APPENDIX C

Mean monthly temperature values in Figure 14.

Supplementary Table 6. Mean monthly temperature values of the single average 33-year modern record from Cherskiy, and modeled mean monthly temperature across each fossil year and the single averaged seven-year fossil record. *Outlier fossil year.

Identifier	
Month	T_{month} (°C)
33-Year Modern Avg	
Jan	-32.44
Feb	-31.08
Mar	-23.48
Apr	-14.06
May	-0.04
Jun	10.03
Jul	12.99
Aug	20.69
Sept	27.20
Oct	-9.18
Nov	-22.63
Dec	-30.45
7-Year Fossil Avg	
Jan	-37.68
Feb	-33.82
Mar	-27.01
Apr	-17.23
May	-6.16
Jun	2.87
Jul	6.37
Aug	13.56
Sept	19.83
Oct	-17.23
Nov	-27.01
Dec	-33.82
DY2 R1*	
Jan	-55.07
Feb	-48.26
Mar	-36.27

Apr	-19.03
May	0.47
Jun	16.37
Jul	22.55
Aug	35.21
Sept	46.25
Oct	-19.03
Nov	-36.27
Dec	-48.26
DY2 R2	
Jan	-35.50
Feb	-31.82
Mar	-25.34
Apr	-16.04
May	-5.50
Jun	3.09
Jul	6.42
Aug	13.26
Sept	19.23
Oct	-16.04
Nov	-25.34
Dec	-31.82
DY2 R3	
Jan	-36.15
Feb	-32.53
Mar	-26.15
Apr	-16.99
May	-6.62
Jun	1.84
Jul	5.13
Aug	11.86
Sept	17.73
Oct	-16.99
Nov	-26.15
Dec	-32.53
DY2 R4	
Jan	-38.63

Feb	-34.84
Mar	-28.16
Apr	-18.57
May	-7.71
Jun	1.15
Jul	4.59
Aug	11.64
Sept	17.79
Oct	-18.57
Nov	-28.16
Dec	-34.84
DY4 R5	
Jan	-34.13
Feb	-30.72
Mar	-24.71
Apr	-16.08
May	-6.32
Jun	1.65
Jul	4.74
Aug	11.08
Sept	16.61
Oct	-16.08
Nov	-24.71
Dec	-30.72
DY4 R6	
Jan	-39.28
Feb	-35.16
Mar	-27.90
Apr	-17.47
May	-5.67
Jun	3.96
Jul	7.70
Aug	15.36
Sept	22.04
Oct	-17.47
Nov	-27.90
Dec	-35.16

DY4 R7	
Jan	-43.74
Feb	-38.83
Mar	-30.16
Apr	-17.71
May	-3.62
Jun	7.87
Jul	12.34
Aug	21.48
Sept	29.46
Oct	-17.71
Nov	-30.16
Dec	-38.83
DY4 R8	
Jan	-36.32
Feb	-32.81
Mar	-26.63
Apr	-17.74
May	-7.69
Jun	0.51
Jul	3.70
Aug	10.23
Sept	15.92
Oct	-17.74
Nov	-26.63
Dec	-32.81

BIOGRAPHICAL SKETCH

Collin Scott Moore received a Bachelor of Science in geology from the Sam Houston State University in August of 2013. Collin began studies at the University of Louisiana Lafayette in August of 2014 as a graduate student to pursue a Master of Science degree in geology. During 2015 and 2016 summer recess, Collin served as an Intern Geologist for a mid-major oil and gas exploration and production company. While stationed in the Tulsa, Oklahoma regional and Denver, Colorado cooperate headquarters, Collin worked on West Texas and Southern Wyoming crude oil and natural gas assets. In March of 2017, Collin gave an oral presentation on the findings from this thesis research at the 51st Annual Meeting of the Geological Society of America South-Central Section session, "Advances in the Application and Development of Terrestrial Paleoclimate Proxies."